MUON INTERACTION WITH LEAD SHIELDING PRODUCING ACTIVATION: IMPLICATIONS FOR GAMMA-RAY SPECTROMETRY.

A thesis submitted in fulfilment of the requirements
for the degree of Master of Applied Science (Applied Physics)

Sean Turnbull

B App Sci (Appl Phys) (Hons)

School of Applied Science
College of Science, Engineering and Health
Royal Melbourne Institute of Technology

August 2011

DECLARATION

Except where due acknowledgement or reference has been made, the work in this thesis is original. To the best of my knowledge no other person's work has been used without due acknowledgement. This work has not been previously submitted in whole or part to qualify for any other degree. The experimentation and analysis of data are largely my own work, with the support and constructive assistance of my supervisors. This thesis is the result of work completed after the official commencement of this degree.

Sean Turnbull

August 2011

ACKNOWLEDGMENTS

I would like to thank my original supervisor Peter Johnston for initiating me on the course of this Masters. For staying with me right up until he moved on from RMIT and further via correspondence. His belief that I could do this work and finish it was encouraging. His guidance, assistance and desire to help and give advice are much appreciated.

For my second supervisor, Salvy Russo: a big thank you for taking up the role and seeing me through to the end. Thanks also to Rick Franich for his great help when I needed it.

Thanks to my friends who always seemed interested in what I was doing and supportive that I was doing the right thing. Thanks for the use of the Victorian Partnership for Advanced Computing (VPAC) computer facilities and CERN for use of the GEANT4 code.

Finally, a big thank you to my partner who always believed that I could do it and more importantly, finish the thesis, once I actually started writing it!

SUMMARY

This work investigates the generation of neutron flux inside lead shielding due to cosmic rays as a function of shielding thickness by use of the GEANT Monte-Carlo modelling code. GEANT allows for the Monte-Carlo modelling of the transport of particles in matter. This includes muons, the particles of interest here, which originate from cosmic ray showers.

Shielding limits background radiation reaching detector systems involved with low-level measurement of radiation. Varying shielding thickness allows a trade off between blocking background radiation and the generation of particles from interaction of particles (such as muons) interacting with the shielding material. Modelling the interaction between background radiation and shielding material and its effect on gamma ray spectrometry measurements is the object of this study.

Results obtained from this work are of importance for the optimisation of materials used in shielding for gamma-ray spectrometry and will model experiments carried out at the Institute of Reference Materials and Measurements in Geel, Belgium.

TABLE OF CONTENTS

LIST OF FIGURES

LIST OF GEANT4 CODE DEVELOPED IN THIS THESIS

LIST OF TABLES

LIST OF PUBLICATIONS

Article in preparation to be submitted:

S. Turnbull, S.P. Russo Muon interactions with lead shielding producing activation: Implications for Gamma Ray Spectrometry

LIST OF ABBREVIATIONS

GRS:	Gamma Ray Spectrometry
NAA:	Neutron Activation Analysis
HPGe	High Purity Germanium Detector
LGS	Low-level gamma-ray spectrometry
ULGS	Ultra low-level gamma-ray spectrometry
GEANT4	Geometry and Tracking v4
CRY	Cosmic Ray Generator
PDG	Particle Data Group
NaI(Tl)	Thallium doped Sodium Iodide Detector
HPGe	High Purity Germanium

1. Introduction

1.1. Overview of Gamma Ray Spectrometry

Gamma-ray spectrometry (GRS) is a key technique in the measurement of low level and ultra low level background gamma (γ) radiation. As such, accurate measurement of γ-rays using GRS requires an understanding of background sources, the experimental setup including the detector, detector signal electronics, the source and source–detector arrangement, data measurement and analysis [1]. GRS originated from research into rare events such as neutrino physics research, however of late the field had broadened. Reviews of GRS can be found in [2-4].

GRS is classified into two categories. The first is ultra low-level gamma-ray spectrometry (ULGS). The system is located deep underground where the effects of muon and neutron background radiation are reduced or absent. The second category is low level gamma-ray spectrometry (LGS) where the system is located either at ground level or in shallow underground locations. At shallow depths an active filter is required to discard the (cosmic) muon component allowing for lower levels of background counting [5].

The GRS technique spans a broad range of subject areas in its applicability. These include: testing for impurities in radioactive and non radioactive solution or materials [3], underwater testing to investigate different marine environments to determine levels of anthropogenic radionuclides at locations such as Mururoa Athol [6], aerial surveying using GRS to gain an understanding of the patterns of radioactivity over large areas of land [7], assisting in the determination of absorbed dose rates of Radon over small areas for Radon prognosis maps [7].

The components of a GRS system include a detector, a test sample and detector electronics to collect the output signals produced by the detector. A typical GRS 2” x 2” NaI(Tl) photo multiplier tube (PMT) scintillation detector set up is shown in figure 1.1. As can be seen in figure 1.1, the laptop serves as the data analysis tool, a NaI(Tl) detector with multi-channel analyser is attached to the computer and lead shielding surrounds the detector. The components of a GRS detection system are discussed below.

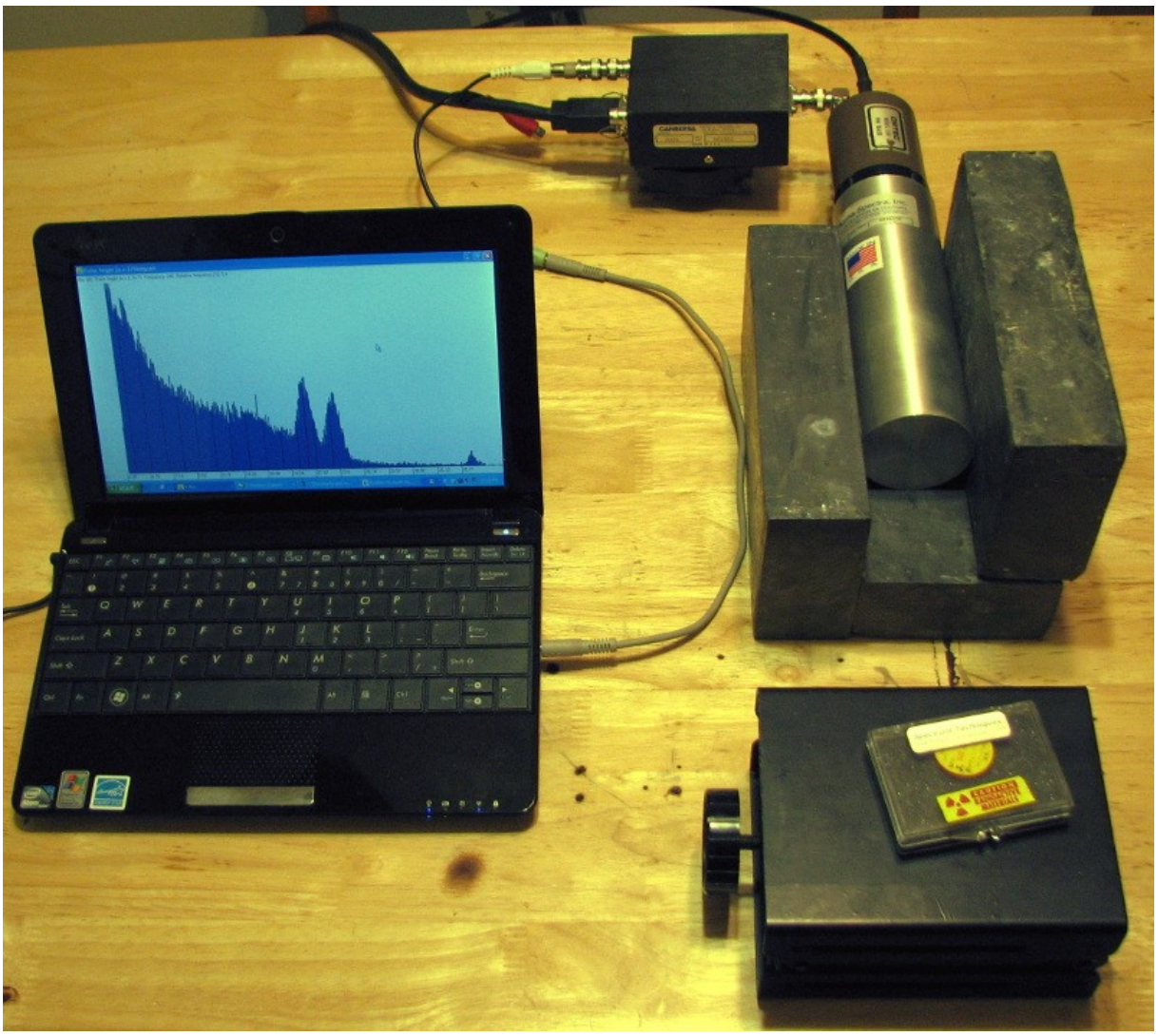

Figure 1.1. GRS system components. Laptop, source, detector, pre-amplifier and shielding. Figure taken from http://www.fusor.net/board/view.php?bn=fusor_neutrons&key=1281247740.

1.1.1. What is a typical GRS set up?

A common set up for GRS includes a detector, detector electronics to collect and process signals from the detector and a computer with specialised software to generate and display the signal spectrum. In addition, much analysis of GRS is done via computer modelling.

Detectors can be classed into three groups according to energy resolution [8]. The first is the scintillation detector such as the NaI(Tl) detector. Second include the hyper-pure germanium (HPGe) detectors whilst the third include organic or plastic detectors.

The Thallium doped Sodium Iodide NaI(Tl) detector is very common for smaller experiments. It is inexpensive and convenient to use at room temperature and is portable. For experiments

requiring a high signal resolution and ability to separate gamma ray signals, a NaI(Tl) detector is not adequate. A standard 3" x 3" NaI(Tl) detector has an energy resolution of 7.0% at 662 keV [9].

A High-Purity Germanium (HPGe) detector is significantly more accurate. This system whilst larger, often difficult to transport and requiring a liquid nitrogen cooled cryostat has signal resolution typically 40-50 times better than a NaI(Tl) detector [10].

A laptop for portability can be loaded with specialised software used for spectrum acquisition, analysis and display. To shape and control the signal, multi channel analysers and preamplifiers are used.

Shielding and shielding methods used for GRS strongly depend on the sensitivity required for the experiment. Often experiments must be carried out underground in laboratories to reduce background radiation to a level where low level signal acquisition due to specific events of interest is not overwhelmed by background noise.

1.1.2. Simulation of a GRS spectra

Computer simulation of GRS is often used in parallel with experiment or as an alternative to experiment where difficulty or cost prohibits experimental measurement to be performed.

As far as computer simulation of GRS is concerned, many simulation toolkits are designed to operate in a wide energy band ranging from thermal energies less than 1 eV to TeV. An example is the software code GEANT4, which is seen as an industry standard for the simulation of particles through matter. It allows control of tracking, geometry and sensitive detector events (hits) along with a complete set of physics processes and particles available to the user. The toolkit is written in C++ using a modular framework where classes can be overridden to create a user defined simulation.

Another simulation toolkit is Transport of Ions in Matter (TRIM). TRIM specialises in the transport of ions in matter. TRIM, GEANT4 and many similar systems use Monte Carlo modelling as the process whereby repeated random sampling is done to simulate transport of particles through matter and their consequent particle interactions [11].

1.1.3. Sources of background radiation

Appropriate GRS shielding is a complex issue hindered by the fact that background radiation can come from various sources. Using shielding limits background radiation reaching the detection system involved with low-level measurement of radiation. Many natural sources contribute to background radiation including include terrestrial gamma sources such as ^{238}U, ^{232}Th and ^{40}K, in addition to Radon and associated daughters [12]. With half lives comparable to the age of the Earth radioactive trace elements are present in almost all materials. Care must be taken to ensure all equipment is radioactively pure or clean.

Typically shielding materials are composed of lead. Whilst lead is a very good shielding material with a high atomic number, additional materials and methods are used to reduce the background levels further for low level counting. These include anticoincidence or anti muon shields to detect and block cosmic radiation, specifically muons.

Neutron production from muon capture follows an atomic number $(Z)^4$ probability distribution [13]. With a high Z number, lead is a good candidate for this process. Increasing lead shielding thickness enhances the production of tertiary neutrons [14]. The neutron production rate is dependent on muon energy. Higher muon energy increases the number of neutrons produced in lead shielding. This can influence the effectiveness of the shielding used [15] as the neutrons produced can interact with other atomic nuclei in the GRS constituent materials and produce γ-rays through (n,γ) reactions.

1.1.4. Muons and their interaction with Pb shielding

Muons (**μ**) belong to the lepton family and have a rest mass of 105.7 MeV/c^2 and an average lifetime of $2.2x10^{-6}$ seconds [16]. The mass of a muon is approximately 207 times that of an electron and is not subject to the strong force [16]. Their dominant energy loss mechanism is ionisation and their penetration distance through rock can be up to a few kilometres. Muons are created from the decay of pions which are generated from the interaction of atomic nuclei in the upper atmosphere with cosmic rays. The mean muon stopping range is governed by a range of factors including the total energy, the electronic stopping power and associated radiative processes [16].

Once generated muons can easily pass through ground level shielding and affect underground GRS without shielding. Figure 1.2 summarises effects of muons producing background radiation. As muons travel they lose energy via electromagnetic processes including photon

emission from bremsstrahlung, muon capture and photonuclear reaction of fast muons inside lead. As a result of its increased mass, muon scattering angles are reduced, allowing deeper penetration underground. This energy loss is continual until the muon is captured by a nucleus or decays.

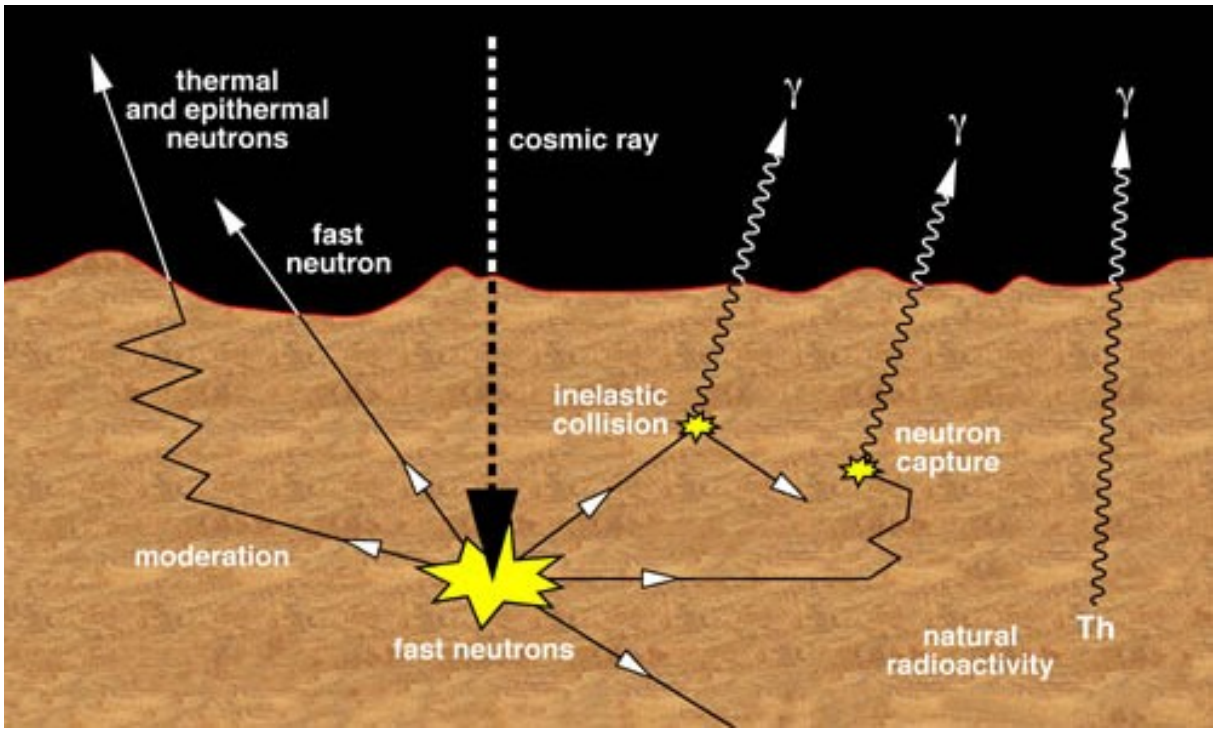

Figure 1.2. Background radiation sources resulting from cosmic rays. Figure taken from http://en.wikipedia.org/w/index.php?title=Gamma_ray_spectrometer&oldid=426250673.

1.2. Scope of this thesis

This project aims to investigate the extent to which GRS events can be generated by emission of gamma rays resulting from neutron capture reactions with target materials where the creation of neutrons is from muon interaction with lead nuclei in the lead shielding.

The GEANT4 simulation package is used to model:

(i) The transport of muons through the lead shielding material

(ii) The creation of tertiary neutrons from the interaction of muons with the lead nuclei

(iii) The neutron capture of tertiary neutrons with the target material (^{197}Au leading to ^{198}Au)

(iv) The emission of gamma rays from the decay of ^{198}Au

The Cosmic Ray Generator (CRY) simulation package is used to generate a muon spectrum resulting from cosmic rays interacting with the Earth's atmosphere.

An understanding of neutron flux generated by the shielding material is very important in the design of detectors and this work will provide valuable data in elucidating this effect. These results will be useful to experimental groups working in GRS such as those at the Institute of Reference Materials and Measurements in Geel, Belgium.

1.3. Thesis Roadmap

This thesis is arranged in 5 chapters.

Chapter 1 gives a brief discussion of the relevant background for this project and discusses the project aims.

Chapter 2 describes the theory of Gamma Ray Spectrometry. A literature review and discussion on the various types of background radiation is given. The importance of various types of shielding to reduce the background count is highlighted and discussed. Neutron activation and isotope production theory is also discussed.

Chapter 3 discusses the project methodology. The setup of GEANT4 simulations is discussed along with the design of a setup to model neutron production in lead shielding via neutron activation of a gold disk. A discussion of the geometry design, material selection, physics list, isotope tracking, simulation code files and muon production is given.

Chapter 4 presents a validation of the results from the GEANT4 simulations and discusses these results and their implications for gamma ray spectrometry.

Chapter 5 concludes with a summary of the aims of the project, and suggestions for future work to expand and build on this area of research.

2. Background Theory

This chapter consists of six sections. Section 2.1 gives a broad outline of the factors which contribute to the background spectrum especially for low level GRS experiments which are set up in underground locations. It is divided into subsections detailing the sources of background: (i) radioactivity sources in the environment and detector equipment, (ii) Radon and its progenies, (iii) muon production from cosmic rays and muon decay methods, (iv) neutron production. Section 2.2 discusses the use of shielding, the effectiveness of using the various types of lead (Pb) shielding available and implications of ^{210}Pb levels in gamma ray experiments. Section 2.3 describes the process of activation resulting from a neutron flux. Section 2.4 discusses the theory of radioactive decay, and specifically relating to the decay of the gold isotope ^{198}Au. The last two sections both detail the modelling codes used in the simulation of cosmic radiation.

2.1. Sources of Background Radioactivity

The definition of measured background can be defined as *the response of the detector in the absence of any source* [12]. Measuring detector response using low level γ-ray spectrometry requires reducing the background by several orders of magnitude. Factors affecting the background include environmental radioactivity, detector construction material impurities, Radon and its progenies, cosmic radiation and neutrons from natural fission and (α, n) reactions. Eliminating or significantly reducing these factors is essential in performing accurate low-level γ-ray measurements.

2.1.1. Environmental Radioactivity Sources

Environmental radiation sources include the natural occurring radioactive decay elements: radium, thorium and potassium. These naturally occurring elements are known as the natural series. In addition, there are cosmogenic and man-made radiation sources.

High concentrations of natural elements, (U, Th and K) are found in mineral rock such as granite, limestone and sandstone. Man-made isotopes such as ^{60}Co and ^{137}Cs from fission reactants exist in smaller quantities. Most shielding materials contain trace amounts of the natural series including Radon. A typical count rate from these elements is 10 photons cm^{-2} s^{-1} at 1 m above sea level [17]. The primordial contribution to the environmental activity is negligible.

Cosmogenic radiation is dominated by the elements ^{14}C, ^{3}He and ^{7}Be [18]. These nuclides are problematic if materials containing these substances are used in for example, scintillation or gas counters.

The main source of anthropogenic sources is nuclear weapons testing. Nuclear accidents such as Chernobyl and the recent Fukushima incident in Japan raised the concentration of ^{137}Cs worldwide.

2.1.2. Radioactivity of Detector Materials

A detector system for low level GRS can only be as good or as pure as the materials used to construct it. Similarly the radioactivity level of the detector components must be carefully controlled during construction. Primordial elements such as ^{238}U, ^{232}Th and ^{40}K are found in almost all materials used today. It is therefore important to choose radioisotope-pure materials to construct a sensitive detector so as not to compound the level of radioactivity from the source being measured. Care must also be taken during each stage of the construction of a detection system to avoid exposure to cosmic radiation and tertiary neutron production sources [19].

2.1.3. Radon

A major portion of the natural radioactive background on Earth is the result of the radioactive decay of elements Uranium and Thorium. With their long half lives, 4.47×10^{9} years for Uranium and 1.41×10^{10} years for Thorium [20], significant background radioactivity from these sources is still observed today.

During the decay sequence of Uranium and Thorium to stable Lead, many isotopes are produced. To classify these, the decay sequence is grouped into families or chains as shown in figure 2.1. The two main decay chains are called the Radium (Uranium) series and Thorium series. Both produce an isotope of Radon via the decay of Radium during their progression to stable Lead, namely ^{222}Rn and ^{220}Rn.

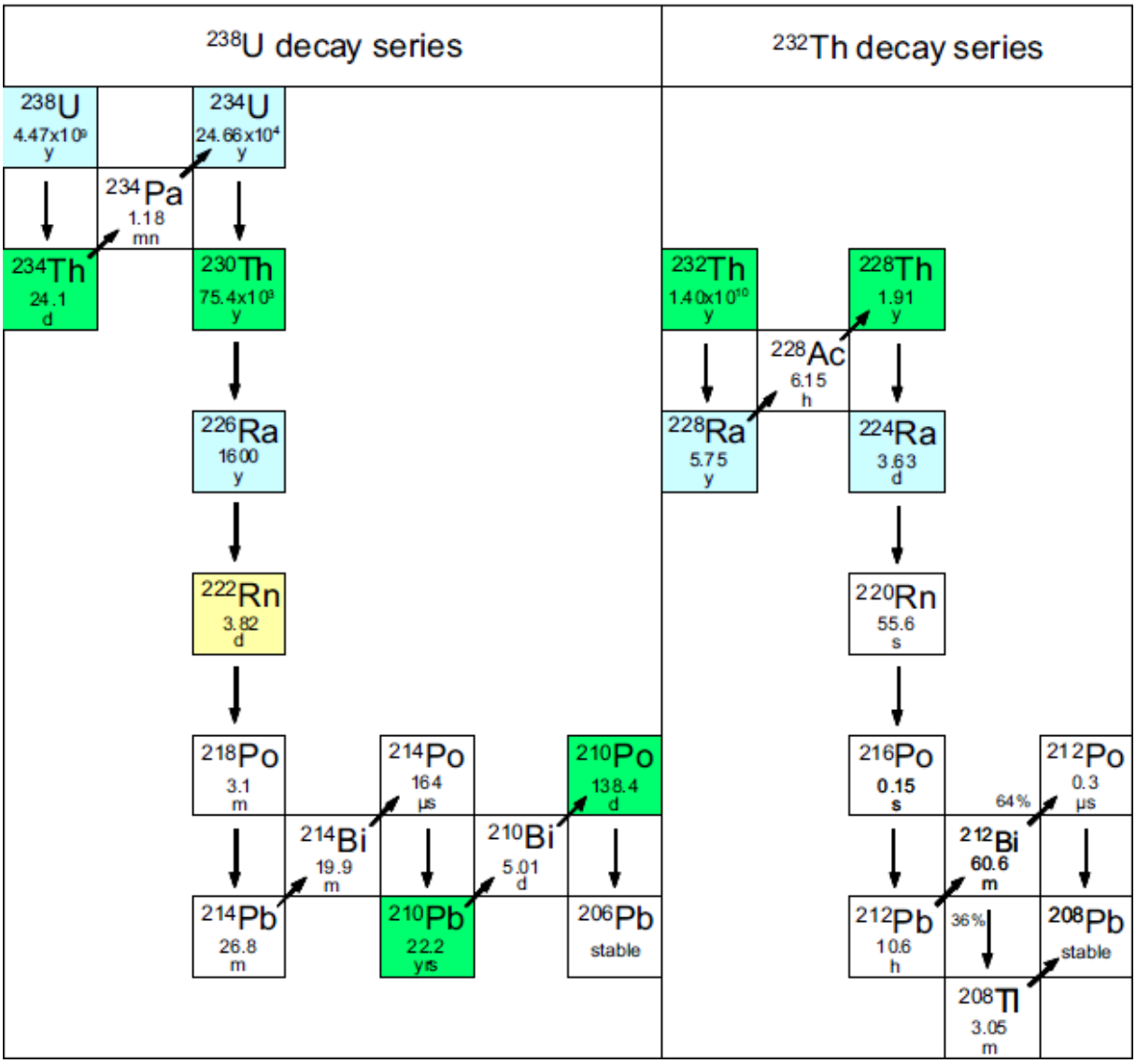

Figure 2.1. The Uranium and Thorium decay chain showing the stages of the decay and associated half-lives of the decay products. Figure from Schmidt 2010 (Ref.[21]).

The half lives for ^{220}Rn and ^{222}Rn are 55.6 seconds and 3.82 days respectively. A shorter half life of ^{220}Rn ensures a reduced chance of contamination during experimental set up from this isotope whilst the longer half life of ^{222}Rn is very problematic in areas such as mining when granite is exposed releasing the radioactive element [22].

Radon is an inert, odourless, colourless and very dense gas. As an inert gas, it easily diffuses through fragmented soil and fault lines. Radon exposure is especially significant during mining operations where concentrations can reach lethal concentrations if ventilation is not in operation. In addition, almost all building materials and equipment contain traces of Radon.

One of the strongest sources of airborne radioactivity is Radon and therefore it is a major consideration when using shielding and detector equipment for underground GRS experiments. With low level γ-ray experiments it is especially prevalent as a background source. Together with dust, Radon gas penetrates detector systems producing lines of ^{214}Pb, ^{214}Bi and ^{210}Pb (see figure 2.1 Uranium series). To mitigate this, a top down ventilation system can be used. Nitrogen is introduced at the top of a detection system and vented at the bottom [12]. Suppressing air altogether from a detector system is another method. Plastic materials should not be used as electrostatic attraction can draw in dust containing Radon [17].

2.1.4. Cosmic Radiation

The discovery of cosmic rays was made by two separate people: Domenico Pacini (1911) and Victor Hess (1912) [23]. Pacini was the first to state that "the results of many experiments on radiation could not be explained by radioactivity in the Earth's crust" [23]. Hess's experiment in 1911 aimed to measure the decrease of the Earth's radioactivity with increasing altitude using a balloon. After a year of testing he noticed as the balloon ascended an increased rate of ionising radiation was shown. An analysis and categorisation of this radiation was needed. Then in 1931 Auguste Piccard and Paul Kipfer performed an experiment sending a balloon to 15785 m confirming Hess's prediction of ionising radiation increasing with height [24]. This radiation called cosmic rays by R. Millikan [25] is now known to contain high energy nuclei: primarily protons, neutrons, muons and electrons.

Cosmic rays as they are now called are divided into two groups. These are galactic cosmic rays (GCR) with energies ranging from below 10^{17} to 10^{18} eV [25] emanating from sources such as supernovae and the interstellar medium [26], and solar cosmic rays (SCR), typically with energies < 100 MeV [25] emitted by solar flares from the sun. Whilst both have a similar composition, approximately 87% protons, 12% alpha particles and 1% heavy ions, there is a marked difference in their energy distribution and intensity [27].

Table 2.1 shows the flux and energy differences in both GCR and SCR. GCR nuclei have high energies with low fluxes, (number of particles per square centimetre per second), whilst SCR have lower energies and higher fluxes.

Table 2.1. Energies and mean fluxes for solar and galactic cosmic rays. Table from Reedy 1983 (Ref .[26]).

Radiation	Energies (MeV nucleon $^{-1}$)	Mean flux (particles cm^{-2} s^{-1})
Solar Cosmic Rays		
Protons and helium nuclei	5-100	~ 100
Iron-group and heavier nuclei	1-50	~ 1
Galactic Cosmic Rays		
Protons and helium nuclei	100-3000	3
Iron-group and heavier nuclei	~ 1	0.03

The variation in cosmic ray flux for SCR is influenced by the 11 and 22 year solar cycle. Evidence of solar cycles is borne out by measurements of sun spots as far back as the 1600s. In addition, the reversal of the heliospheric magnetic field, the bubble of material from the sun blown by the solar wind, is related to the 22 year solar cycle [28].

Another cause of cosmic ray flux variation is the so-called Forbush minima [29]. This is a rapid decrease in the galactic cosmic ray intensity caused by thin hot plasma emitted by the sun following a coronal mass ejection, a solar flare. Shaped into a lobe of the Sun's magnetic field, cosmic rays are deflected away from the Earth by the solar wind [30, 31] creating the fluence drop.

Fluence rate is also affected by altitude as Hess discovered [32]. Shielding from the atmosphere reduces the dose rate at sea level to 0.3 mSv per year whilst at around 30 000 feet, the dose rate is more than two orders of magnitude higher [33].

2.1.5. Generation of Muons

Galactic cosmic rays entering the atmosphere interact with nitrogen, oxygen and argon nuclei present in the air. This interaction produces neutrons, protons and pions leading to a hadron cascade in subsequent collisions via excitation and evaporation [34]. Pions decay to muons or

photons and muons decay to electrons and photons via pure leptonic electroweak decays. Muons are the dominant particle of cosmic rays at sea level, see figure 2.2.

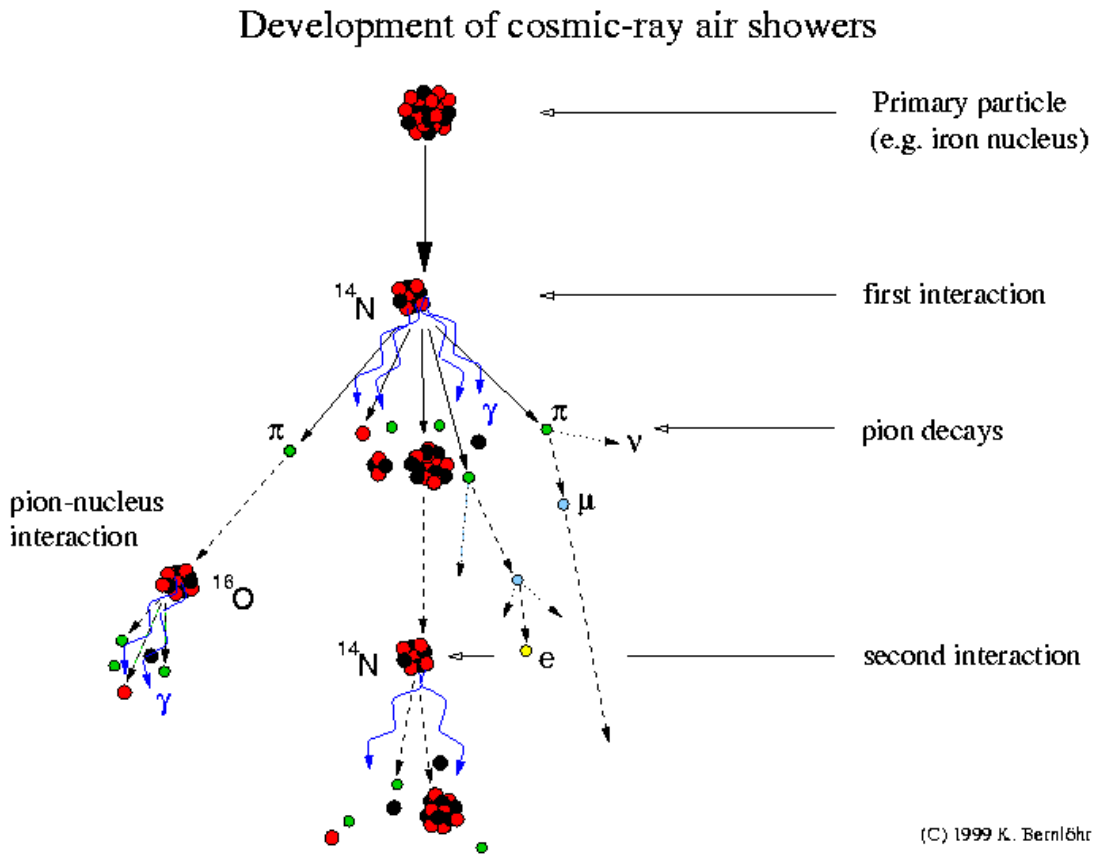

Figure 2.2. Cosmic shower showing creation of muons from pion decays.Figure from Bernlöhr 1999 (Ref. [35]).

In parallel to the cascade of figure 2.2, figure 2.3 shows the dose equivalent for the cosmic ray spectrum as a function of the altitude above sea-level. Neutrons, protons and electrons are produced at approximately 25 km above sea-level during the first interaction with the atmosphere. At an altitude of approximately 8 km the dose rate drops fairly rapidly resulting from the generation of the secondary particles, pions and neutrons. These secondary particles produced during cosmic showers reach a maximum dose rate at approximately 12km. Because muons penetrate so far underground, the dose rate at ground level is still quite large. Conversely the pion dose rate drops quite sharply to ground level. This is mainly due to the fact that pions decay to muons as shown in (2.1).

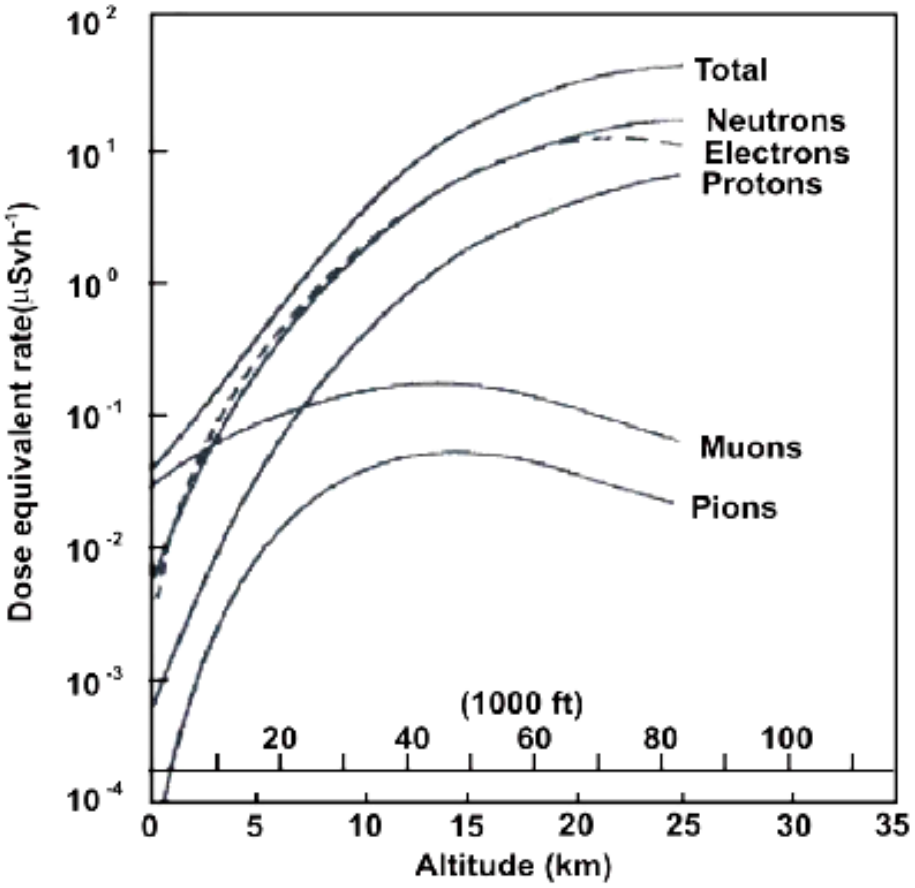

Figure 2.3. Dose equivalent of primary and secondary particles at various heights. The neutron, electron and proton dose rate is much higher at the top of the atmosphere whereas after secondary collisions muons and pions are produced. Muons only show a small variation in dose equivalent rate to the ground. Figure from Singh 2011(Ref.[36]).

Muons (μ^-), anti-muons (μ^+) and muon neutrinos (υ_μ) are created by the decay of pions (π**)** via (2.1) and (2.2),

$$\pi^- \rightarrow \mu^- + \bar{\upsilon}_\mu, \qquad 2.1$$

$$\pi^+ \rightarrow \mu^+ + \upsilon_\mu. \qquad 2.2$$

Muon mass is approximately 207 the mass of an electron. The typical energy range for muons is 0.2 - 20 GeV with the median value of 2 GeV [34].

When muons reach sea level their fluence rate is approximately 1.9 x 10^{-2} $cm^{-2}s^{-1}$ (for the United States) [34], the absolute value is dependent on the latitude of the detector. The Earth's

magnetic field, atmospheric absorption and muon decay all affect angle of incidence upon the Earth [17].

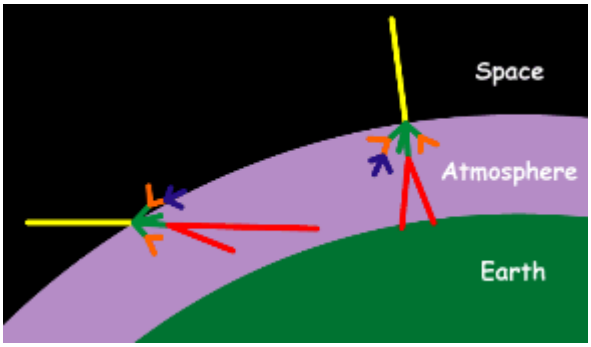

Figure 2.4. Schematic showing longer distance travelled by muons far from zenith angle.

To clarify the zenith angle, figure 2.5 shows the Earth's surface with the angle θ representing different incident angles travelled by muons to the surface. The zenith angle is measured at 90° to the Earth's surface. Large angular deviation from the zenith represents longer distances as shown in the left section of figure 2.4.

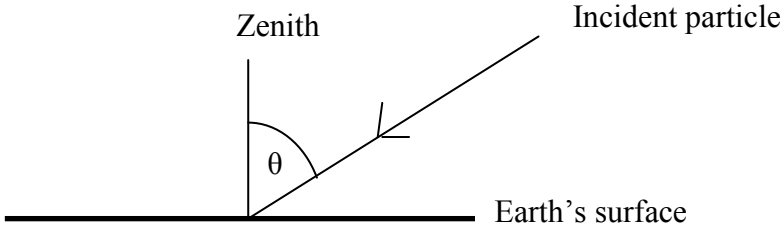

Figure 2.5. Schematic showing Earth's surface and zenith angle θ.

Figure 2.4 shows the different path lengths muons travel when they are far from the zenith (vertical). Correspondingly for lower energy muons at large θ, a lower flux is recorded. These muons lose energy through decay or ionisation. More precisely, a helical path is traversed with magnetic fields bending muons depending on charge in different directions toward the magnetic poles. The fluence rate as a function of angle $\varphi(\theta)$ follows a $cos^n\theta$ relationship relative to the zenith as given by (2.3) for $\theta \leq 75°$,

$$\varphi(\theta) = \varphi_0 cos^n\theta \ , \qquad 2.3$$

where φ_0 is the angular fluence rate at $\theta=0^0$, n is a function of momentum, $n=n(p)$. An increasing muon momentum equates to a higher n value. For muons with energies greater than 1 GeV, n is approximately 1.85 [34, 37].

2.1.6. Energy loss Processes in Muons

Energy loss processes for muons in rock include catastrophic interaction mechanisms such as ionisation, pair production, muon decay, bremsstrahlung and nuclear interaction. For dense materials, the primary energy loss mechanism is ionisation [19]. These will briefly be discussed.

2.1.6.1. Muon Ionisation

Muon Ionisation is a two stage process dependent on its energy. For low energy, energy loss is a continuous process whereas with high energies the process is discrete with the production of energetic delta electrons [17]. The energy loss rate in the atmosphere is approximately 2MeV / gcm^{-2} [38].

2.1.6.2. Pair Production

Pair production involves the production of a particle antiparticle pair, represented by though not exclusive to, the following group of interactions,

$$e^+e^- \rightarrow \mu^+\mu^-, \tag{2.4}$$

$$\gamma\gamma \rightarrow \mu^+\mu^-. \tag{2.5}$$

This can be an electron-positron, gamma-gamma or muon-anti-muon pair [39, 40]. Equation (2.5) can be represented by the Feynman diagram as shown in figure 2.6.

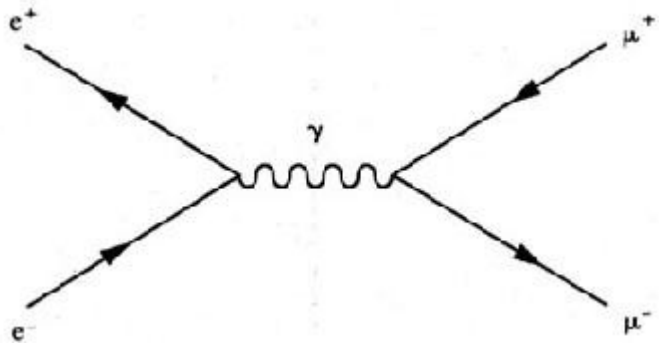

Figure 2.6. Feynman diagram of muon pair production. Figure from Brandt 2009 (Ref.[41]).

Charge conservation requires that these pairs be opposite in charge. For this process to occur, the incident particle requires twice the rest energy of the created pair. In the case of an electron, this is 1022 MeV [42]. Excess energy is carried away equally by the pair.

2.1.6.3. Muon decay

Muon decay is represented by the following [43],

$$\mu^- \rightarrow e^- + \bar{\upsilon}_e + \upsilon_\mu, \quad 2.6$$

$$\mu^+ \rightarrow e^+ + \upsilon_e + \bar{\upsilon}_\mu. \quad 2.7$$

where μ, μ^+ is a muon/anti muon, e^-, e^+ is an electron/positron, υ_e, $\bar{\upsilon}_e$ is an electron neutrino/anti electron neutrino and υ_μ, $\bar{\upsilon}_\mu$ is a muon neutrino/anti muon neutrino.

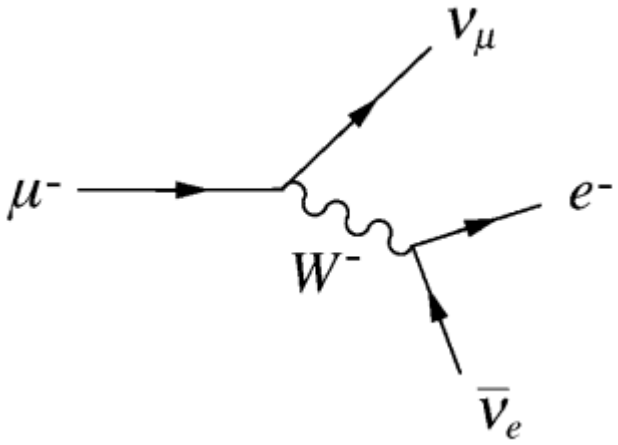

Figure 2.7. Feynman diagram of muon decay via weak interaction of W boson. Figure from Martin 2008 (Ref.[44]).

The weak interaction governs the decay via means of the exchange of a W boson and to conserve lepton number there are always two neutrinos, an electron and muon neutrino and one electron produced, matching the input muon charge as shown in figure 2.7.

2.1.6.4. Bremsstrahlung

Braking radiation or Bremsstrahlung occurs when a muon or electron is scattered by the presence of a charged particle, emitting a photon. Specifically the Coulomb field of the nuclear charge affects the incoming particle. During the scattering the muon accelerates, losing kinetic energy and emitting a photon to conserve energy [17] .

Due to the increased mass of a muon, (207 times the mass of an electron), scattering angles are reduced during encounters with Coulomb fields producing less Bremsstrahlung [45]. This accounts for the greater penetrating depth of muons in materials such as granite.

2.1.6.5. Nuclear interaction

High energy particles such as muons can lose energy via virtual photon exchange whilst undergoing inelastic collisions. This is dependent upon the energy of the incoming particle. For energies below 1 GeV protons and neutrons are emitted primarily but above this number pion production dominates [19].

Attenuation length of muons in rock is typically around 2 kg cm^{-2} near sea level [46]. Figure 2.8 shows the dependence of muon intensity for various underground experimental sites. The muon intensity is considerable down to eight kilometres and has a direct influence on neutron production rates. Higher muon energies increase neutron production [15].

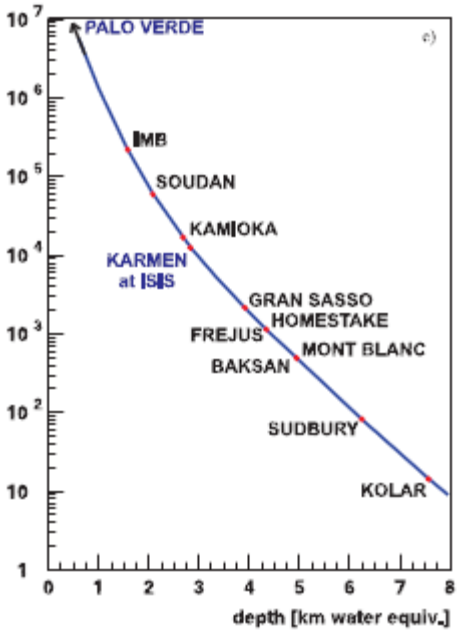

Figure 2.8. Muon flux as a function of depth for underground laboratory detection sites. Figure from Wolf 2002 (Ref. [47]).

2.1.7. Neutron Production

Neutron production in the context of this project is primarily a result of cosmogenic muons interacting with atomic nuclei in the detector setup such as the lead shielding. Neutron production is a significant factor in GRS experiments as the generated neutrons can interact

with nuclei in the detector and surrounding material and produce γ-rays through neutron-capture events. Gamma rays produced in such events must be accounted for in accurate GRS measurements. The production of neutrons is brought on by several processes. This first is negative muon capture. This is a weak interaction shown by (2.8),

$$\mu^- + p \rightarrow n + \nu_\mu. \qquad 2.8$$

Muons are slowed then captured in the atomic K shell orbit of a nucleus. Various electromagnetic processes occur in this orbit such as Bremsstrahlung allowing the muon to drop down to the inner orbital 1s, then the muon either decays or undergoes nuclear capture. At low atomic number (Z < 11) the muon capture process dominates, whereas around (Z = 11), the probabilities of capture and decay are approximately equal, however, for high Z nuclei (e.g. Lead) the muon capture processes again dominate [48]. After capture the nucleus de-excites by the emission of a neutron and neutrino from the nucleus [18]. The resulting atom is known as a muonic atom.

This process is the dominant source of tertiary neutron production at shallow to moderate rock depth. With a high Z material such as lead, the probability of muon capture is proportional to Z^4 [13].

The second process is direct muon induced spallation where a heavy nucleus ejects large numbers of nucleons (neutrons in this case) resulting from collisions by protons from cosmic rays. In addition there is photon induced spallation of muons whereby photons produced in muon showers cause the spallation of the neutron [49, 50].

Making measurements inside a lead shielded gamma ray spectrometer poses many challenges, not least of which is reducing the energy deposited by muons as they traverse the shield. In addition to the neutrons originating outside the shield from natural radioactivity and secondary neutrons from cosmic showers, neutrons can also be created inside the lead. Tertiary neutrons can increase the background neutron flux by an order of magnitude [51]. By moving the experiment to a different laboratory site underground, secondary neutrons are absorbed by the intervening rock and the tertiary neutron flux can be significantly reduced [52]. For example, The Institute for Reference Materials and Measurements (IRMM) low level laboratory is located 500 m underground, enabling a muon flux reduction factor of 800 compared to ground level. Also the cosmic radiation nucleonic component is reduced by five to six orders of magnitude [53].

2.2. Shielding

Shielding material made of lead is very efficient at reducing the radiation background. It has a manageable cost, is easily machinable and has a high Z number and low cross section for activation of environmental neutrons. It is often categorised by the level of ^{210}Pb contamination. Commercial lead suffers large contamination from the uranium or thorium series [54]. Much of the literature states that the main cause of radioactivity in lead is caused by ^{210}Pb and its progenies ^{210}Bi and ^{210}Po. The decay details of ^{210}Pb follow. ^{210}Pb decays to ^{210}Bi then ^{210}Po with a half life of 22.3 years. Specifically:

(i) ^{210}Pb emits γ-rays of energy 46.530 keV via β^- decay with half life of 22 years.

(ii) ^{210}Bi emits no γ-rays but decays via β^- decay to ^{210}Po with half life of 5.013 days.

(iii) ^{210}Po emits γ-rays of 803.1 keV via α decay to ^{206}Pb with half life of 138 days [55].

Lead is classified by the ^{210}Pb count with different levels of radioactivity including Modern Lead with a ^{210}Pb count ranging from 2500 Bq kg^{-1} up to 50000 Bq kg^{-1}. Lead used in underground experiments typically has a background count of 200 Bq kg^{-1}. Reducing the count to around 20 Bq requires specially made lead by suppliers such as Johnson & Mahey or acquiring lead that is old enough for the several half lives (^{210}Pb half life is approximately 22 years) of ^{210}Pb to have passed [46]. This is commonly called ancient lead with a typical age of 200 years or more. Not surprisingly it is difficult locating lead at this age but sources of ancient lead have been found in ship wrecks and old French lattice lead work and near the Sardinian coast. Lead found here has been dated back to Roman times. This lead is named after the location of origin, Oristano.

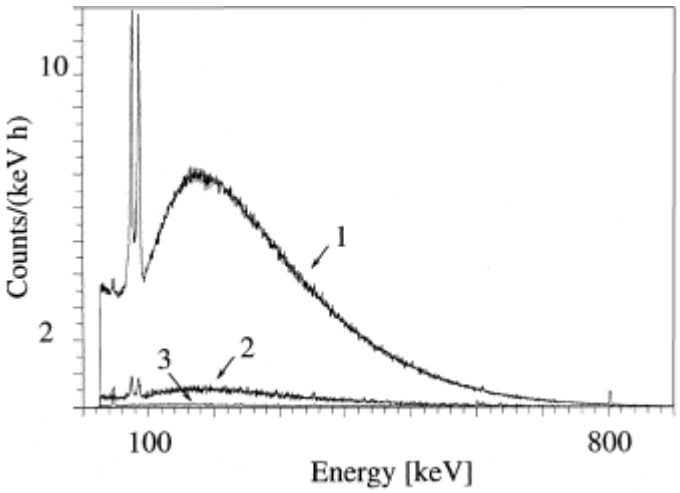

Figure 2.9. Types of lead shielding containing ^{210}Pb. 1. Common modern lead. 2. Modern lead with low ^{210}Pb count. 3. Roman lead from Oristano. Figure from Alessandrello 1991 (Ref. [56]).

Figure 2.9 illustrates the γ-ray count difference in keV of the decay of ^{210}Pb to ^{210}Bi. Three types of lead: common lead, modern lead and Oristano lead are shown. The ^{210}Pb γ-ray level in Roman lead is significantly smaller showing the usefulness in low level background setups. The β^- decay equation for ^{210}Pb is given in (2.9),

$$^{210}_{82}Pb \rightarrow {}^{210}_{83}Bi + {}^{0}_{-1}e. \qquad 2.9$$

A common challenge in rare-event searches using GRS is an accurate and precise understanding of all background radiation components [57]. While moving a detector set up underground and using lead shielding can remove most of the background, often the muon background is the last component to be reduced or eliminated. With the requirement for increasingly sensitive detection methods, different types of shielding methods are called for. Shielding material can include water or paraffin for neutron moderation and borax or cadmium for absorption or a plastic scintillator surrounding the detector and shielding.

One such system is called a veto, also known as an active shield. By monitoring which particles cross the veto counter, often made in the form of a plastic scintillator surrounding the detector, a signal or coincidence event is triggered that stops the acquisition of that particle. When the counter operates in coincidence mode, direct measurement of the muon background is possible [58]. When a particle crosses the veto, a signal is transmitted that stops the acquisition of the current event. This does however lead to an increase in dead time; this is time that is not used for counting. Figure 2.10 shows the effects of no shielding compared to

using passive shielding such as lead and active shielding such as a muon veto or anti-cosmic shielding veto.

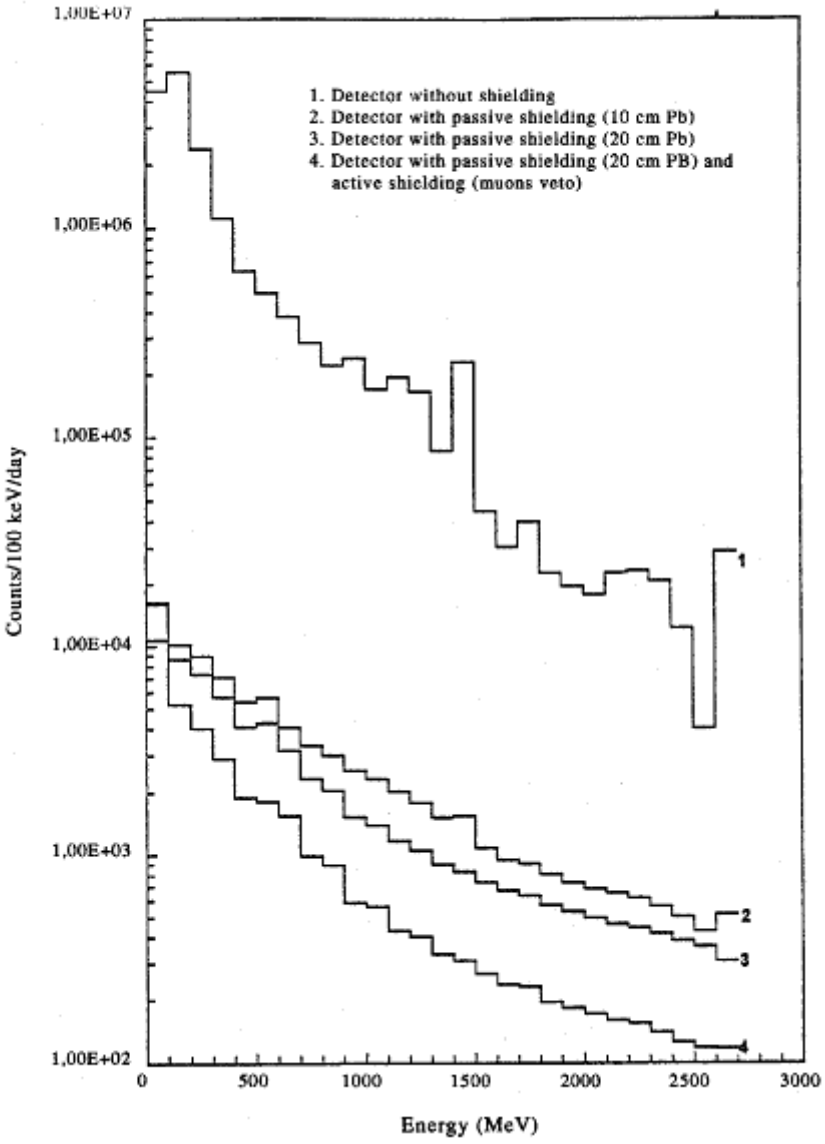

Figure 2.10. Results after using shielding and a veto on count rate. Figure from Núñez-Lagos, 1996 (Ref.[12]).

2.3. Neutron Activation

Activation analysis is a method for the determination of elements based upon the conversion of stable nuclei to other, mostly radioactive nuclei via nuclear reactions, and measurement of the reaction products [59].

Neutron Activation Analysis (NAA) consists of taking a small sample of material and exposing it to a neutron flux, typically thermal neutrons, such as those from a nuclear reactor, where neutron capture (n, γ) predominates. When the metal target such as Au is exposed to the neutron flux, the number of ^{198}Au nuclei builds until saturation is reached. The saturation activity A_{sat} is caused by both thermal and epithermal (0.025 eV – 0.1 eV) neutrons and is given by (2.10),

$$A_{sat} = \left(\sigma_{th}\varphi_{th} + I_{\gamma}\varphi_{epi}\right)\left(\frac{N_a m\theta}{A}\right), \qquad 2.10$$

where σ_{th} is the thermal neutron capture cross section, φ_{th} the thermal neutron flux, I_{γ} the resonance integral, φ_{epi} the epithermal neutron flux, N_a the Avogadro number, m is the mass of the target, θ the natural abundance of the activated isotope in the target and A is the atomic number of activated isotope [52].

When the disintegration rate of the nuclide ^{197}Au is equal to the production rate of ^{198}Au, a steady state is formed known as saturation. Bombarding an element with neutrons allows a neutron to be absorbed by the target nucleus, creating an excited nucleus (^{198}Au) with an additional neutron. The unstable nucleus de-excites usually occurs through emission of gamma rays [60]. This process is known as neutron capture.

De-excitation occurs through emission of one or more prompt gamma rays. As the emitted gamma ray energies are characteristic of a particular nuclide, measurement of these gamma energies allows for quantitative determination of the composition of materials. There are two types of NAA, depending on whether measurements are taken during irradiation (Prompt NAA) or after the irradiation following radioactive decay (Delayed NAA).

PNAA is used for elements with a very short half life. The advantages of PNAA include being a non-destructive technique requiring no sample preparation. The neutron flux used for irradiation is typically lower than 10^9 $cm^{-2}s^{-1}$ [61]. The number of converted nuclei is 7-8 orders of magnitude less than the number of atoms in the sample [61]. Radiation damage caused by irradiation is often negligible. Every element except ^{4}H can be analysed. Excitation of the sample and detection occur at the same time, with the gamma radiation detected off axis to the beam. DNAA is the conventional method and requires the user to irradiate the material for a length of time then typically the analysis is done offsite. Time between irradiation and analysis is dependent on half life of the material. A very short half life in the order of minutes often precludes DNAA.

The probability of a neutron interacting with a nucleus is a function of the neutron energy. Assuming a density of particles in the incident beam of n_a, the flux (φ) in units of particles per unit area per unit time through the target is given by (2.11),

$$\varphi = n_a v_i, \tag{2.11}$$

where v_i is the incident beam velocity relative to target. Assuming also that all of the target particles have an effective cross-section σ, the probability that any particle a will hit a target is

$$\varphi = \sigma n_b \, dx, \tag{2.12}$$

where n_b is the fraction of target area obscured by b particles and dx is the target thickness [62].

The capture cross-section (on the rhs of equation 2.12) is measured in units called barns (with 1 barn = 10^{-28} m^2 or 10^{-24} cm^2) and each nuclide has a unique neutron energy – capture cross-section relationship. For many nuclides, the capture cross-section is greatest for low energy neutrons referred to as thermal neutrons. Some nuclides have greater capture cross-sections for higher energy neutrons called epithermal neutrons. NAA analysis primarily uses nuclides that are activated by thermal neutrons. Refer to table 2.2 for a classification of neutron energies.

Table 2.2. Classification of neutrons according to neutron energy.

Classification	**Energy**
Thermal	Around 0.025 eV
Slow	< 1 eV
Resonance	1 keV - 0.5 MeV
Fast	0.5 MeV - 10 MeV
High Energy	> 10 MeV

The neutron capture scheme for ^{198}Au is shown in (2.13),

$$^{197}_{97}Au + \ ^{1}_{0}n \rightarrow \ ^{198}_{97}Au + \ \gamma. \qquad 2.13$$

Using the neutron capture cross section, the activity for a particular nuclide, at any time *t*, during an irradiation, (2.14) can be found,

$$A_t = \sigma_{act}\varphi N(1 - e^{-\lambda t}), \qquad 2.14$$

where A_t = the activity in units of number of decays per unit time, σ_{act} = the activation cross-section, φ = the neutron flux (neutrons cm^{-2} s^{-1}), N = the number of parent atoms, λ = the decay constant (number of decays per unit time) and t = the irradiation time.

NAA is a very popular method as the samples used during the process are not destroyed or altered [59]. Small doses of induced radioactivity are often present but with a short half life. A brief review of the literature highlights the usefulness of the non destructive nature of NAA. Examples include the age determination of pottery, the estimation of the gold in mines in southern Egypt and analysis of Hellenistic pottery from Boeotia Greece.

For this project, NAA is used to activate a ^{197}Au sample. Muons are directed to the lead target that functions as a muon to neutron converter. Thermal neutrons of energies of a few eV are produced from muon energy loss processes. Through neutron capture, the gold sample is activated producing the isotope ^{198}Au. Characteristic energies of 411.8 keV occur through the decay of ^{198}Au. This isotope production rate will be counted and convolved or multiplied with the natural muon spectrum giving a third graph, the activation rate as a function of muon energy. A ^{198}Au decay scheme is shown in figure 2.11.

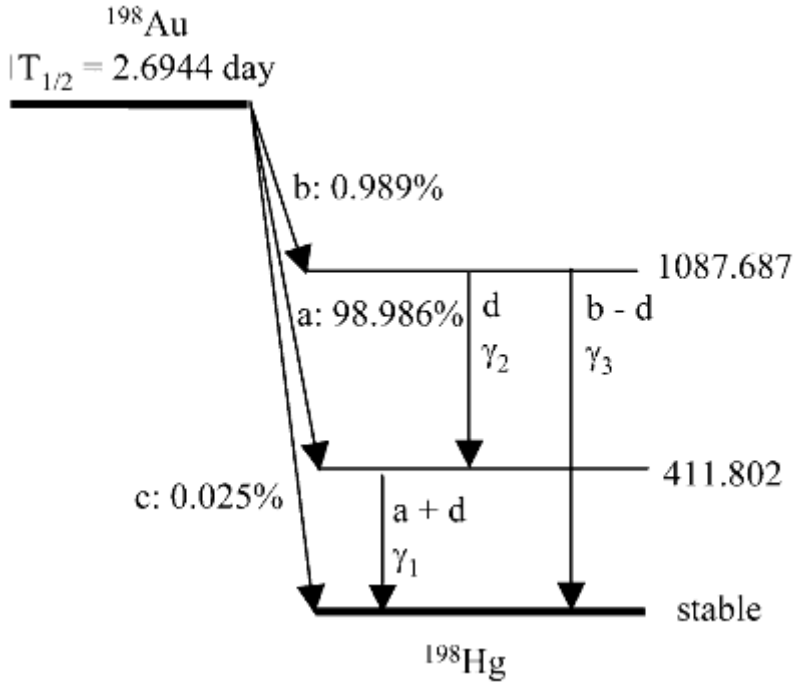

Figure 2.11. Branching ratio for ^{198}Au. Figure from Mo, 2007 (Ref.[63]).

2.4. Isotope Production and Decay

By definition, materials whose nuclei spontaneously emit radiation and thereby change the state of the nucleus are considered radioactive [20].

The principle of radioactive decay dictates that radioactive nuclei will emit particles or photons according to well a defined probability specific to the nucleus. Whilst it is impossible to know when decay will occur within an atom, it is possible to know how many nuclei will have statistically decayed after a certain time. The probability of the decay over the life time of the atom remains constant. This is given by (2.15) [20],

$$\lambda = -\frac{(dN/dt)}{N}, \qquad 2.15$$

where N is the number of nuclei present at a time t, and λ is the decay constant. Integrating (2.15) yields,

$$N(t) = N_0 e^{-\lambda t}, \qquad 2.16$$

where N_0 is the number of original nuclei present at t = 0. Setting N(t) = ½N_0 in (2.16) gives the half life $t_{1/2}$ which is a measure of the time required for ½ the original nuclei to have decayed and is given by,

$$t_{1/2} = \frac{\ln 2}{\lambda}. \qquad 2.17$$

Three main types of decay exist in nature. These are α - alpha, β - beta and γ - gamma decay. Both alpha and beta decay emit a particle and change the nuclear species. In the case of alpha decay a helium nucleus, ^{4}He is ejected. In β decay, an electron (e^-) and electron anti-neutrino ($\bar{\upsilon}_e$) (or their anti particle pairs) are emitted, converting a neutron to a proton or vice versa as given by (2.18(a)) and (2.18(b)),

$$n \rightarrow p + e^- + \bar{\upsilon} \qquad \beta^- \text{ decay,} \qquad 2.18a$$

$$p \rightarrow n + e^+ + \upsilon \qquad \beta^+ \text{ decay.} \qquad 2.18b$$

In cases where β^+ decay occurs, electron capture can also take place as given by (2.19),

$$p + e^- \rightarrow n + \upsilon_e \qquad \text{electron capture } (\varepsilon). \qquad 2.19$$

Gamma decay involves the emission of a γ-ray resulting from the relaxation of a nucleus from an excited state to a lower energy state. Often a γ-ray emission will follow an α or β decay during decay.

For this project, the reaction of primary importance is the β^- decay of ^{198}Au, (2.13). This reaction governs the process that will be used to gain an estimate of the gold activation rate during irradiation from neutrons in lead environments from natural cosmic radiation. For the GEANT4 simulations in this project the incident neutrons involved in the neutron activation of ^{197}Au result from the muons incident on the lead shielding and thus measurement of ^{198}Au γ-rays allows an estimate of the effect of cosmic rays (muons) on the lead shielding which is relevant for accurate GRS measurements.

Often these decays do not go straight to the end product or the stable product, but via a series of steps. These steps have a certain probability, energy and decay time. Multiple decay processes may also be involved for each step. Competing decay modes and intensities are shown usually on a diagram by their branching ratios. An example is the element ^{226}Ac. It has α, β^- and ε decay modes all competing during nuclei decay.

Analysing the ^{198}Au isotope and its decay scheme, figure 2.11 yields many interesting features. The half life is 2.69 days making it an ideal candidate for NAA. It allows placement within a neutron source and transport back to the detector within one half life.

The isotope ^{198}Au decays to ^{198}Hg through 100% β^- emission through three branching ratios. These are labelled a, b and c. The (a branch) is the primary branch with 98.98% intensity. It decays to the ground state with emission of 411.802 keV (γ_1). The second branch (b branch) decays to the 1087.687 keV (γ_3) state of ^{198}Hg then promptly decays again via emission of 675.885 keV (γ_2). The intensity for this decay is 0.989% whilst the (c branch) is lower still with 0.025% intensity. This branch decays straight to stable ^{198}Hg with no γ-ray emission.

GEANT4 simulation runs show for each activation the corresponding 411.802 keV gamma energy demonstrating the main branch intensity.

Two competing rates exist in measuring radioactivity, the activation rate and decay rate. As stated previously, *this project is concerned with the activation rate*, or the number of ^{198}Au isotopes produced during irradiation from neutrons. The decay rate, as previously mentioned defines the number of decays of the irradiated or activated nuclei over a specified time assuming no increase to the nuclei in the sample. Comparing the activation rate with decay rate requires knowledge of the N_0 of target nuclei, the half life and the activation cross section σ, measured in barns (10^{-24} cm^2). This defines the probability of a particular reaction occurring, a higher cross section indicates a greater interaction probability.

To highlight the competing nature of the two rates: if a sample is placed in a thermal neutron source such as a nuclear reactor for 10 minutes, the original nuclei N_0 present in the sample are irradiated due to the high neutron flux. Now the number of radioactive nuclei N_1 increases due to the irradiation whilst also decreasing due to radioactive decay forming stable nuclei N_2.

If the half life of the sample is very short, in the order of milliseconds, the decay rate of the radioactive nuclei will match the activation rate. The N_1 production will be very small and hence as soon as one nucleus is activated, decay will follow. Depending on the cross section, the production of N_1 will be a significant proportion of N_0. Once the neutron source is switched off, it will decay according to the exponential rate law (2.16).

Another possibility occurs where the sample during decay produces daughter nuclei which are also radioactive. An example is ^{132}Te with $t_{1/2}$ = 78 h. It decays to an unstable ^{132}I with $t_{1/2}$ = 2.28 h then to stable ^{132}Xe. As the decay of ^{132}Te produces daughter ^{132}I nuclei, the decay

rates for both reach secular equilibrium after approximately twelve hours [20] . Therefore in order to model the complexities associated with the various activation and decay schemes possible, a Monte-Carlo method is required such as GEANT4.

The decay of ^{198}Au is modelled using the GEANT4 toolkit described below.

2.5. The GEANT4 Toolkit

This project uses the computer simulation toolkit GEANT4. GEANT4 is a toolkit for the simulation of the passage of particles through matter [11].

The development of a simulation code for background measurement is useful in optimising a detection system with respect to the background radiation. It enables the system to be tested and experimental measurements compared to theoretical results before the detector is used in sensitive GRS measurement. In addition, experimental results gained from a physical detector can be compared to simulation to test whether results are in line with expected results based on various theoretical models and activation/decay schemes.

GEANT4 uses the Monte Carlo method. The Monte Carlo technique is a numerical method based on random number generation [64]. Using GEANT4 as an example, the probabilities for different particle interactions, step length between particles, direction of movement as well as other parameters can be simulated [64].

Toolkits using the Monte Carlo method include GEANT4, MCNPX, FLUKA, TRIM, MICAP, MUSIC, EGSNRC, MEGALib and GAMLIB to name a few. Although some theoretical models have been developed to account for low energy effects, currently the most accurate method for predicting thermal neutron transport is via computer simulation of particle transport.

GEANT4 consists of an open source collection of C++ classes freely available that are compiled into libraries. The code provides tools for a complete simulation toolkit including modelling processes such as geometry, materials, properties of materials involved in the measurement process, primary event generation, tracking of particles through materials and a wide range of other physical processes.

Classifying the various processes is accomplished by an object orientated technology approach allowing the architecture to be divided into key sections or class categories that handle the passage of particles through matter. They are labelled as: run and event, tracking and track, geometry and magnetic field, particle definition and matter, physics, hits and digitization, visualisation and interfaces. A representation of the scheme is shown in figure 2.12.

Developing an application using the toolkit requires a user to write or modify their own C++ program using classes which inherit behaviour from the inbuilt classes.

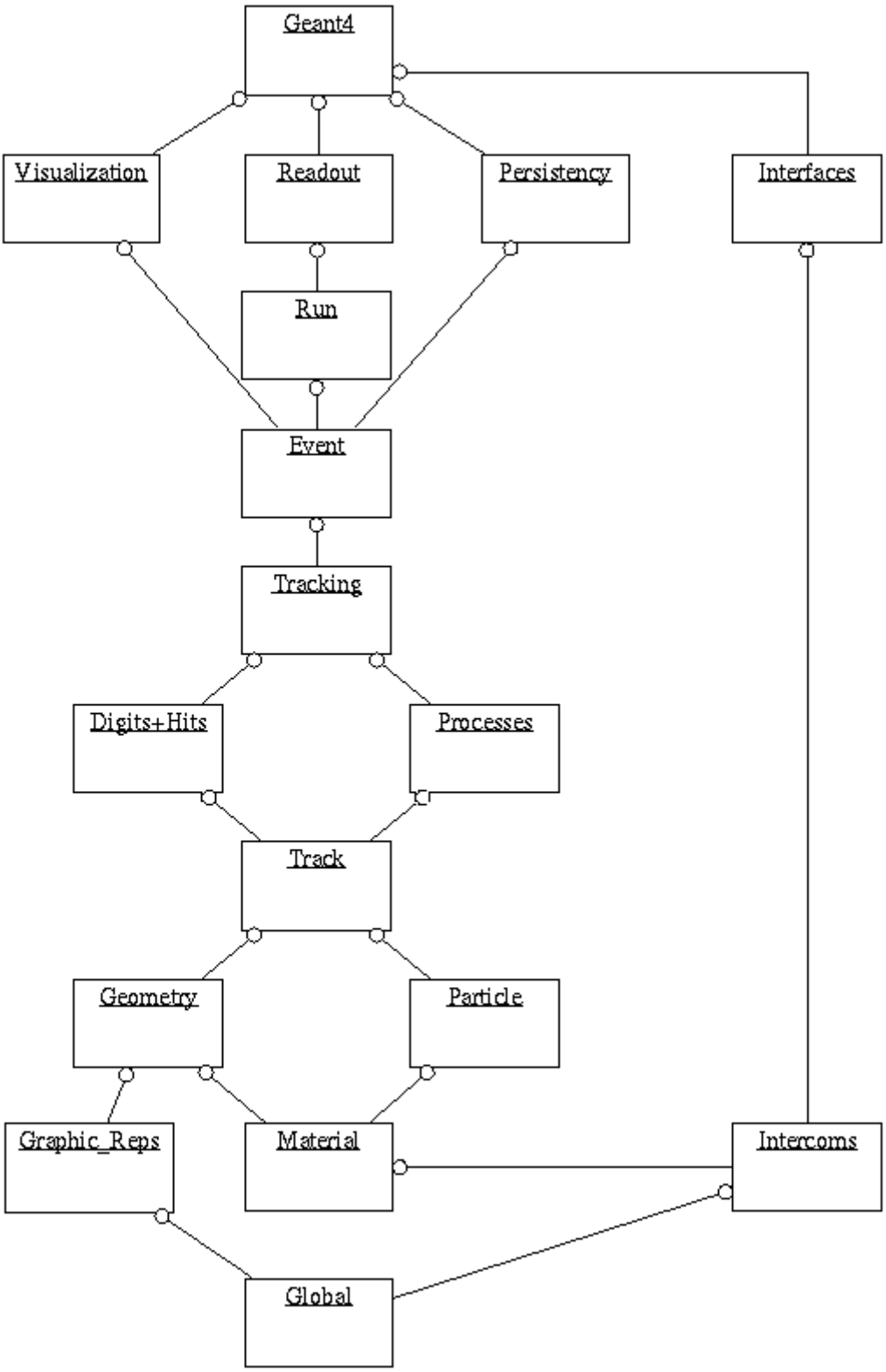

Figure 2.12. GEANT4 class categories.

GEANT4 requires three virtual classes to be overridden to create a concrete class for a simulation. These control the geometry of the detector, the definition of particles and physics processes and generation of primary particles.

2.5.1. User Action Classes

In order to use GEANT4 for a specific modelling application a number of user defined (or user action) class files need to be written which detail the specifics of the simulation. These files are detailed below.

G4UserDetectorConstruction

This class defines the detector and its geometry. The detector definition requires the representation of the geometry and associated materials, assigning visualisation and other user defined properties. The geometrical representation involves a hierarchical approach containing the world volume, the physical volume and its logical counterpart. Simple and complex shapes can be built and repeated or geometry can be interfaced with STEP compliant CAD systems. Materials used in GEANT4 are built from elements of the periodic table and in turn are built from isotopes. The user can create their materials, elements and isotopes or use predefined ones from the National Institute of Standards and Technology (NIST) inbuilt database. Hits and sensitive detector regions in the detector geometry can be assigned. A hit contains the track, energy deposition, particle characteristics, and location within the volume and spatial coordinates of the hit. An example showing the simplest application of the DetectorConstruction.cc file is included.

```
//
// $Id: ExN01DetectorConstruction.cc,v 1.9 2006-06-29 17:47:19 gunter Exp $
// GEANT4 tag $Name: geant4-09-04-patch-02 $
//

#include "ExN01DetectorConstruction.hh"

#include "G4Material.hh"
#include "G4Box.hh"
#include "G4Tubs.hh"
#include "G4LogicalVolume.hh"
#include "G4ThreeVector.hh"
#include "G4PVPlacement.hh"
#include "globals.hh"

ExN01DetectorConstruction::ExN01DetectorConstruction()
 :  experimentalHall_log(0), tracker_log(0),
    calorimeterBlock_log(0), calorimeterLayer_log(0),
    experimentalHall_phys(0), calorimeterLayer_phys(0),
    calorimeterBlock_phys(0), tracker_phys(0)
{;}
```

```
ExN01DetectorConstruction::~ExN01DetectorConstruction()
{
}

G4VPhysicalVolume* ExN01DetectorConstruction::Construct()
{

  //------------------------------------------------------ materials

  G4double a;  // atomic mass
  G4double z;  // atomic number
  G4double density;

  G4Material* Ar =
  new G4Material("ArgonGas", z= 18.,a= 39.95*g/mole, density=1.782*mg/cm3);

  G4Material* Al =
  new G4Material("Aluminum", z= 13., a= 26.98*g/mole, density= 2.7*g/cm3);

  G4Material* Pb =
  new G4Material("Lead", z= 82., a= 207.19*g/mole, density= 11.35*g/cm3);

  //------------------------------------------------------ volumes

  //------------------------------ experimental hall (world volume)
  //------------------------------ beam line along x axis

  G4double expHall_x = 3.0*m;
  G4double expHall_y = 1.0*m;
  G4double expHall_z = 1.0*m;
  G4Box* experimentalHall_box
    = new G4Box("expHall_box",expHall_x,expHall_y,expHall_z);
  experimentalHall_log = new G4LogicalVolume(experimentalHall_box,
                                             Ar,"expHall_log",0,0,0);
  experimentalHall_phys = new G4PVPlacement(0,G4ThreeVector(),
  experimentalHall_log,"expHall",0,false,0);

  //------------------------------ a tracker tube

  G4double innerRadiusOfTheTube = 0.*cm;
  G4double outerRadiusOfTheTube = 60.*cm;
  G4double hightOfTheTube = 50.*cm;
  G4double startAngleOfTheTube = 0.*deg;
  G4double spanningAngleOfTheTube = 360.*deg;
  G4Tubs* tracker_tube = new G4Tubs("tracker_tube",innerRadiusOfTheTube,
                                    outerRadiusOfTheTube,hightOfTheTube,

startAngleOfTheTube,spanningAngleOfTheTube);
  tracker_log = new G4LogicalVolume(tracker_tube,Al,"tracker_log",0,0,0);
  G4double trackerPos_x = -1.0*m;
  G4double trackerPos_y = 0.*m;
  G4double trackerPos_z = 0.*m;
  tracker_phys = new G4PVPlacement(0,
             G4ThreeVector(trackerPos_x,trackerPos_y,trackerPos_z),
             tracker_log,"tracker",experimentalHall_log,false,0);

  //------------------------------ a calorimeter block

  G4double block_x = 1.0*m;
  G4double block_y = 50.0*cm;
  G4double block_z = 50.0*cm;
  G4Box* calorimeterBlock_box = new G4Box("calBlock_box",block_x,
                                          block_y,block_z);
```

```
  calorimeterBlock_log = new G4LogicalVolume(calorimeterBlock_box,
                                             Pb,"caloBlock_log",0,0,0);
  G4double blockPos_x = 1.0*m;
  G4double blockPos_y = 0.0*m;
  G4double blockPos_z = 0.0*m;
  calorimeterBlock_phys = new G4PVPlacement(0,
            G4ThreeVector(blockPos_x,blockPos_y,blockPos_z),

calorimeterBlock_log,"caloBlock",experimentalHall_log,false,0);

return experimentalHall_phys;
}
```

Code 2.1. DetectorConstruction class file. GEANT4 example N01.

G4UserPhysicsList

There are no default physics lists inbuilt to a user's application, rather the user must choose from a range of processes. This allows for the fact that the scope for a default set of processes is too large. A *PhysicsList* is built containing all the particle definitions and processes including the transportation process. Conversely the user can select prebuilt physics lists that cover a wide range of application areas and energies. This has the benefit of ensuring validation for the list has previously been done by the GEANT4 body at large. For this project the following G4UserPhysicsList processes are used: QGSP_BIC_HP physics list and G4RadioactiveDecayPhysicsList physics list. This is discussed further in section 3.3 Physics List on page 46.

G4UserPrimaryGeneratorAction

The generation of particles is done via the G4ParticleGun class. This allows the definition of particles, momentum and direction, energy, particle time, position, polarisation and the number of particles to be considered for the event. In addition, the particle source can be either a beam or an emitting surface or volume (circle, annulus, ellipse, rectangle, sphere, ellipsoid, cylinder or parallelepiped).

G4UserEventAction

An event in GEANT4 starts with the initiation of tracking particles and finishes with the completion of tracking all generated secondaries. The G4UserEventAction class possesses two virtual methods which are invoked at the beginning and end of each event. The *beginOfEventAction* method is invoked before converting the primary particles to G4Track objects. The method *endOfEventAction* is invoked at the very end of event processing. A typical use of the *EventAction* class is to analyse the collection of hits to the sensitive region of the detector in order to extract information such as energy deposition.

G4UserRunAction

A run is the largest component in the simulation. It represents a sequence of events and controls the detector geometry, sensitive detectors and physics processes. The *G4UserRunAction* class has several methods. A run starts with the invocation of the *BeamOn* command. The number of simulation events required during the run is also entered.

G4UserSteppingAction

The tracking category manages the propagation of a particle through the detector taking into account its physics interaction with matter. A step in GEANT4 describes the transport of a particle between two points in space. At this level the user can access information such as energy, position, particle direction and energy deposition.

G4UserStackingAction

For customising access to the track stacks, GEANT4 uses three stacks, *urgent*, *waiting* and *postpone-to-next-event.* All tracked particles are stored in the *urgent* stack in a last in first out (LIFO) manner. The *G4UserStackingAction* class can be overridden to move tracked objects to the *waiting* or *postpone-to-next-event* stacks.

2.5.2. GEANT4 Interface commands

GEANT4 has various built-in user interface commands. These commands can be used interactively via a user interface, in batch mode or in a macro file. Examples of these commands include controlling the verbosity of output during a run, checking for any overlapping volumes when designing the detector and listing defined processes. A messenger class can also be used to alter variables such as detector geometry, primary beam, or physics parameters between simulation runs without recoding. Control of the simulation can be placed in a macro file allowing execution of several simulations using a macro file.

2.5.3. Visualisation

GEANT4 has the capability to visualise detector geometries, particle trajectories and tracking steps and particles hits. Functions include producing high quality graphics for publication, debugging complex geometries and detector geometry selection. There are a variety of visual drivers that can be used including DAWNFILE, RayTracer, VRML, QT, OpenInventor and OpenGL each with their specialities.

Many methods of visualisation are possible. The OpenGL, VRML and G4HepRepFile styles were used for this project to analyse geometry, particle hits and incident beam directions and location of detector within the world volume.

2.5.4. Physics of GEANT4

The design of physics processes in GEANT4 is done in a generic way to enable a user to design their own process.

The major physics process categories for GEANT4 are:

- Electromagnetic
- Hadronic
- Decay
- Photolepton-hadron
- Optical
- Parameterisation
- Transportation

For this project, the relevant processes are electromagnetic, hadronic and radioactive decay.

The energy range of electromagnetic processes is extensive, ranging from 250 eV to 1000 PeV. The electromagnetic model comes in two packages defined by the range of energy required. The "standard" electromagnetic processes range from 1 keV to 1000 PeV. The processes included for photons are: Compton scattering, γ-conversion, photo-electric effect and muon pair production. Electron/positrons: ionisation and δ-ray production, bremsstrahlung, multiple scattering and positron annihilation. Muons: pair production, multiple scattering, ionisation and δ-ray production and finally Hadron/ions: multiple ionisation processes. The standard process averages the effects of atomic shell structure and does not work below 1 keV [11].

The low energy electromagnetic processes can use external data libraries such as the Livermore data library, the ICRU73 data tables or Penelope Monte Carlo Code. The data

libraries are freely available with the GEANT4 release and are located via the G4LEDATA environment variable.

The hadronic category ranges from thermal energies through 15 orders of magnitude to cosmic ray energies. This project tracks thermal energy neutrons generated from muons ranging from a few MeV to a few GeV.

A simulation of the total cosmic-muon induced spectrum in the energy region below 1500 keV calculated using GEANT compared with a measured background spectrum is shown in figure 2.13.

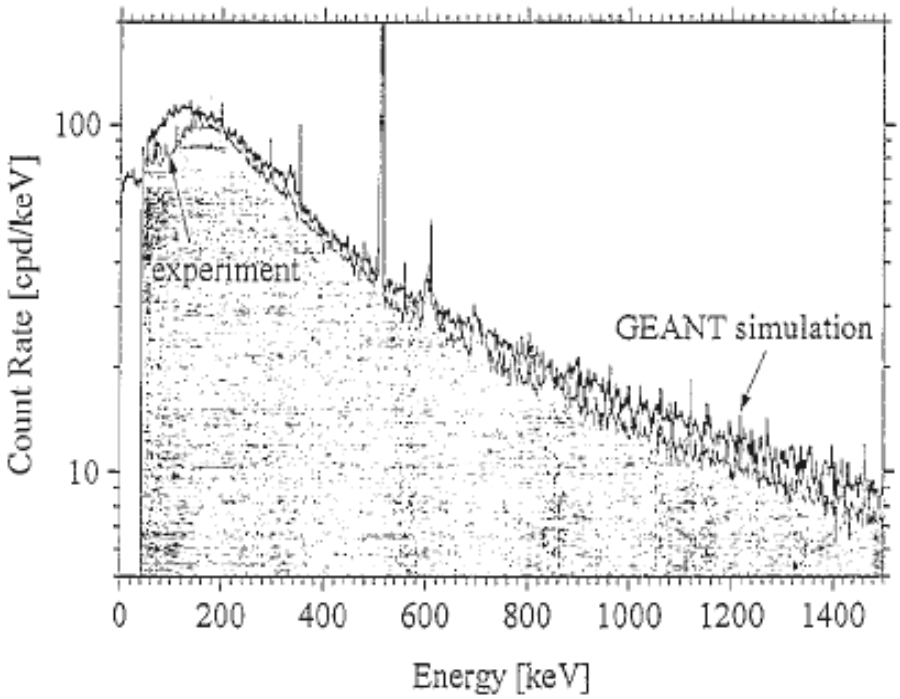

Figure 2.13. Comparison between measured background spectrum and calculated cosmic-muon induced spectrum. Figure from Vojtyla 1995 (Ref.[65]).

Referring to figure 2.13, the agreement between simulation and measured background is very good with some small differences in the low and high-energy range. The differences arise because the measured background contains many influences including the cosmic muon component, secondary and tertiary neutrons and ^{210}Bi.

Three basic errors can potentially manifest between simulation and experiment. The first is the input muon flux is an approximation with many simplifications. It does not take into account variables such as latitude and longitude of the detector. Second, some of the modelled physics processes are simplified. Lastly, some physical processes are not included at all.

Although these errors are important, very useful and important results still can be found using the GEANT simulation code.

The geometry, material definition and description of the physics list used for the simulation are described in the next chapter.

2.6. CRY Software

The Cosmic Ray Generator software generates correlated cosmic-ray particle showers from three different elevations, sea level, 2100 m and 11300 m. The showers can be used as input data for transport and detector simulation codes. A wide range of energies are modelled from 1 GeV to 100 TeV for primary and secondary particles using data tables. The tables are derived and tested against simulation packages MCNPX, Fluka2005 and GEANT4. Shower generation is done within an area defined up to 300 m by 300 m. Particle production includes muons, neutrons, protons, electrons, photons and pions [66].

Further options available are: (i) the types of secondary particles returned, all particles are simulated by default; (ii) the latitude in metres, used to simulate the effect of the Earth's magnetic field; (iii) the date, the eleven year sunspot cycle is modelled with the effects of solar minimum and solar maximum; (iv) the number of input particles, where a minimum and maximum can be set [66].

The atmosphere through which the shower is generated is a series of 42 constant-density flat layers, each composed of 78% N_2, 21% O_2, and 1% Ar by volume. The density change between adjacent layers was set to 10%, and the densities were derived from the 1976 US Atmosphere Model [66].

The primary particle used for the shower generation is the proton.

3. Geometry and Sources - Method

This chapter will outline the computational method used to measure the isotope production rate of ^{198}Au as a function of incident muon energy. As stated in Section 2.3, this is required because it will enable the activation rate as a function of muon energy to be calculated and provide a guide as to the contribution of γ-rays which result from muon interactions with Pb atoms in lead shielding.

The various sections in this chapter will discuss the design of the detector, both the geometry and materials used to simulate it, the physics processes required for the realistic simulation including particle generation, the tracking of produced isotopes and concluding with the use of the Cosmic Ray Generator (CRY) software used for generating a muon spectrum.

3.1. Geometry design

The design of the detector and its placement within space is detailed below using code from the simulation.

Detector design followed these steps.

I. Defining the detector geometry

II. Placing the detector within a volume.

III. Placing volume within the world volume.

IV. Designing the detector messenger

V. Visualising the components

Table 3.1 shows the dimensions of all components of the detector. As the gold disk is located centrally, the lead shield does not form a solid cylinder. It is similar to a torus with the internal diameter of 50 mm, matching the diameter of the gold disk. Both the Pb caps and Au disk are solid cylinders.

Table 3.1. GEANT4 shield detector dimensions.

(mm)	Pb shield	Pb caps	Au disk
Radius	600	50	50
Inner radius	50	-	-
Height	400	199.25	1.5

Figure 3.1 highlights the central column (coloured magenta) within which the gold disk resides and the two lead "caps" either side of the central gold disk. All the detector elements are described in section 3.1.1 below. The 3 dimensional axes can be seen. Blue, red and green are the Z, X and Y axes respectively.

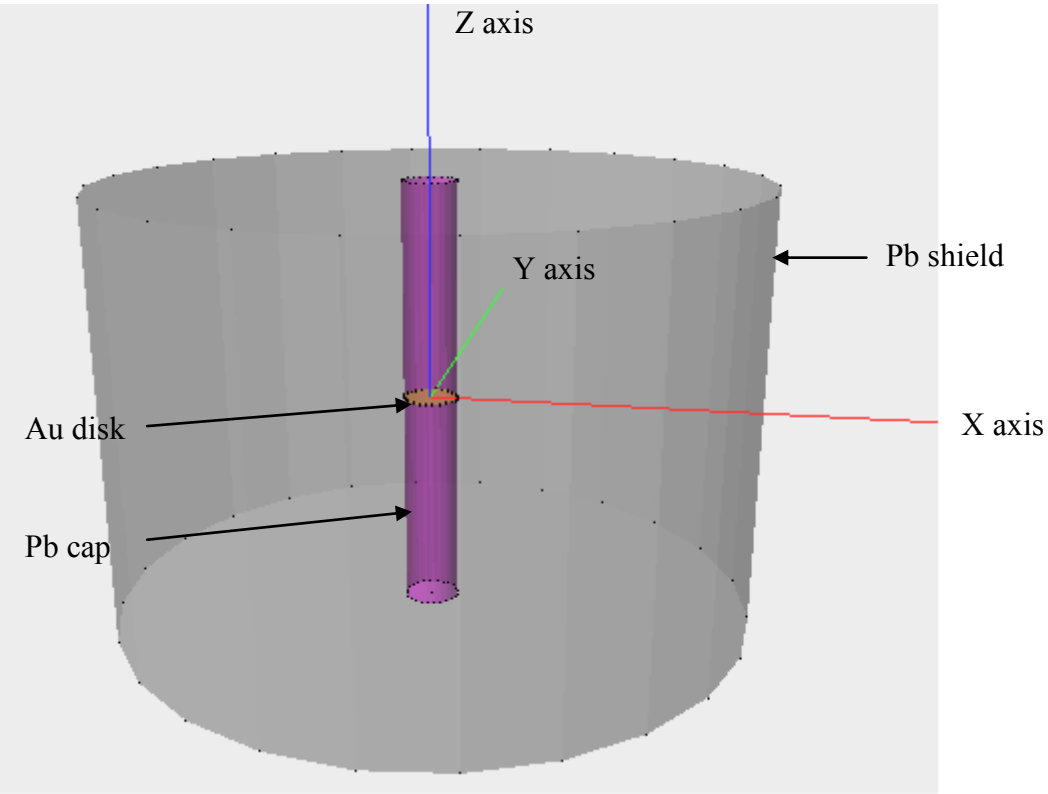

Figure 3.1. Detector showing Pb shield construction and axes.

3.1.1. Defining the detector

Defining the detector components requires the construction of physical volumes. This is described below.

The Pb shield is shown first. The G4Tubs class defines the cylinder here. The dimensions of the shield outer and inner widths and the location in space are shown below.

```
// Pb shield - grey
G4double outerRadiusDisk   = 600.*mm;
G4double innerRadiusDisk   = 50.*mm;
G4double heightDisk        = 400.*mm;

//placing cylinder in a logical volume
lead_disk_Vol = new G4Tubs("lead_disk",innerRadiusDisk,
      outerRadiusDisk,heightDisk,
      startAngle,spanningAngle);
      lead_log_Vol =new
      G4LogicalVolume(lead_disk_Vol,pbMaterial,"lead_log",0,0,0);

// logical volume
G4double Pos_x = 0.*mm;
G4double Pos_y = 0.*mm;
G4double Pos_z = 0.*mm;

lead_phys_Vol = new G4PVPlacement(0,      // no rotation
      G4ThreeVector(Pos_x,Pos_y,Pos_z),   // at coordinates
      lead_log_Vol,                       // its logical name
      "lead_phys",                        // its name
      expHall_log,                        // its mother name
      false,                              // no boolean operators
      0);
```

Code 3.1. Definition of Pb shield using the GEANT4 DetectorConstruction class.

The shield was constructed as a cylinder of lead. As table 3.1 shows, the cylinder has a radius of 600mm and a height of 400mm. GEANT4 defines all lengths from origin to desired length, therefore the full length is 800 mm.

Next are the lead caps that fill the 50mm gap made by the gold disk.

```
// ------------------------------------ Physical volumes next
G4double startAngle    = 0.*deg;
G4double spanningAngle = 360.*deg;
// ------------------------------------ some defaults

// Pb casing – Top - magenta
G4double innerRadiusOfLeadCylTop = 0.*mm;       // Solid cylinder
G4double outerRadiusOfLeadCylTop = 50.*mm;      //
G4double heightOfLeadCylTop = 199.25*mm;        // Cylinder height

leadcyl1_Vol = new G4Tubs("lead_cyl_top",innerRadiusOfLeadCylTop,
            outerRadiusOfLeadCylTop,heightOfLeadCylTop,
            startAngle,spanningAngle);
leadcyl1_log_Vol  = new
G4LogicalVolume(leadcyl1_Vol,pbMaterial,"leadcyl1_log",0,0,0);

Pos_x = 0*mm;
Pos_y = 0.*mm;
Pos_z = 200.75*mm; // doubled

leadcyl1_phys_Vol = new G4PVPlacement(0,        // no rotation
```

```
            G4ThreeVector(Pos_x,Pos_y,Pos_z),   // at coordinates
            leadcyl1_log_Vol,                   // its logical name
            "leadcyl1_phys",                    // its name
            expHall_log,                        // its mother name
            false,                              // no boolean operators
            0)                                // no field specific to volume
// ------------------------------------------------------------------------
// Pb casing –Bottom - magenta
leadcyl2_Vol = new G4Tubs("lead_cyl_bot",innerRadiusOfLeadCylTop,
            outerRadiusOfLeadCylTop,heightOfLeadCylTop,
            startAngle,spanningAngle);
leadcyl2_log_Vol = new
G4LogicalVolume(leadcyl2_Vol,pbMaterial,"leadcyl2_log",0,0,0);

Pos_x = 0*mm;
Pos_y = 0*mm;
Pos_z = -200.75*mm;

leadcyl2_phys_Vol = new G4PVPlacement(0,
            G4ThreeVector(Pos_x,Pos_y,Pos_z),
            leadcyl2_log_Vol,
            "leadcyl2_phys",
            expHall_log,
            false,
            0);
```

Code 3.2. Definition of top and bottom lead caps using GEANT4 G4Tubs cylinder class.

Code 3.2 shows the implementation of two Pb caps using the GEANT4 G4Tubs class.

```
// Gold disk - yellow
outerRadiusDisk   = 50.*mm;
innerRadiusDisk   = 0.*mm;
heightDisk        = 1.5*mm;

G4Tubs* gold_disk_Vol = new G4Tubs("gold_disk",innerRadiusDisk,
            outerRadiusDisk,heightDisk,
            startAngle,spanningAngle);
gold_log_Vol  = new
G4LogicalVolume(gold_disk_Vol,auMaterial,"gold_log",0,0,0);

Pos_x = 0.*mm;
Pos_y = 0.*mm;
Pos_z = 0.*mm;

gold_phys_Vol = new G4PVPlacement(0,            // no rotation
            G4ThreeVector(Pos_x,Pos_y,Pos_z),   // at coordinates
            gold_log_Vol,                       // its logical name
            "gold_phys",                        // its name
            expHall_log,                        // its mother name
            false,                              // no boolean operators
            0)                                // no field specific to volume
```

Code 3.3. Definition of gold detector disk.

Code 3.3 shows the implementation of a gold disk using the G4Tubs cylinder class.

3.1.2. Placement within a volume

GEANT4 uses the concept of a logical volume to contain the properties of the material components used. These properties include the geometrical properties of the solid and the physical characteristics: volume of material; any sensitive detector elements and the magnetic field.

Referring to code 3.4 (below), gold_log_Vol declares the logical volume containing the gold disk. The volume is filled with Au material, (to be discussed in section 3.2); the logical volume name is "gold_log" with the final three fields not used in this simulation. This process is replicated for all constructed physical volumes. Refer to code 3.2 and 3.3 given above.

```
gold_log_Vol  = new G4LogicalVolume(
            gold_disk_Vol,
            auMaterial,
            "gold_log",
            0,0,0);
```

Code 3.4. Definition of logical volume of Au disk.

3.1.3. Placement within world volume

Next the logical volume is placed within a world volume as shown in code 3.5. This is the largest volume containing all volumes in the detector geometry. For simplicity and efficiency the volume is defined as a box called expHall_box. This box is placed within a physical volume called expHall_phys. The dimensions of the physical volume are 5 m^3.

```
//------------------------------ experimental hall box (world volume)
// BoxWidth,BoxWidth,BoxHeight // defined in macro file au.g4mac
// world volume
G4Box* expHall_box
      = new G4Box("expHall_box",BoxWidth,BoxWidth,BoxHeight);
// logical volume
expHall_log = new G4LogicalVolume(expHall_box,
            Air,"expHall_log",0,0,0);

// physical volume and its placement
expHall_phys  = new G4PVPlacement(0,      //no rotation
            G4ThreeVector(),              //at (0,0,0)
            "physContainer",              //its name
            expHall_log,                  //its logical volume
            0,                            //its mother name
            false,                        //no boolean operators
            0)                            //no field specific to volume
```

Code 3.5. Definition of world volume of the detector using the GEANT4 DetectorConstruction class.

3.1.4. Designing the detector messenger

Allowing the detector and the world volume to extend in the z direction whilst the simulation is running allows the user to alter the width and height of the world volume easily. The simulation does not need to be stopped, the code altered for the new world volume value and then recompiled. Between a run, the user can run the commands shown in code 3.6 for "on the fly" changes.

Two variables defining the height of the detector and the width of the expHall_phys box were constructed, `setHeight` and `setWidth` respectively. After changing either of these commands, the `update` command is run to update the detector geometry to reflect the change.

```
Command directory path : /mydet/

Guidance :
World box height.

 Sub-directories :
 Commands :
   setHeight * Select height in (m) of box.
   setWidth * Select width in (m) of box.
   update * Update volume size.
```

Code 3.6. Menu option for updating geometry between runs.

Usage of the commands shown in code 3.6 enables variation in the height and width of the world volume. To simulate various heights of incident muons above the detector requires altering the detector geometry and the world height before the run.

When the model is initialised, code 3.7 shows the output of the current values in metres for the detector geometry.

```
G4cout << "-----------------------------------------" << G4endl;
G4cout << "Box Height " << BoxHeight/m << " m" << G4endl;
G4cout << "Box Width "  << BoxWidth/m << "  m" << G4endl;
G4cout << "-----------------------------------------" << G4endl;
```

Code 3.7. Printout during run for detector geometry.

3.1.5. Visualisation

Colours can be assigned to logical volumes similar to figure 3.1. This is useful as it allows detector components to be easily seen and magnified revealing any inconsistencies between components such as an air gap or volume overlaps.

This is shown in code 3.8.

```
//  visualisation attributes ------------------------------------------

// attributes for World
expHall_log->SetVisAttributes (G4VisAttributes::Invisible);
G4VisAttributes* expHall_log = new G4VisAttributes (G4Colour(1.0,1.0,1.0));
                  // white
// expHall_log->SetVisibility(true);
expHall_log->SetForceWireframe(true);

G4VisAttributes* worldVolVisAtt = new G4VisAttributes
            (G4Colour(1.0,1.0,1.0));                  // white
worldVolVisAtt->SetVisibility(true);
worldVolVisAtt->SetForceWireframe(true);

// attributes for lead
G4VisAttributes* leadlogVolVisAtt = new G4VisAttributes
            (G4Colour(0.5,0.5,0.5));                  // grey
leadlogVolVisAtt->SetForceWireframe(true);
lead_log_Vol->SetVisAttributes(leadlogVolVisAtt);

// attributes for lead caps
G4VisAttributes* leadlogTopBotVolVisAtt = new G4VisAttributes
            (G4Colour(1.0,0,1.0));                    // magenta

leadlogVolVisAtt->SetForceWireframe(true);
leadcyl1_log_Vol->SetVisAttributes(leadlogTopBotVolVisAtt);
leadcyl2_log_Vol->SetVisAttributes(leadlogTopBotVolVisAtt);

// attributes for gold
G4VisAttributes* aulogVolVisAtt = new G4VisAttributes(G4Colour(1.0,1.0,0));
                        // yellow
gold_log_Vol->SetVisAttributes(aulogVolVisAtt);
```

Code 3.8. Colour and transparency assignment for volumes.

The first line of code from code 3.8 shows the world volume expHall_log is set to invisible. When this situation is reversed the world volume box is shown, figure 3.2 is the result.

Colours shown in figure 3.2 are defined from RGB colours defined by GEANT4.

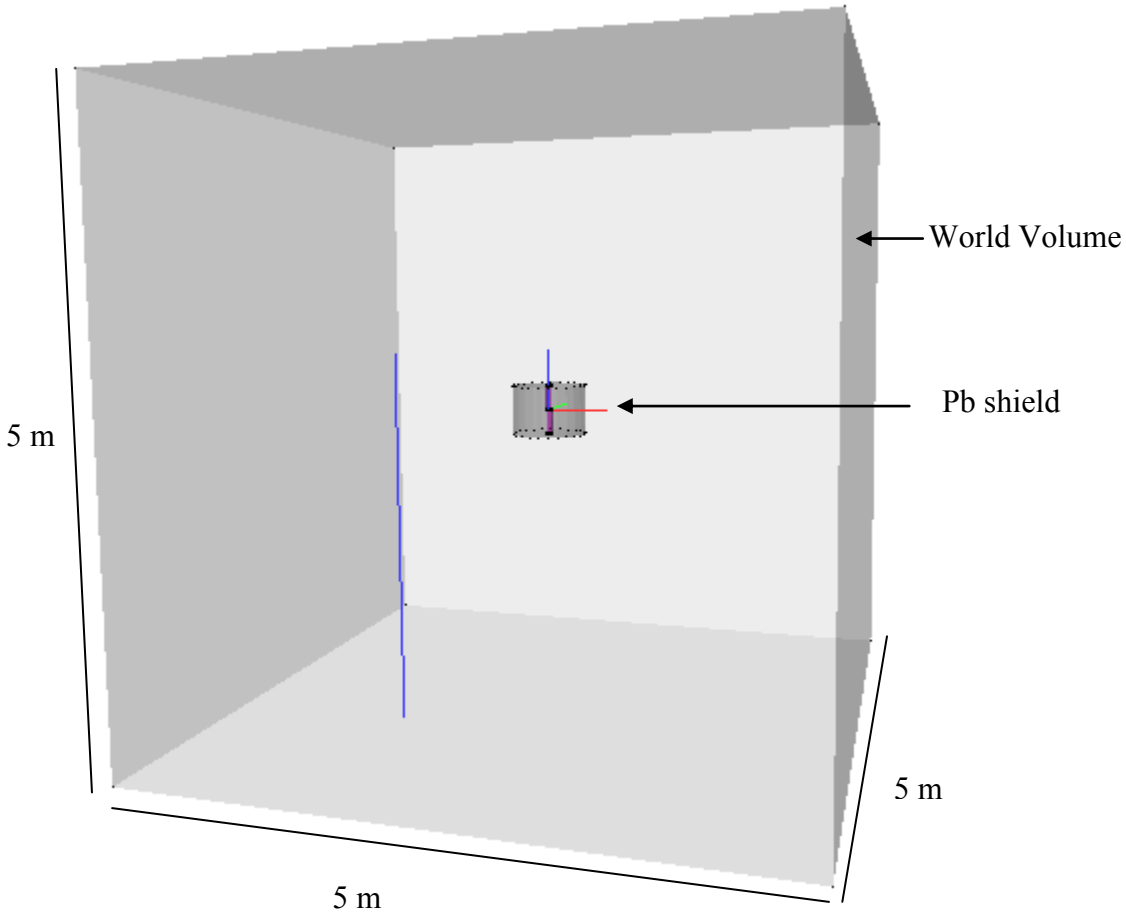

Figure 3.2. Detector with world box visibility enabled highlighting the size of the volume.

A single muon is shown in blue highlighting the world volume size is much larger than the detector. The design allows a much larger shower of muons to be tracked incident on the detector and world volume, thus increasing the statistical accuracy of results.

This process was used for testing geometry configuration and debugging. A program called VRMLView enabled visualisation of the incident muons in the form of a rotatable and free form model. The user could use this tool to rotate the model and zoom into various sections of the geometry to check correct geometry definitions, analyse where muons were being initialised and incident upon the detector.

Note that during data runs the visualisation was turned off to speed up computation time and reduce memory footprint.

3.2. Material selection

The materials used in the simulation are defined using inbuilt definitions provided by GEANT4. To define the materials, a call to the internal database is done and the materials assigned to a variable.

For this simulation, the only materials defined are lead, gold and air. These are then inserted into the logical volume definition to fill that detector component with the required material, as shown in code 3.9.

```
G4Material* pbMaterial;
G4Material* auMaterial;
G4Material* Air;

pbMaterial = G4NistManager::Instance()->FindOrBuildMaterial("G4_Pb");
auMaterial = G4NistManager::Instance()->FindOrBuildMaterial("G4_Au");
Air        = G4NistManager::Instance()->FindOrBuildMaterial("G4_AIR");
```

Code 3.9. Defining materials for detector using GEANT4 G4Material class.

A brief definition for G4_Pb material follows in code 3.10. A full listing of the material and elemental definitions for all materials is available in the Appendix 1

```
Material: G4_Pb   density: 11.350 g/cm3   RadL: 5.613 mm
      Nucl.Int.Length: 18.261 cm
Element: Pb (Pb)  Z = 82.0    N = 207.2   A = 207.22 g/mole

Isotope: Pb204    Z = 82      N = 204     A = 203.97 g/mole
      abundance: 1.40 %

Isotope: Pb206    Z = 82      N = 206     A = 205.97 g/mole
      abundance: 24.10 %

Isotope: Pb207    Z = 82      N = 207     A = 206.98 g/mole
      abundance: 22.10 %

Isotope: Pb208    Z = 82      N = 208     A = 207.98 g/mole
      abundance: 52.40 %      ElmMassFraction: 100.00 %     ElmAbundance
100.00 %
```

Code 3.10. Material definitions for Pb shielding in GEANT4 using DetectorConstruction class.

3.3. Physics list

Design of the various electromagnetic and hadronic physics processes in the simulation required careful consideration of the processes needed and their respective energy bounds.

After much testing, it was decided to use two predefined reference physics lists. The first is the QGSP_BIC_HP class, chosen for suitability in simulating protons and neutrons with energies below ~10 GeV. This physics list is a container that supports a range of physics processes within it as shown in code 3.11. It ensures accurate particle and process creation with almost no coding required to implement, compared to a hand built physics list source file containing hundreds of lines of code. Careful selection of the correct physics list for the simulation enables a great deal of complexity and potential bugs to be removed.

```
// EM Physics
  this->RegisterPhysics( new G4EmStandardPhysics(ver) );

  // Synchroton Radiation & GN Physics
  this->RegisterPhysics( new G4EmExtraPhysics(ver) );

  // Decays
  this->RegisterPhysics( new G4DecayPhysics(ver) );

   // Hadron Elastic scattering
  this->RegisterPhysics( new G4HadronElasticPhysicsHP(ver) );

   // Hadron Physics
  this->RegisterPhysics(  new HadronPhysicsQGSP_BIC_HP(ver));

  // Stopping Physics
  this->RegisterPhysics( new G4QStoppingPhysics(ver) );

  // Ion Physics
  this->RegisterPhysics( new G4IonBinaryCascadePhysics(ver));
```

Code 3.11. Physics lists contained within QGSP_BIC_HP list.

The binary cascade (BIC) model within this module better describes production of secondary particles produced in interactions of protons and neutrons with nuclei. In addition the High Precision neutron package version of QGSP_BIC_HP allows transport of neutrons below 20 MeV down to thermal energies using external data libraries read during simulation run. The G4RadioactiveDecayPhysics builder class enables the simulation of the decay of radioactive nuclei by α, β^+ and β^- emission and electron capture. A physics process builder is different to a physics list described in the previous paragraph. It is not a complete list containing a range of processes such as QGSP_BIC_HP, but rather an additional process that can be added to a GEANT4 simulation for the required functionality. This simulation involves the creation and decay of the ^{198}Au isotope and thus the G4RadioactiveDecayPhysics class was added. Data describing intensities, decay mode and energies is collated from external radioactive decay tables provided by GEANT4.

After choosing the lists, implementation of the reference list is straightforward. Code 3.12 below shows how this is done. This code is entered in the au-muon.cc main file. All the necessary processes and models are thus taken care of.

```
G4VUserPhysicsList* physics = new QGSP_BIC_HP;
G4RadioactiveDecayPhysics* radPhysics = new G4RadioactiveDecayPhysics();
physics->RegisterPhysics(radPhysics);
runManager->SetUserInitialization(physics);
```

Code 3.12. Implementation of reference list.

The electromagnetic and hadronic models and processes can be found in tables 3.2 and 3.3 respectively. For the *nCapture* process, the energy range difference is evident between G4LCapture ranging from 19.9 MeV to 20 TeV and *NeutronHPCapture* ranging from 0 eV to 20 MeV. High precision allows tracking of thermal neutrons.

Table 3.2. Electromagnetic models and processes with energy ranges in GEANT4 QGSP_BIC_HP class module.

Particle	**Process name**	**Process**	**Model**	**Energy Min**	**Energy max**
Muon mu^-	muIoni	Muon ionisation	ICRU73QO	0 eV	200 keV
			BetheBloch	200 keV	1 GeV
			MuBetheBloch	1 GeV	10 TeV
	muBrems	Bremsstrahlung		0	10 TeV
	muPairProd	Pair production		0	10 TeV
	CoulombScat	Coulomb scattering		0	10 TeV

Table 3.3. Hadronic models and processes with energy ranges in GEANT4 QGSP_BIC_HP class module.

Particle	Process name	Process	Model	Energy min (GeV)	Energy max (GeV)
Muon	muMinusCaptureAtRest	Muon capture			
Neutron	hadElastic	Elastic scattering	hElasticCHIPS	0.0195	100000
			NeutronHPElastic	0	0.02
	NeutronInelastic	Inelastic scattering	QGSP	12	100000
			G4LENeutronInelastic	9.5	25
			Binary Cascade	0.0199	9.9
			NeutronHPInelastic	0	0.02
	nCapture	Neutron capture	G4LCapture	0.0199	20000
			NeutronHPCapture	0	0.02
	nFission	Neutron fission	G4LFission	0.0199	20000
			NeutronHPFission	0	0.02

The G4RadioactiveDecayPhysicsList list is also used to model the decay of ^{198}Au isotopes, created from neutron capture during activation. A listing of the isotope created is shown in code 3.13.

The particle definition for ^{198}Au:

```
--- G4ParticleDefinition ---
 Particle Name : Au198[0.0]
 PDG particle code : 1000791980 [PDG anti-particle code: 0]
 Mass [GeV/c2] : 184.366     Width : 0
 Lifetime [nsec] : 3.36004e+14
 Charge [22]: 79
 Spin : 0/2
 Parity : 1
 Isospin : (I,Iz): (0/2 , 0/2 )
 Quark contents     (d,u,s,c,b,t) : 277, 317, 0, 0, 0, 0
 AntiQuark contents               : 0, 0, 0, 0, 0, 0
 Lepton number : 0 Baryon number : 198
 Particle type : nucleus [generic]
```

```
 Atomic Number : 79  Atomic Mass : 198
```

Code 3.13. Listing of Au198 definition in GEANT4.

Code 3.13 shows the definition of the Au198[0.0] radioactive nucleus. The Particle Data Group (PDG) particle code of 1000791980 is calculated from the *G4IonTable* class using the following key:

```
// PDG code for Ions
// Nuclear codes are given as 10-digit numbers +-100ZZZAAAI.
// For a nucleus consisting of np protons and nn neutrons
// A = np + nn and Z = np.
// I gives the isomer level, with I = 0 corresponding.
// to the ground state and I >0 to excitations
```

The number written in brackets [] is the energy of the generated ion.

3.4. Isotope Tracking

With the two lists, QGSP_BIC_HP and G4RadioactiveDecayPhysics working to create ^{198}Au isotopes and associated processes, isotope tracking and counting is required. During the initial phase of the project, the *G4UserSteppingAction* class was used for isotope counting. The *G4UserSteppingAction* class manages the propagation of particles through the detector. The physics interactions with matter, energy, energy deposition, position, particle direction can all be accessed through this class. After discussion with the online GEANT4 forum and the realisation that G4UserSteppingAction is called at every step for every particle, the isotope counting algorithm was altered to utilise the *G4USerStackingAction* class. The *G4USerStackingAction* class is useful for easily counting particles that are created during a run. The ClassifyNewTrack method, part of the *G4UserStackingAction* class is called during the tracking process when new particles need to be added to the stack for tracking. It ensures highly efficient accumulation of the data needed and only once for each particle when it is newly created.

In addition to making the code more efficient, two energy checks were made for electrons and gammas created over 1.0 MeV and 1.5 MeV respectively. This ensured no unnecessary computation time was used for the tracking of these particles. If either particle is above the threshold, it is killed, as shown in code 3.14. A significant increase in efficiency was gained as there was no need to track these particles at these energies.

```
G4ClassificationOfNewTrack StackingAction::ClassifyNewTrack(const G4Track*
aTrack)
{
    //keep primary particle
    if (aTrack->GetParentID() == 0) return fUrgent;
      G4double particleValue = G4double(aTrack->GetDefinition()-
      >GetPDGEncoding())

    acount = 0;
    // Au198 isotope count check
    if ( particleValue == 1000791980 )
    {
        acount++;
        runAction->aCount(acount); // add to activation count
    }

    G4ClassificationOfNewTrack classification = fUrgent;

    // kill secondary electron production to save time
    if  (aTrack->GetDefinition() == G4Electron::ElectronDefinition())
    {
        if (aTrack->GetKineticEnergy() > 1.0*MeV)
            {
                classification = fKill;
//              return classification;
            }
    }
    // kill secondary gamma production to save time
    if  (aTrack->GetDefinition() == G4Gamma::GammaDefinition())
    {
        if (aTrack->GetKineticEnergy() > 1.5*MeV)
            {
                classification = fKill;
            }
    }
    return classification;
}
```

Code 3.14. Listing for StackingAction and isotope tracking in GEANT4 StackingAction class.

Tracking isotopes is performed by checking the Particle Data Code (PDG) encoding for ^{198}Au isotopes. The PDG is an international collaboration whose goal is summarising Particle Physics and assigning various particles a unique number or code. To count isotopes: If an isotope is found, add one to the count for that isotope and pass the value to runAction to display at the end of a run.

3.5. Simulation Code Files

The design of the code follows the GEANT4 layout: The main file - au-muon.cc, GNUMakefile to build the system and multiple header and class definition files. These are listed in table 3.4. Much time in this project was devoted to understanding how to develop and

modify the GEANT4 code (using C++) to design the detector and physical processes relevant to the detection of ^{198}Au isotopes and associated decay products thus validating the decay process and then testing these modifications for validation of the model.

Table 3.4. File listing of code developed for simulation.

Class file	**Header File**
DetectorConstruction.cc	DetectorConstruction.hh
DetectorMessenger.cc	DetectorMessenger.hh
EventAction.cc	EventAction.hh
PrimaryGeneratorAction.cc	PrimaryGeneratorAction.hh
RunAction.cc	RunAction.hh
StackingAction.cc	StackingAction.hh
SteppingAction.cc	SteppingAction.hh

Files of interest include DetectorConstruction, describing the construction of the detector components.

GEANT4 has three stacks, *urgent*, *waiting* and *postpone-to-next-event*. By default, all tracked objects are stored in the urgent stack and handled in a "last in first out" manner. In this case, the other two stacks are not used. However, tracks may be routed to the other two stacks by the user-defined *StackingAction* class. Another use for StackingAction is to check the 411.8 keV gamma ray ejected during neutron capture inside the ^{198}Au nucleus.

SteppingAction tracks each particle step for position, energy and process change. This class was originally used to check for isotope production but this code was moved to StackingAction.cc.

3.6. Muon production

In the simulations negative muons were directed towards the detector. A range of muon energies from 100 MeV to 1.5 GeV in steps of 50 MeV were used in the simulation. An initial run with muon energies ranging from 100 MeV to 10 GeV was done but no gold activation isotopes were found above 1.5 GeV therefore this value was used as the maximum muon energy in the GEANT4 simulations.

The class General Particle Source (GPS) allows non hard coded manipulation of the incident muons from a text file. Specifically, it allows the specifications of the spectral, spatial and angular distribution of the primary source particles.

Before and during the run, these commands can be altered to test and execute data runs. See code 3.15 and descriptions of au-rec.g4mac

```
# creates a rectangular plane source, isotropic radiation
# 1 m from start of Au.

/gps/particle mu-       // incident particle
#rectangle plane source // create a plane source over the detector
/gps/pos/type Plane
/gps/pos/shape Rectangle
/gps/pos/centre 0. 0. 1.0 m         // muon start position
/gps/pos/halfx 5 m                  // 5 m by 5 m plane
/gps/pos/halfy 5 m
# isotropic angular distribution.
#
/gps/energy 500 MeV                 // example incident energy

# commands below are independent of gps
#/mydet/setHeight 5 m
#/mydet/setWidth 5 m
#/mydet/update
#/run/beamOn 1000000                number of events to create.
```

Code 3.15. au.g4mac listing showing GPS commands.

Code 3.15 describes an incident particle type (mu-) and a 5 m x 5 m virtual rectangular plane located 1.0 m above the detector from which the muons are sent. The example energy of the incident muons is 500 MeV. When the simulation starts, these commands are sent to the GEANT4 kernel. All of the commands in code 3.15 can be hard coded into the

G4PrimaryGeneratorAction class but this removes the flexibility of changing the parameters without recoding and recompiling.

Figure 3.3 shows a shower of muons (blue) incident 1 m above the detector. Neutrons are shown in red.

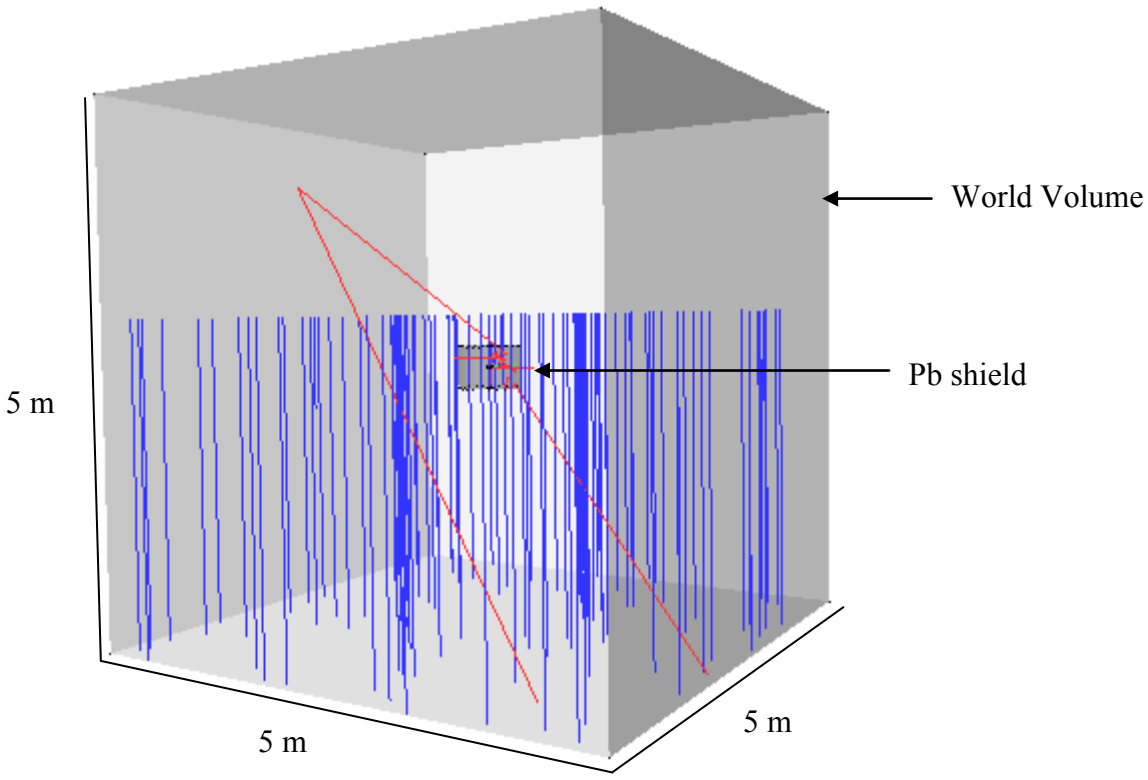

Figure 3.3. Simulation of muon shower using GPS commands in GEANT4.

The processes used by GEANT4 for muon energy loss include *muMsc* (multiple scattering), *muIoni* (muon ionisation), *muBrems* (muon bremsstrahlung) and *muPairProd* (muon pair production).

The CRY software generated a muon spectrum as a function of altitude, latitude and energy. To find the expected ^{198}Au production rate, the ^{198}Au count and the muon flux spectrum were convolved. A test program provided with the CRY software was modified to discard all particles from analysis excluding the muon, (testRoot.cc).

The data analysis software ROOT was used to display the generated data from CRY. Two hundred bins with the X-axis range between 0.001 MeV to 1500 MeV were used. After the secondary particles were added to the histogram, the flux was calculated and the histogram y axis recalibrated to units of flux, $m^{-2}s^{-1}MeV^{-1}$.

With the detector geometry defined, physics processes implemented and tracking of ^{198}Au isotopes enabled, data generation and acquisition can begin. Chapter 4 shows the results of the GEANT4 simulations.

4. Results and Discussion

4.1. Introduction

As stated earlier in this thesis, this project aims to investigate the muon interaction with lead shielding producing γ-rays through Au activation and its associated implications for Gamma Ray Spectrometry.

To do this, the simulation toolkit GEANT4 was used to do a series of Monte Carlo modelling simulations of the detector, physical processes and particle transport interactions. All simulations were performed using the Victorian Partnership for Advanced Computing (VPAC) supercomputer cluster.

As discussed in the last chapter, a detector was constructed using lead as the shielding material. The activation target material was stable gold ^{197}Au which was placed in the centre of the shield. To simulate a cosmic particle shower, muons were directed onto the detector in a 5 m x 5 m planar beam. As the muons penetrated the lead shield, energy loss mechanisms caused muon capture and decay, producing secondary and tertiary neutrons. These neutrons then caused the activation of the gold disk producing ^{198}Au isotopes.

The design of the simulation system was set to model those in place at the Institute of Reference Materials and Measurements (IRMM), Geel Belgium. The dimensions of the detector and target were set to model as closely as possible the preconfigured model. To generate a similar result set, much work in this thesis was directed towards the correct design of the detector geometry, the generation of events as well as the selection of relevant physics processes and data analysis. Care was taken to ensure that all the required physical processes were included thus enabling correct particle generation whilst ensuring simulation efficiency was not compromised.

The computational efficiency of the GEANT4 simulations was improved by moving the activation counting mechanism from the *SteppingAction* to *StackingAction* class. In addition the counting algorithm for ^{198}Au in GEANT4

```
if ( (particleName=="Au198[0.0]")
```

used a very slow string comparison check. Using a string comparison requires all characters to be checked sequentially whilst an integer comparison can be done in one CPU cycle. All

particles created during the run are tracked so computational speed and efficiency is essential. Therefore this part of the code was replaced with

```
if ( particleValue == 1000791980 )
```

using the PDG code for an ^{198}Au nucleus, which improved the counting algorithm considerably.

Another improvement in computational performance was found by checking the energy of γ-rays and electrons produced during a simulation run. If their respective energies were over 1.5 MeV and 1.0 MeV, tracking of these γ-rays and electrons was terminated. These computational improvements were adopted as it was found, after testing, that they did not lead to inaccuracies in the neutron activation rate of the atoms in the gold disk.

4.1.1. Simulation times and muon energies

Two types of GEANT4 simulations were initially conducted in this project. The first type involved directing muons one metre above the z axis surface of the detector, as this simulated muons at ground level. The second type involved directing muons 2100 metres above the z axis of the detector. Typical simulation times were in the range of eight to ten hours for the first type and a few hundred hours for the second type. In both cases the muon beam geometry was set to a five by five metre square planar source as shown in chapter 3, figure 3.3.

The simulations set at 2100 m were found to take one to two orders of magnitude longer to run, hence GEANT4 simulations involving incident muons placed one metre above the detector were used. This did not invalidate conclusions drawn as the effect of placing the muons at an increased altitude would only reveal the muons lost energy via a range of processes leading to the muon energy spectrum at one metre.

For the z =1 m simulations, the spectrum of muon energies used ranged from 50 MeV to 1500 MeV in steps of 50 MeV. Initially the range 50 MeV to 10 GeV was chosen however it was noticed that for muon energies greater than 1500 MeV, no activation of gold atoms resulted. Further testing at higher muon energies ranging from greater than 1500 MeV to 10 GeV confirmed that interactions of these muons with lead shielding did not lead to gold activation, presumably because the energy of the created neutrons was too high for the activation process to occur therefore the muon energy range was set from 50 MeV to 1.5 GeV.

4.2. Data validation

4.2.1. GEANT4 Validation

In order to have confidence in the predictions of the GEANT4 simulations, as many of the simulation predictions as possible were tested. In this project GEANT4 was used to model:

(i) production and transport of secondary/tertiary neutrons from interaction of incident muons (originating from cosmic rays) with protons in the Pb atoms of the lead shielding via the reaction given by (equation 2.8),

$$\mu^- + p \rightarrow n + \nu_\mu, \qquad 2.8$$

(ii) The interaction and neutron capture of these neutrons with ^{197}Au atoms in the gold disk leading to the activation of the Au atoms and the production of γ-rays via the reaction given by (equation 2.13),

$$^{197}_{97}Au + \, ^{1}_{0}n \rightarrow \, ^{198}_{97}Au + \, \gamma. \qquad 2.13$$

After searching the literature, referenced data showing neutron production rate from a cosmic muon flux could not be found. However data on the activation of ^{197}Au atoms for specific neutron fluxes and irradiation times was available from the World Information Service on Energy [67] and this information was used to validate this aspect of the GEANT4 simulations. In order to do this (4.1) was used which represents the activity or decay rate, or the number of ^{198}Au isotopes decaying per second,

$$A_t = \sigma\varphi N(1 - e^{-\lambda t}), \qquad 4.1$$

where A_t = the activity in units of Becquerels, σ = the activation cross-section, φ = the neutron flux (neutrons cm^{-2} s^{-1}), N = the number of parent atoms, λ = the decay constant (number of decays per unit time), and t = the irradiation time.

If the irradiation time t is much less than one half life $t_{½}$, the exponential term in (4.1) can be expanded to keep the linear term as given in (4.2),

$$A_t = \sigma\varphi N\lambda t. \qquad 4.2$$

A GEANT4 simulation was designed where the detector geometry consisted of a gold disk with identical dimensions to those used in the main simulations discussed in later sections of this chapter. The dimensions are shown in table 4.1 and the detector is shown in figure 4.1. The mass of the gold disk was given as 455 g.

Table 4.1. GEANT4 gold disk geometry dimensions for validation.

(mm)	**Au disk**
Outer Radius	50
Inner radius	-
Height	1.5

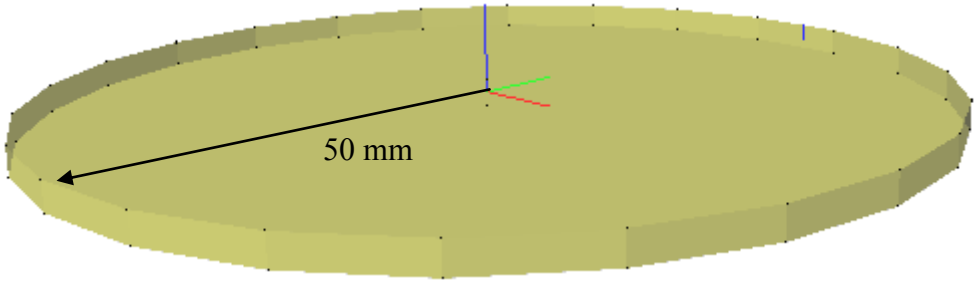

Figure 4.1. Au detector used for validation of the activation process

The simulations used $1x10^6$ incident neutrons on the gold disk, with energy of 0.025 eV corresponding to thermal neutron energy. The simulation ran for 757 seconds. The neutron beam area was 78.53 cm^2 giving a flux of $1.27x10^4$ $cm^{-2}s^{-1}$. The neutron beam area matched the gold disk surface area for maximum capture probability. Using the determined values: t = 757 s and $\varphi = 1.27x10^4$ $cm^{-2}s^{-1}$ enabled substitution into (4.1).

In order to calculate the activity of Au from (4.1), the following values were used.

σ = thermal neutron cross section: 98.8 (barns) (9.88×10^{-23} cm^{-2}) [67]

φ = neutron flux: 1.27×10^4 (cm^{-2} s^{-1}) [determined from GEANT4 simulation, see above]

N = number of Au parent particles: 1.390×10^{24} ((mass/Molar mass)N_A)

λ = decay constant: 2.98×10^{-6} (s^{-1}) [67]

t = irradiation time: 757 (s) [determined from GEANT4 simulation, see above]

Substitution of these values into (4.1) yielded a value for the activity of 3.93 kBq. Data from [67] for the same input values gave a result of 3.92 kBq. The excellent agreement between these results verified that our methodology in our GEANT4 simulations was sound.

4.2.2. External GEANT4 library validation

The libraries described below were used in GEANT4 simulations. They were included via the use of an environmental variable pointing to their location. During a simulation run the libraries were called and the appropriate data contained within was used for the simulations.

The Radioactive Decay library version 3.3 used with the *G4RadioactiveDecayPhysics* class originates from the *Evaluated Nuclear Structure Data File (ENSDF)* maintained by National Nuclear Data Centre, Brookhaven USA. The G4NDL library used to model thermal neutrons originates from the *ENDF/B-VI* library maintained by the Cross Section Evaluation Working Group (CSEWG), also from the National Nuclear Data Centre, Brookhaven USA. The version used - ENDF/B-VII.0 released December 15, 2006 can be found at [68].

The QGSP_BIC_HP physics list header file *QGSP_BIC_HP.hh* incorporates seven physics processes within it. They are EM Physics, Synchrotron Radiation & GN Physics, Decays, Hadron Elastic Scattering, Hadron Physics, Stopping Physics and Ion Physics.

Neutron production from the capture of muons by a nucleus is done by the *G4MuMinusCaptureAtRest* process. This involves the Fermi model of muon capture in compounds [11], the simplified EM cascade model and muon decay from K-shell and muon nucleus capture reaction. These libraries have been sufficiently tested by the physics community to be considered valid for use.

4.2.3. Cosmic Ray Generator Software Validation

As stated in section 3.6, the software program Cosmic Ray Generator (CRY) was used to create a muon spectrum used in the GEANT simulations. A self-modified program *testRoot* was used to test and validate the CRY software. The package was compiled and optimised until test inputs yielded the same results as CRY reference programs.

4.3. GEANT4 simulation results

Data collected during simulation runs is presented and discussed below.

4.3.1. GEANT4 Simulation Run Output

Referring to the GEANT4 data output, the particles formed during the radioactive decay of the excited ^{198}Au nucleus are shown with tracking set to verbose. GEANT4 verbose output is shown below highlighting the process of radioactive nuclei creation and decay. The results emphasise the accuracy of the radioactive model chosen. A summary of the results show Au198[0.0] decays to an unstable Hg198[411.8] excited state nucleus. The nucleus then de-excites by emitting a 411.8 keV γ-ray to stable Hg198[0.0]. A description of the various aspects of the output is shown below.

```
*************************************************************************
* G4Track Information: Particle = neutron,   Track ID = 29,   Parent ID = 1
*************************************************************************
```

A neutron is tracked for 265 steps until neutron capture (nCapture) occurs in the gold disk:

```
Step# X(mm) Y(mm) Z(mm) KinE(MeV) dE(MeV) StepLeng TrackLeng NextVolume
ProcName

265    -10.4    -26.6   -0.118 0  0  3.21  7.23e+03   gold_phys nCapture
```

A ^{198}Au radioactive nucleus is formed,

```
*************************************************************************
* G4Track Information:   Particle = Au198[0.0],   Track ID = 344,   Parent
ID = 29
*************************************************************************
```

decaying via *RadioactiveDecay* in the gold disk.

```
Step# X(mm) Y(mm) Z(mm) KinE(MeV) dE(MeV) StepLeng TrackLeng NextVolume
ProcName
2    -10.4  -26.6 -0.118  0     0  0  2.25e-06  gold_phys RadioactiveDecay
```

An electron and an anti electron neutrino are ejected during β^- decay

```
*************************************************************************
* G4Track Information:   Particle = e-,   Track ID = 347,   Parent ID = 344
*************************************************************************
*************************************************************************
* G4Track Information: Particle = anti_nu_e,Track ID = 346, Parent ID = 344
*************************************************************************
```

to create an unstable Mercury isotope Hg198[411.8] of energy 411.8 keV.

```
*************************************************************************
* G4Track Information: Particle = Hg198[411.8], Track ID = 345,Parent ID =
344
*************************************************************************
```

During branch decay, (figure 2.11, pg 25), a 411.8 keV gamma is ejected from the nucleus.

```
*************************************************************************
* G4Track Information: Particle = gamma, Track ID = 349, Parent ID = 345
*************************************************************************

Step# X(mm) Y(mm) Z(mm) KinE(MeV) dE(MeV) StepLeng TrackLeng NextVolume
ProcName
0    -10.4 -26.6  -0.118 0.412        0        0        0     gold_phys
```

to create after decay a stable nucleus of mercury.

```
*************************************************************************
* G4Track Information: Particle = Hg198[0.0],Track ID = 348,Parent ID = 345
*************************************************************************
```

Below is a complete printout of GEANT4 output during a run. Note that the printout below is the result of executing the *au-muon* executable which was compiled by the author of this thesis. Appendix II contains the full run after executing /run/beamOn to initialise a run.

The au.g4mac file is shown first containing initial parameters

```
# creates a rectangular plane source, isotropic radiation
# 10 cm from start of Au.

/gps/particle mu-
#rectangle plane source
/gps/pos/type Plane
/gps/pos/shape Rectangle
/gps/pos/centre 0. 0. 1. m
/gps/pos/halfx 5 m
/gps/pos/halfy 5 m
# isotropic angular distribution.
#/gps/ang/type cos

/gps/energy 1 MeV

# commands below are independent of gps
#
#/mydet/setHeight 5 m
#/mydet/setWidth 5 m
#/mydet/update
#/tracking/verbose 1
#/run/beamOn 100000000
```

```
[sturnbull@tango Au-muon]$ au-muon

*************************************************************
 Geant4 version Name: geant4-09-04-patch-02    (24-June-2011)
                      Copyright : Geant4 Collaboration
                      Reference : NIM A 506 (2003), 250-303
                            WWW : http://cern.ch/geant4
*************************************************************

The materials defined are :

***** Table : Nb of materials = 3 *****

 Material:    G4_Pb     density: 11.350 g/cm3   RadL:   5.613 mm   Nucl.Int.Length:  18.261 cm   Imean: 823.000 eV
   --->  Element: Pb (Pb)    Z = 82.0   N = 207.2   A = 207.22 g/mole
   --->  Isotope: Pb204   Z = 82   N = 204   A = 203.97 g/mole   abundance:   1.40 %
```

```
   --->  Isotope: Pb206   Z = 82   N = 206   A = 205.97 g/mole   abundance:  24.10 %
   --->  Isotope: Pb207   Z = 82   N = 207   A = 206.98 g/mole   abundance:  22.10 %
   --->  Isotope: Pb208   Z = 82   N = 208   A = 207.98 g/mole   abundance:  52.40 %  ElmMassFraction: 100.00 %
ElmAbundance 100.00 %

 Material:    G4_Au     density: 19.320 g/cm3   RadL:   3.344 mm   Nucl.Int.Length:  10.539 cm   Imean: 790.000 eV
   --->  Element: Au (Au)   Z = 79.0   N = 197.0   A = 196.97 g/mole
   --->  Isotope: Au197   Z = 79   N = 197   A = 196.97 g/mole   abundance: 100.00 %  ElmMassFraction: 100.00 %
ElmAbundance 100.00 %

 Material:   G4_AIR     density:  1.205 mg/cm3  RadL: 303.921 m    Nucl.Int.Length: 710.261 m    Imean:  85.700 eV
temperature: 273.15 K  pressure:   1.00 atm
   --->  Element: C (C)   Z =  6.0   N =  12.0   A =  12.01 g/mole
   --->  Isotope:   C12   Z =  6   N =  12   A =  12.00 g/mole   abundance:  98.93 %
   --->  Isotope:   C13   Z =  6   N =  13   A =  13.00 g/mole   abundance:   1.07 %  ElmMassFraction:   0.01 %
ElmAbundance   0.02 %
   --->  Element: N (N)   Z =  7.0   N =  14.0   A =  14.01 g/mole
   --->  Isotope:   N14   Z =  7   N =  14   A =  14.00 g/mole   abundance:  99.63 %
   --->  Isotope:   N15   Z =  7   N =  15   A =  15.00 g/mole   abundance:   0.37 %  ElmMassFraction:  75.53 %
ElmAbundance  78.44 %
   --->  Element: O (O)   Z =  8.0   N =  16.0   A =  16.00 g/mole
   --->  Isotope:   O16   Z =  8   N =  16   A =  15.99 g/mole   abundance:  99.76 %
   --->  Isotope:   O17   Z =  8   N =  17   A =  17.00 g/mole   abundance:   0.04 %
   --->  Isotope:   O18   Z =  8   N =  18   A =  18.00 g/mole   abundance:   0.20 %  ElmMassFraction:  23.18 %
ElmAbundance  21.07 %
   --->  Element: Ar (Ar)   Z = 18.0   N =  40.0   A =  39.95 g/mole
   --->  Isotope:  Ar36   Z = 18   N =  36   A =  35.97 g/mole   abundance:   0.34 %
   --->  Isotope:  Ar38   Z = 18   N =  38   A =  37.96 g/mole   abundance:   0.06 %
   --->  Isotope:  Ar40   Z = 18   N =  40   A =  39.96 g/mole   abundance:  99.60 %  ElmMassFraction:   1.28 %
ElmAbundance   0.47 %



***** Table : Nb of elements = 6 *****

 Element: Pb (Pb)   Z = 82.0   N = 207.2   A = 207.22 g/mole
   --->  Isotope: Pb204   Z = 82   N = 204   A = 203.97 g/mole   abundance:   1.40 %
   --->  Isotope: Pb206   Z = 82   N = 206   A = 205.97 g/mole   abundance:  24.10 %
   --->  Isotope: Pb207   Z = 82   N = 207   A = 206.98 g/mole   abundance:  22.10 %
   --->  Isotope: Pb208   Z = 82   N = 208   A = 207.98 g/mole   abundance:  52.40 %
```

```
 Element: Au (Au)   Z = 79.0   N = 197.0   A = 196.97 g/mole
   --->  Isotope: Au197   Z = 79   N = 197   A = 196.97 g/mole   abundance: 100.00 %

 Element: C (C)   Z =  6.0   N =  12.0   A =  12.01 g/mole
   --->  Isotope:   C12   Z =  6   N =  12   A =  12.00 g/mole   abundance:  98.93 %
   --->  Isotope:   C13   Z =  6   N =  13   A =  13.00 g/mole   abundance:   1.07 %

 Element: N (N)   Z =  7.0   N =  14.0   A =  14.01 g/mole
   --->  Isotope:   N14   Z =  7   N =  14   A =  14.00 g/mole   abundance:  99.63 %
   --->  Isotope:   N15   Z =  7   N =  15   A =  15.00 g/mole   abundance:   0.37 %

 Element: O (O)   Z =  8.0   N =  16.0   A =  16.00 g/mole
   --->  Isotope:   O16   Z =  8   N =  16   A =  15.99 g/mole   abundance:  99.76 %
   --->  Isotope:   O17   Z =  8   N =  17   A =  17.00 g/mole   abundance:   0.04 %
   --->  Isotope:   O18   Z =  8   N =  18   A =  18.00 g/mole   abundance:   0.20 %

 Element: Ar (Ar)   Z = 18.0   N =  40.0   A =  39.95 g/mole
   --->  Isotope:  Ar36   Z = 18   N =  36   A =  35.97 g/mole   abundance:   0.34 %
   --->  Isotope:  Ar38   Z = 18   N =  38   A =  37.96 g/mole   abundance:   0.06 %
   --->  Isotope:  Ar40   Z = 18   N =  40   A =  39.96 g/mole   abundance:  99.60 %
<<< Geant4 Physics List engine packaging library: PACK 5.5
<<< Geant4 Physics List simulation engine: QGSP_BIC_HP 1.3

------------------------------------------
Box Height 5 m
Box Width 5  m
------------------------------------------

------------------------------------------------------------------
---> The World Box height is  5 m
------------------------------------------------------------------
NeutronHP: /Elastic/ file for Z = 6, A = 13 is not found and NeutronHP will use
/nfs/user1/sturnbull/geant4/data/G4NDL3.14/Elastic///CrossSection/6_nat_Carbon
NeutronHP: /Elastic/ file for Z = 8, A = 18 is not found and NeutronHP will use
/nfs/user1/sturnbull/geant4/data/G4NDL3.14/Elastic///CrossSection/8_17_Oxygen
NeutronHP: /Capture file for Z = 6, A = 13 is not found and NeutronHP will use
/nfs/user1/sturnbull/geant4/data/G4NDL3.14/Capture//CrossSection/6_nat_Carbon
NeutronHP: /Elastic file for Z = 6, A = 13 is not found and NeutronHP will use
/nfs/user1/sturnbull/geant4/data/G4NDL3.14/Elastic//CrossSection/6_nat_Carbon
```

```
NeutronHP: /Inelastic file for Z = 6, A = 13 is not found and NeutronHP will use
/nfs/user1/sturnbull/geant4/data/G4NDL3.14/Inelastic//CrossSection/6_nat_Carbon
NeutronHP: /Capture file for Z = 8, A = 18 is not found and NeutronHP will use
/nfs/user1/sturnbull/geant4/data/G4NDL3.14/Capture//CrossSection/8_17_Oxygen
NeutronHP: /Elastic file for Z = 8, A = 18 is not found and NeutronHP will use
/nfs/user1/sturnbull/geant4/data/G4NDL3.14/Elastic//CrossSection/8_17_Oxygen
NeutronHP: /Inelastic file for Z = 8, A = 18 is not found and NeutronHP will use
/nfs/user1/sturnbull/geant4/data/G4NDL3.14/Inelastic//CrossSection/8_17_Oxygen
/nfs/user1/sturnbull/geant4/data/G4NDL3.14
NeutronHP: /Capture/ file for Z = 6, A = 13 is not found and NeutronHP will use
/nfs/user1/sturnbull/geant4/data/G4NDL3.14/Capture///CrossSection/6_nat_Carbon
NeutronHP: /Capture/ file for Z = 8, A = 18 is not found and NeutronHP will use
/nfs/user1/sturnbull/geant4/data/G4NDL3.14/Capture///CrossSection/8_17_Oxygen
Idle>
```

Code 4.1. GEANT4 initial run output for a simulation showing defined material properties.

4.3.2. Cosmic Ray Generator Simulation Output

Running simulations using the Cosmic Ray Generator (CRY) code required the following inputs in the CRY setup file.

The parameter file `setup.file` is shown in code 4.2.

```
returnNeutrons 1
returnProtons 1
returnGammas 1
date 7-1-2008     // dates account for 11 year solar cycle
latitude 37       // set to Melbourne latitude
altitude 2100     // 3 altitudes to choose – 0 , 2100 and 11300 m
subboxLength 300  // lateral size of interest 300 x 300 m
```

Code 4.2. CRY setup.file showing input parameters.

A simulation run using the CRY code to test the muon flux variation for various altitudes was performed. Using CRY, the muon flux at sea-level (0 m) and 2100 m was determined and the results are shown in Table 4.2.

Table 4.2. Muon flux determined using CRY at 0 m and 2100 m.

Altitude (m)	**0**	**2100**
Flux ($m^{-2}s^{-1}$)	113.9	165.23

4.3.3. Data Run: Muons at 1 m above Pb shield

A series of GEANT4 simulations were run to enable the counting of ^{198}Au isotopes produced at different incident muon energies. Code 4.3 below shows the au.g4mac file used for the input setup parameters. The activation count of ^{198}Au was output at the end of each run.

```
# creates a rectangular plane source, isotropic radiation
# 10 cm from start of Au.

/gps/particle mu-                   // incident particle
#rectangle plane source
/gps/pos/type Plane                 // plane rectangular source 5 m x 5 m
/gps/pos/shape Rectangle
/gps/pos/centre 0. 0. 1. m          // 1 m above Pb shield
/gps/pos/halfx 5 m
/gps/pos/halfy 5 m
#
/gps/energy 750 MeV                 // example muon energy

# commands below are independent of gps
```

```
#
#/mydet/setHeight 5 m
#/mydet/setWidth 5 m
#/mydet/update
/run/beamOn 100000000                  // # muon event number
```

Code 4.3. au.g4mac setup parameters used for GEANT4 simulation data run.

Table 4.3 gives the results of 30 GEANT4 simulations where the muons are incident from 1 m above the Pb shield.

Table 4.3. Data table for 30 GEANT4 simulation runs with muons at 1 m above detector shield.

Run #	**Energy (MeV)**	**Act. count**
1	50	75
2	100	128
3	150	157
4	200	237
5	250	274
6	300	368
7	350	350
8	400	364
9	450	388
10	500	475
11	550	520
12	600	579
13	650	545
14	700	466
15	750	451
16	800	389
17	850	348
18	900	290

Run #	Energy (MeV)	Act. count
19	950	256
20	1000	193
21	1050	163
22	1100	108
23	1150	42
24	1200	11
25	1250	2
26	1300	1
27	1350	1
28	1400	0
29	1450	0
30	1500	1

Using table 4.3, figure 4.2 was plotted showing the activation count of ^{198}Au isotopes against muon energy.

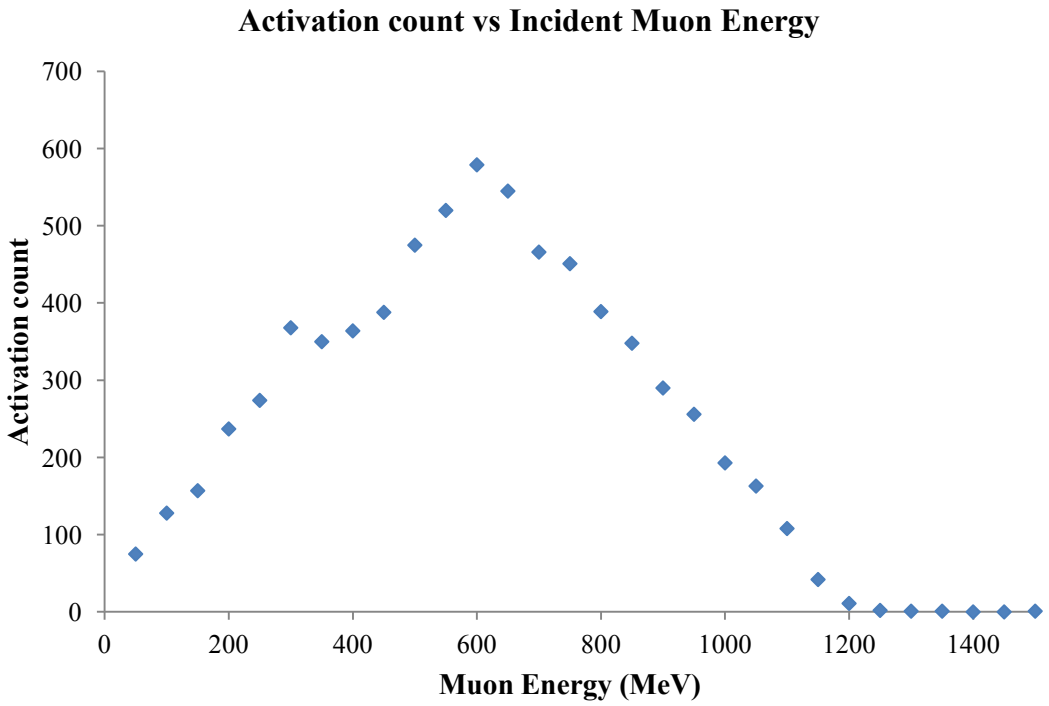

Figure 4.2. Activation count of ^{198}Au isotopes for incident muon energies.

Figure 4.2 shows the optimal muon energy range for neutron activation of ^{198}Au is 550 - 650 MeV. As discussed in chapter 2, muons interact with the lead nuclei in the lead shielding to produce neutrons via the interaction given by (equation 2.8),

$$\mu^- + p \rightarrow n + \nu_\mu. \qquad 2.8$$

Therefore in order to investigate the reasons why the optimal muon energy range for neutron activation of ^{198}Au is around 600 MeV, further simulations, using the same input variables (i.e. detector geometry, physics processes, setup parameters etc.) were conducted to determine the neutron production over the same muon energy range. The number of events was reduced to 1 x 10^6 from 1 x 10^8 to reduce the computation time.

For these simulations GEANT4 used two different physics processes to produce neutrons; *MuMinusCaptureAtRest* and *NeutronInelastic*. GEANT4 utilises further neutron creation processes such as neutron fission, although this process was not utilised as it was not relevant to this project. In order determine which of the above processes created the neutron, an algorithm was designed as shown below in code 4.4.

```
if (aTrack->GetDefinition() == G4Neutron::Neutron())
{
      nProcess = (aTrack->GetCreatorProcess()->GetProcessName());
      G4cout << " neutron process: " << nProcess << G4endl;
}
```

Code 4.4. Check to test neutron creation process within the GEANT4 *StackingAction* class.

Code 4.4 tests the current track for a neutron and if true; the creator process name is stored in the variable *nProcess*. The G4cout command outputs the neutron process. This output was redirected to a text file where the ratio of *MuMinusCaptureAtRest* to *NeutronInelastic* processes were counted and the results plotted in figure 4.3.

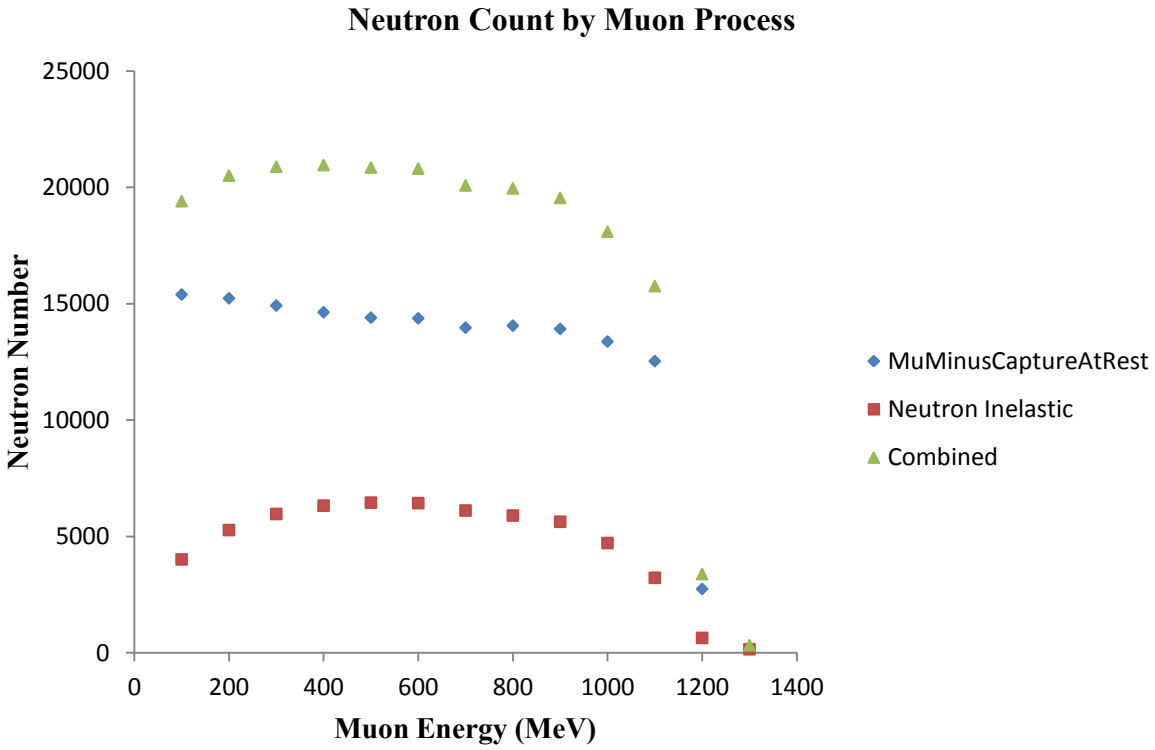

Figure 4.3. Neutrons generated via the *MuMinusCaptureAtRest* and *NeutronInelastic* process and the total neutron count as a function of incident muon energy.

Analysis of figure 4.3 reveals the following:

(i) The *NeutronInelastic* process shows a similar trend to figure 4.2 whilst the *MuMinusCaptureAtRest* process shows a gradual decline in the neutron count with increasing muon energy.

(ii) Neutron capture drops sharply at 1300 MeV matching the drop in activation number. Around this energy, the *PhotonInelastic* process begins. This process models photonuclear

reactions, (γ, n), which involve the absorption of gamma-ray photons by atomic nuclei with the accompanying emission of protons, neutrons and heavier particles. For ^{208}Pb, the photo-absorption cross-section (σ_γ) is largest for photon energies between 10 – 30 MeV where the maximum photon energy is called a giant resonance [69]. At muon energies of 1.3 GeV, γ-rays fall into this resonance overtaking the *MuMinusCaptureAtRest* process for neutron production.

The total neutron production count (i.e. the sum from both processes) basically follows the same trend as the Au activation count (Figure 4.2) as a function of muon energy. This indicates that incident muon energy of 600 MeV is close to the maximum in the neutron production count.

GEANT4 simulations were also analysed to determine the neutron energy spectrum for neutrons created by incident muons of energy 200, 600 and 800 MeV and the results are shown in figure 4.4.

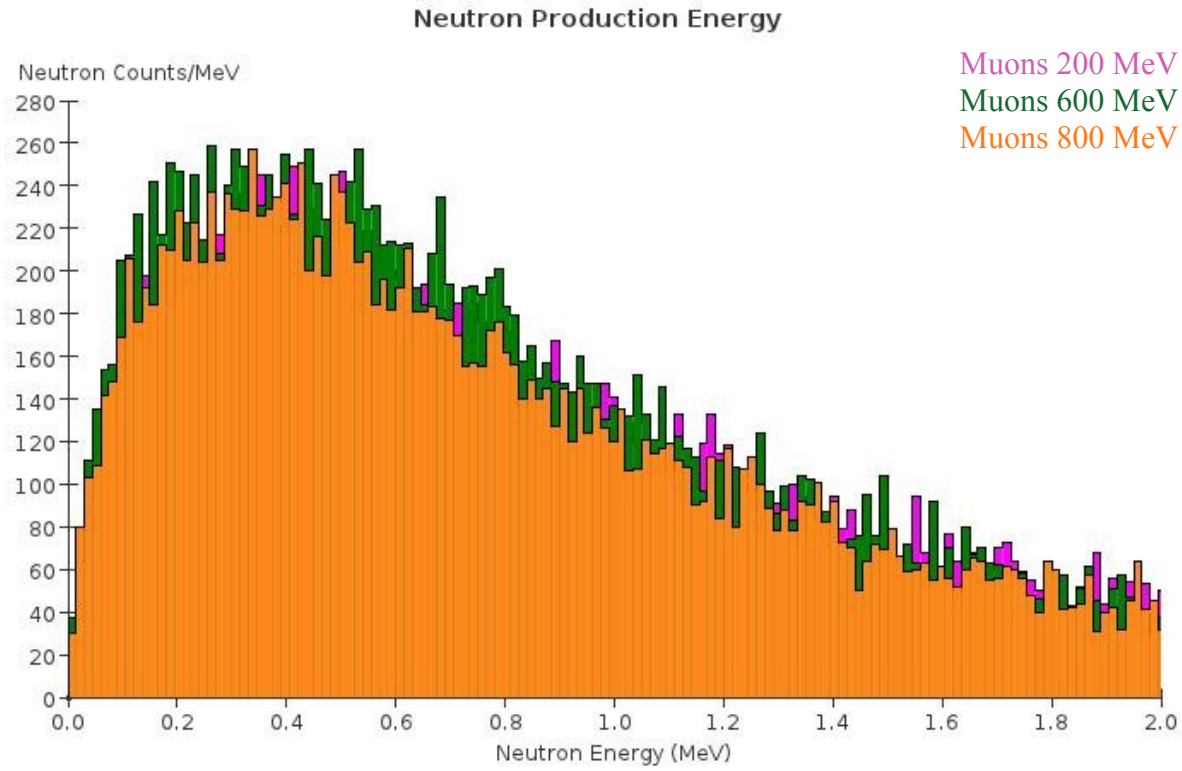

Figure 4.4. Neutron energy spectrum for muons of incident energy 200, 600 and 800 MeV as determined from GEANT4 simulations.

Figure 4.4 reveals that the neutron energy spectrum is effectively the same at these incident muon energies. This data is useful when viewed with figure 4.5 which gives the

$^{197}Au(n,\gamma)^{198}Au$ capture cross-section. The data for figure 4.5 was obtained from the National Nuclear Data Centre, Brookhaven National Laboratory [68].

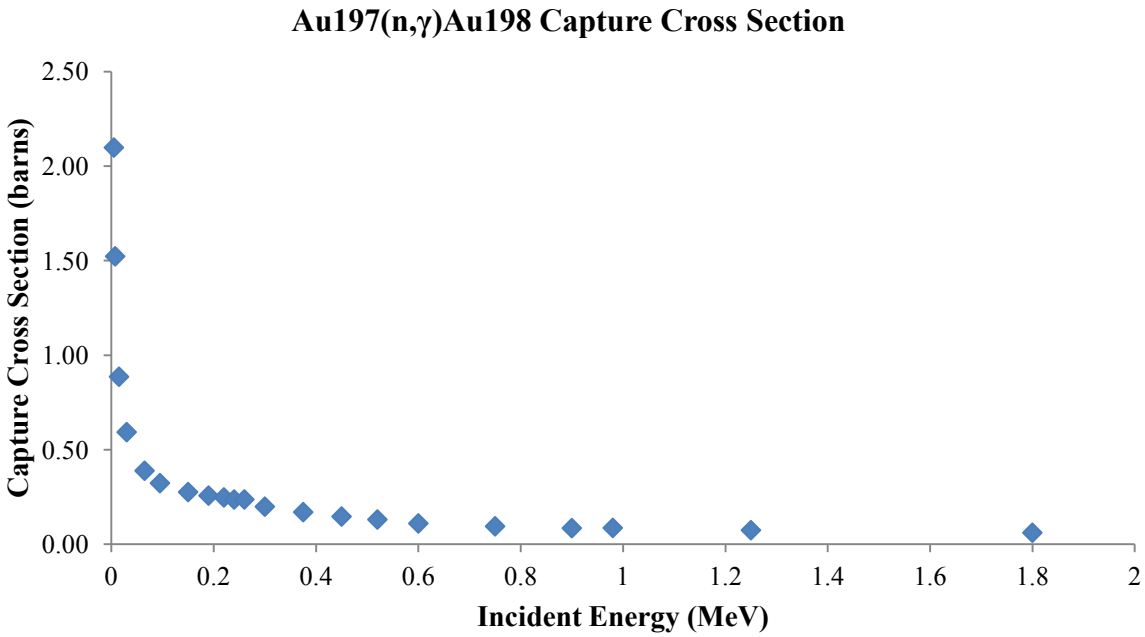

Figure 4.5. $^{197}Au(n,\gamma)^{198}Au$ capture cross-section data from Chadwick 2006 (Ref.[68])

The convolution of data from figures 4.3, 4.4 and 4.5 may explain why the gold activation count curve (figure 4.2) has a maximum at muon incident energy of 600 MeV. The reasons can be summarised as follows:

1. The neutron production is optimal between the incident muon energies of 200-800 MeV (Figure 4.3)

2. The neutron energy spectrum over this muon energy range is effectively the same (Figure 4.4) and shows that the neutron count drops sharply at low neutron energies (0.2 MeV) but more slowly at high neutron energies (>0.8 MeV).

3. At low neutron energies (<0.2 MeV) the $^{197}Au(n,\gamma)^{198}Au$ capture cross-section is highest (but few neutrons have this energy) . The cross-section decays slowly at neutron energies above 0.2 MeV.

A kink in the spectrum of figure 4.2 also appears at 300 MeV showing a slightly higher activation count. This may be due to a kink in one of the scattering cross-sections in the data tables of GEANT4 and an investigation of this is a subject of further work.

4.4. CRY Simulation Results

In section 4.3 the activation of ^{198}Au from ^{197}Au via neutron capture was modelled at various muon energy levels ranging from 50 MeV to 1500 MeV. In order for the GEANT4 simulations to accurately model or be compared to experimental results of ^{198}Au activation an accurate muon flux resulting from cosmic ray interaction with the atmosphere needs to be determined. Therefore the CRY tool was used to generate a simulated spectrum of muon flux at sea level.

To do this, a setup.file with the following input parameters was used as shown in code 4.5

```
returnNeutrons 1
returnProtons 1
returnGammas 1
date 7-15-2011    // date accounts for 11 year solar cycle
latitude 37       // set to Melbourne latitude
altitude 0        // altitude 0 m
subboxLength 100  // lateral size of interest 100 x 100 m
```

Code 4.5. Initial parameters used for muon flux spectrum.

A modified version of the example program *testRoot* included with CRY was used to generate figure 4.6. The program simulates a cosmic spectrum returning a range of particles. Muon energy and count is tallied and output to a histogram. Analysis software called *ROOT*[1] was used to read the histogram and output a graph.

Using the setup.file as input for the *testRoot* program generated a muon flux of 113.9 $m^{-2}s^{-1}$ over 42.2 seconds. Using the muon flux, the y-axis of figure 4.6 could be rescaled to ensure correct units of flux ($m^{-2}s^{-1}$). The CRY default energy unit is MeV therefore no rescaling of energy units was required.

ROOT was used to plot the muon flux spectrum generated using the software program *testRoot* as discussed in chapter 4, section 4.2.3. The activation production rate as a function of muon energy, figure 4.7, was generated from the convolution of figure 4.2, the activation count of ^{198}Au isotopes for incident muon energies, with figure 4.4, the simulated muon spectrum from CRY.

[1] http://root.cern.ch/drupal/

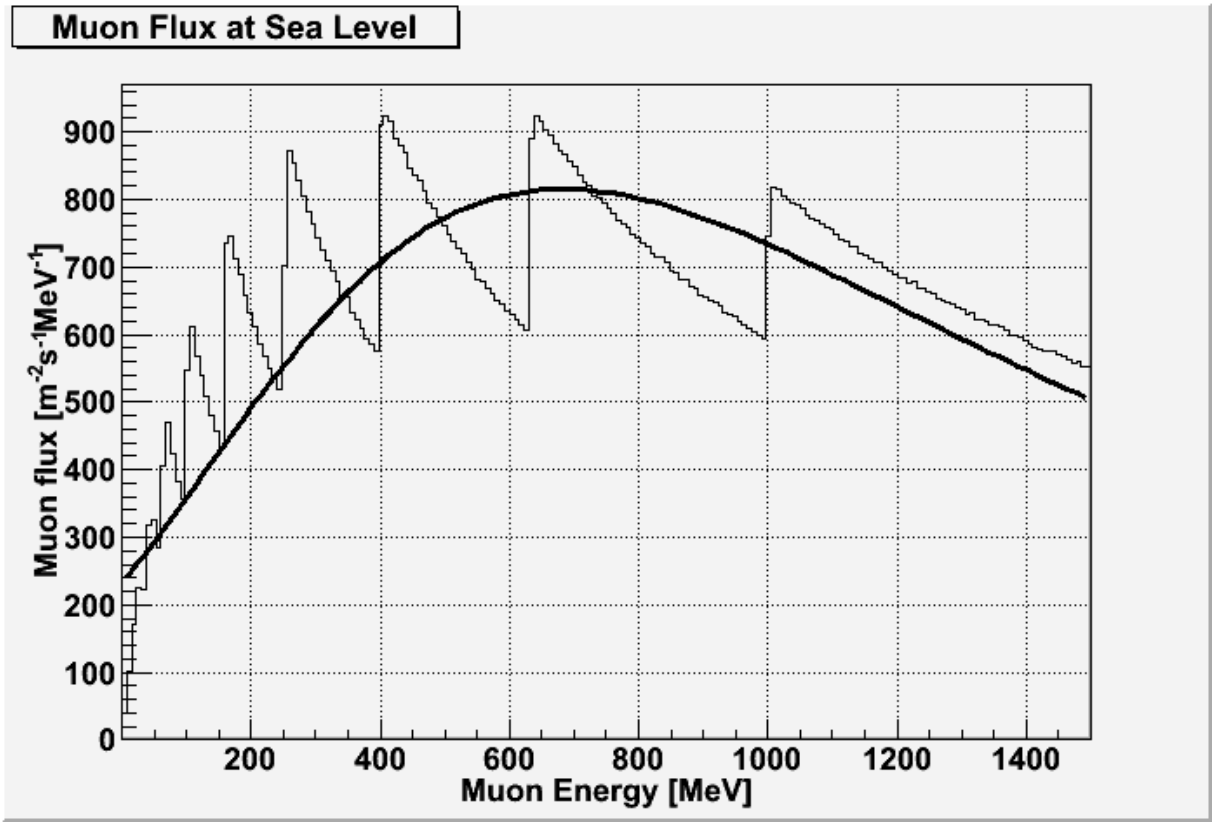

Figure 4.6. Muon spectrum generated from CRY. The thin black line represents the CRY results and the thick black line is a fit using the Landau fitting function as this gave the best fit.

Using figure 4.6, the muon flux per incident muon energy was read from the graph. As an example, 50 MeV muons have a flux of 2.91 x 10^2 $m^{-2}s^{-1}MeV^{-1}$. To calculate the muon rate entering the top of the Pb shield the following calculation is performed.

Step 1:

Area of Pb shield top: 1.33 m^2

Muon Flux at 50 MeV: 2.91 x 10^2 $m^{-2}s^{-1}$ [obtained from figure 4.4]

Number of muons entering detector per second: $(1.33)(2.91 \times 10^2) = 3.86 \times 10^2$

Step 2:

How many ^{198}Au activations per second are detected?

Number of muons entering detector: 3.86 x 10^2 [from step 1]

Number of incident muons: 1×10^8 [from Code 4.3]

Activation count (50MeV): 75 [from Table 4.3]

Therefore ^{198}Au production rate for 50 MeV muons is: $\frac{3.86\ x\ 10^2}{1\ x\ 10^8} x\ 75 = 2.9\ x\ 10^{-4}$

Repeating this process for all energies to 1500 MeV yields table 4.4.

Table 4.4. Activation rate of ^{198}Au as a function of muon energy (MeV).

Muon Energy (MeV)	**Activation Rate (s^{-1})**
50	2.90E-04
100	6.07E-04
150	8.84E-04
200	1.54E-03
250	2.01E-03
300	2.98E-03
350	3.09E-03
400	3.42E-03
450	3.83E-03
500	4.87E-03
550	5.48E-03
600	6.20E-03
650	5.89E-03
700	5.04E-03
750	4.85E-03
800	4.14E-03
850	3.64E-03
900	2.98E-03
950	2.56E-03
1000	1.88E-03

Muon Energy (MeV)	Activation Rate (s^{-1})
1050	1.54E-03
1100	9.88E-04
1150	3.71E-04
1200	9.36E-05
1250	1.64E-05
1300	7.88E-06
1350	7.57E-06
1400	0.00E+00
1450	0.00E+00
1500	6.68E-06

Plotting table 4.4 yields figure 4.7.

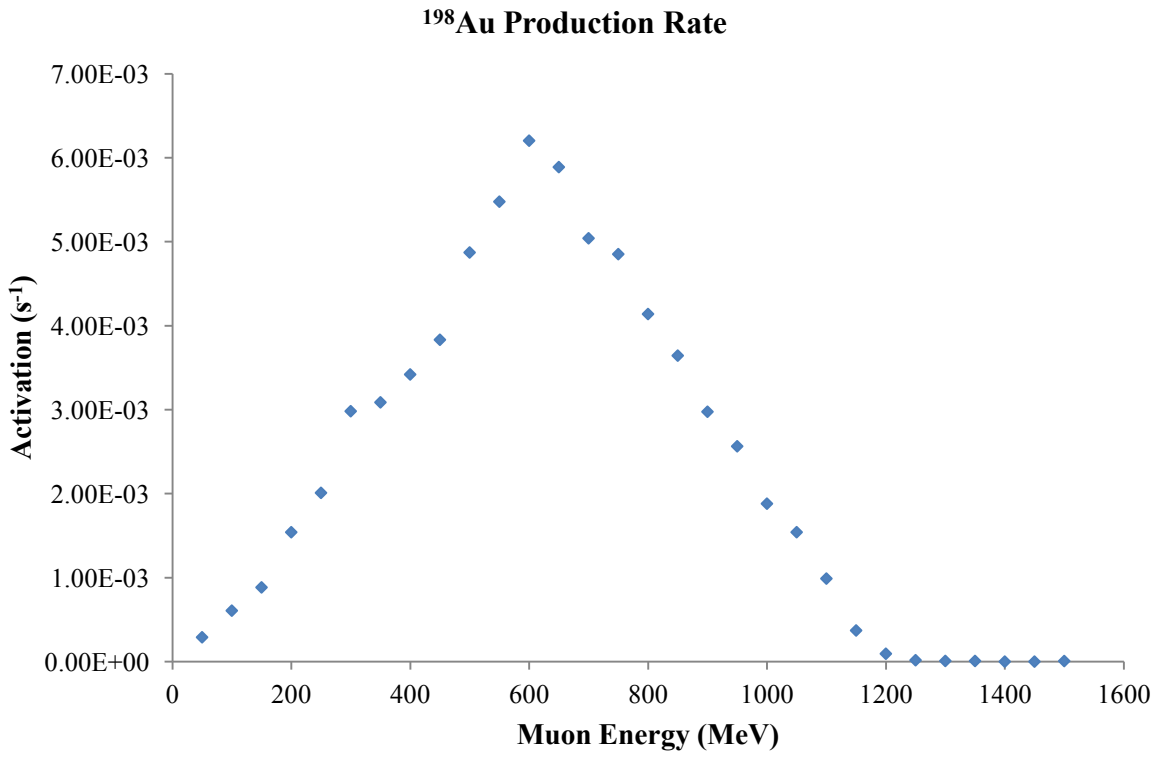

Figure 4.7. Activation rate per muon energy.

The ^{198}Au production rate as a function of muon energy is shown in figure 4.7 and reveals the same overall trend as figure 4.2. Further calculations allow the activation rate per second to be

converted to the activation rate per muon. These calculations yield the expected activation count per muon is 3.46×10^{-6}.

Potential sources of discrepancy between simulations and actual experiments on activation of Au resulting from neutron production in the Pb shielding could be due to:

1. Modelling only muons and not the whole spectrum of particles generated during a cosmic shower. Using only muons reduces secondary particle creation and knock-on neutron production counts, affecting the activation count.

2. The lead used for the detector in the GEANT4 simulations was pure ^{208}Pb. In reality this type of lead is almost impossible to find because most lead is contaminated with trace elements ^{210}Pb, ^{238}U and ^{232}Th, Radon and associated daughters.

3. Calculations involving the activation rate assumed only muons entering the detector from the top face and not the sides of the detector. Muons passing close to the vertical side of the detector could cause a particle shower with the surrounding air and hence enter the side of the detector, adding to the neutron count.

However overall the study has demonstrated that effects such as neutron production in Pb shielding from muon interaction is an important effect in sensitive GRS experiments as the secondary/tertiary neutrons produced may interact with target nuclei to produce γ-ray events which could not be accounted for otherwise.

5. Concluding remarks

This project aimed to gain an estimate of the gold activation rate, the number of ^{198}Au isotopes produced during irradiation from neutrons produced from muon interaction with Pb in the shielding of a GRS detector. The source of the muons was cosmic rays which interacted with particles in the atmosphere. The design and construction of the simulations and analysis of the data proved to be a challenging but a successful enterprise. An outcome was achieved that aligned with the initial aims and research question.

The main results of this project can be summarised as follows:

1. The creation of neutrons from muons interacting with lead shielding is a significant effect which must be taken into account in accurate GRS experiments.

2. The production of neutrons is relatively constant in the muon energy range of 200-800 MeV as shown in figure 4.3.

3. The neutron energy spectrum is effectively the same over the muon energy range 200-800 MeV.

4. From the point of view of neutron activation of gold, the activation rate of gold atoms via (equation 2.13) is maximised at muon energy of 600 MeV and the reasons for this are discussed in chapter 4.

Data obtained from these simulations will be useful in experiments to be carried out at the Institute of Reference Materials and Measurements, Geel, Belgium and are also of general importance for the optimisation of materials used in shielding for gamma-ray spectrometry.

5.1. Further Research

To extend the investigations in this project, simulations could be run using separate simulation toolkits to better analyse data at the low energy range. Example toolkits include the Cosmic Simulator (Cosima), part of the Medium Energy Gamma-ray Astronomy library (MEGALib). Cosima is designed as the interface between MEGALib and GEANT4 and is often used for activation studies. MCNPX and Fluka are suited for low energy neutron transport and would be ideal to run in parallel with GEANT4 for verification.

Although these GEANT4 simulations were designed to model experiments performed above ground, muons can penetrate many hundreds of metres underground losing energy via various physical processes. Therefore performing simulations which model muon interactions through rock, thereby simulating underground GRS experiment environments, would be an interesting additional project. The Muon Simulation Code (MUSIC) is designed for this sole purpose and would be ideal for muon propagation through rock at different depths.

Replacing muons with a cosmic particle spectrum would provide a more realistic input for the GEANT4 physics processes to generate the required neutron flux. Many particles produced in a cosmic ray shower were not modelled in this project and this could impact on the total neutron flux generated.

With the dependence on latitude and altitude, muon propagation through a suitably defined air column is important. This simulation treated the air column through which the muons travelled using a constant density profile. To make a more realistic simulation, a variable density profile would need to be added, similar to the system used for the CRY software.

Altering the isotopic concentrations of the lead isotopes in the GEANT4 model would more accurately simulate the influence of isotropic impurities.

Finally, in order to achieve a greater statistical accuracy during a run, more particles could be simulated. This would require much greater computation times and schemes to maximise computational efficiency such as cross-sectional area reaction biasing.

BIBLIOGRAPHY

1. Debertin, K. and R.G. Helmer, *Gamma- and x-ray spectrometry with semiconductor detectors*1988: North-Holland.

2. Brodzinski, R.L., *Low-level gamma-ray spectrometry.* Journal of Physics G: Nuclear and Particle Physics, 1991. **17**(S): p. S403.

3. Mikael, H., *Low-level gamma-ray spectrometry using Ge-detectors.* Metrologia, 2007. **44**(4): p. S87.

4. Laubenstein, M., et al., *Underground measurements of radioactivity.* Applied Radiation and Isotopes. **61**(2-3): p. 167-172.

5. Semkow, T.M., et al., *Low-background gamma spectrometry for environmental radioactivity.* Applied Radiation and Isotopes, 2002. **57**(2): p. 213-223.

6. Osvath, I. and P.P. Povinec, *Seabed [gamma]-ray spectrometry: applications at IAEA-MEL.* Journal of Environmental Radioactivity, 2001. **53**(3): p. 335-349.

7. Aydin, İ., et al., *An attempt to use aerial gamma-ray spectrometry results in petrochemical assessments of the volcanic and plutonic associations of Central Anatolia (Turkey).* Geophysical Journal International, 2006. **167**(2): p. 1044-1052.

8. Hendriks, P.H.G.M., J. Limburg, and R.J. de Meijer, *Full-spectrum analysis of natural [gamma]-ray spectra.* Journal of Environmental Radioactivity, 2001. **53**(3): p. 365-380.

9. Mengesha, W. and J.D. Valentine, *Benchmarking NaI(Tl) electron energy resolution measurements.* Nuclear Science, IEEE Transactions on, 2002. **49**(5): p. 2420-2426.

10. Ortec. *Gamma Spectroscopy: ORTEC Scientific Equipment*. 2010; Available from: http://www.ortec-online.com/Solutions/gamma-spectroscopy.aspx.

11. Agostinelli, S., et al., *G4--a simulation toolkit.* Nuclear Instruments and Methods in Physics Research Section A: Accelerators, Spectrometers, Detectors and Associated Equipment, 2003. **506**(3): p. 250-303.

12. Núñez-Lagos, R. and A. Virto, *Shielding and background reduction.* Applied Radiation and Isotopes, 1996. **47**(9-10): p. 1011-1021.

13. Measday, D.F., *The nuclear physics of muon capture.* Physics Reports, 2001. **354**(4-5): p. 243-409.

14. Knoll, G.F., *Radiation Detection and Measurement*2010: John Wiley & Sons.

15. Kudryavtsev, V.A., N.J.C. Spooner, and J.E. McMillan, *Simulations of muon-induced neutron flux at large depths underground.* Nuclear Instruments and Methods in Physics Research Section A: Accelerators, Spectrometers, Detectors and Associated Equipment, 2003. **505**(3): p. 688-698.

16. Bevelacqua, J.J., *Health physics in the 21st century*2008: Wiley-VCH.

17. Povinec, P.P., P. Vojtyla, and J.-F. Comanducci, *Monte Carlo simulation of background characteristics of gamma-ray spectrometers--a comparison with experiment*, in *Radioactivity in the Environment*, P.P. Pavel, Editor 2008, Elsevier. p. 163-208.

18. Povinec, P. and ScienceDirect. *Analysis of environmental radionuclides*. 2008; Available from: http://www.sciencedirect.com/science/publication?issn=15694860&volume=11.

19. Niese, S., *Underground laboratories for low-level radioactivity measurements*, in *Radioactivity in the Environment*, P.P. Pavel, Editor 2008, Elsevier. p. 209-239.

20. Krane, K.S., *Introductory nuclear physics*1987: New York : Wiley, c1987. Medium: X; Size: Pages: 550.

21. Schmidt, S. and J.K. Cochran, *Radium and radium-daughter nuclides in carbonates: a brief overview of strategies for determining chronologies.* Journal of Environmental Radioactivity, 2010. **101**(7): p. 530-537.

22. (ATSDR), A.f.T.S.a.D.R., *Toxicological profile for Radon (Draft for Public Comment)*, U.S.D.o.H.a.H. Services, Editor 2008: Atlanta.

23. Carlson, P. and A. De Angelis, *Nationalism and internationalism in science: the case of the discovery of cosmic rays.* The European Physical Journal H, 2011. **35**(4): p. 309-329.

24. Putze, A., *Direct cosmic-ray detection.* Nuclear Instruments and Methods in Physics Research Section A: Accelerators, Spectrometers, Detectors and Associated Equipment. **In Press, Corrected Proof**.

25. Hörandel, J.R., *The origin of galactic cosmic rays.* Nuclear Instruments and Methods in Physics Research Section A: Accelerators, Spectrometers, Detectors and Associated Equipment, 2008. **588**(1-2): p. 181-188.

26. Reedy, R.C., J.R. Arnold, and D. Lal, *Cosmic-ray record in solar system matter.* Science, 1983. **219**(4581): p. 127-135.

27. Lal, D., B. Peters, and i. Originating Research Org. not, *COSMIC RAY PRODUCED RADIOACTIVITY ON THE EARTH.* pp 551-612 of Handbuch der Physik. Band XLVI/2. Fluegge, S. Sitte, K. (eds.). Berlin, Heidelberg, New York, Springer-Verlag, 1967., 1968.

28. Potgieter, M.S., *Solar cycle variations and cosmic rays.* Journal of Atmospheric and Solar-Terrestrial Physics, 2008. **70**(2-4): p. 207-218.

29. Forbush, S.E., *ON DIURNAL VARIATION IN COSMIC-RAY INTENSITY.* Terr. Magn. Atmos. Electr., 1937. **42**(1): p. 1-16.

30. Wordel, R., et al., *Study of neutron and muon background in low-level germanium gamma-ray spectrometry.* Nuclear Instruments and Methods in Physics Research Section A: Accelerators, Spectrometers, Detectors and Associated Equipment, 1996. **369**(2-3): p. 557-562.

31. Svensmark, H., T. Bondo, and J. Svensmark, *Cosmic ray decreases affect atmospheric aerosols and clouds.* Geophys. Res. Lett., 2009. **36**(15): p. L15101.

32. Hess, V.F., *Penetrating Radiation in Seven Free Ballon Flights.* Phys. Zeit, 1912. **13**: p. 1084-1091.

33. Pioch, C., et al., *Measurement of cosmic ray neutrons with Bonner sphere spectrometer and neutron monitor at 79°N.* Nuclear Instruments and Methods in Physics Research Section A: Accelerators, Spectrometers, Detectors and Associated Equipment, 2011. **626-627**: p. 51-57.

34. Lin, J.-W., et al., *Measurement of angular distribution of cosmic-ray muon fluence rate.* Nuclear Instruments and Methods in Physics Research Section A: Accelerators, Spectrometers, Detectors and Associated Equipment, 2010. **619**(1-3): p. 24-27.

35. Bernlöhr, K. *Cosmic-ray air showers*. 1999; Available from: http://www.mpi-hd.mpg.de/hfm/CosmicRay/Showers.html.

36. Singh, A.K., D. Siingh, and R.P. Singh, *Impact of Galactic Cosmic Rays on Earth's Atmosphere and Human Health.* Atmospheric Environment, 2011. **45**(23): p. 3806-3818.

37. Grieder, P.K.F., *Cosmic Rays at Earth* 2001 Elsevier.

38. Grieder, P.K.F., *Preface*, in *Cosmic Rays at Earth*2001, Elsevier: Amsterdam. p. v-vii.

39. Banerjee, S., et al., *Tau and muon pair production cross sections in electron-positron annihilations at s=10.58 GeV.* Physical Review D, 2008. **77**(5): p. 054012.

40. Aktas, A., et al., *Muon pair production in ep collisions at HERA.* Physics Letters B, 2004. **583**(1-2): p. 28-40.

41. Brandt, S., *The harvest of a century: discoveries of modern physics in 100 episodes*2009: Oxford University Press.

42. Gautreau, R. and W. Savin, *Schaum's outline of theory and problems of modern physics*1999, New York [u.a.]: McGraw-Hill.

43. Kuno, Y. and Y. Okada, *Muon decay and physics beyond the standard model.* Reviews of Modern Physics, 2001. **73**(1): p. 151.

44. Martin, B.R. and G. Shaw, *Particle physics*2008: Wiley.

45. Grossman, Y. and Y. Nir, *Lepton mass matrix models.* Nuclear Physics B, 1995. **448**(1-2): p. 30-50.

46. Heusser, G., *Low-Radioactivity Background Techniques.* Annual Review of Nuclear and Particle Science, 1995. **45**(1): p. 543-590.

47. Wolf, J. *Measurement of Muon Induced Neutron Background at Shallow Sites*. 2002; Available from: http://arxiv.org/abs/hep-ex/0211032v1.

48. Mukhopadhyay, N.C., *Nuclear Muon capture.* Physics Reports, 1977. **30**(1): p. 1-144.

49. Araújo, H.M., et al., *Measurements of neutrons produced by high-energy muons at the Boulby Underground Laboratory.* Astroparticle Physics, 2008. **29**(6): p. 471-481.

50. Wang, Y.F., et al., *Predicting neutron production from cosmic-ray muons.* Physical Review D, 2001. **64**(1): p. 013012.

51. Da Silva, A., et al., *Neutron background for a dark matter experiment at a shallow depth site.* Nuclear Instruments and Methods in Physics Research Section A: Accelerators, Spectrometers, Detectors and Associated Equipment, 1995. **354**(2-3): p. 553-559.

52. MartInez Canet, M.J., et al., *Measurements of activation induced by environmental neutrons using ultra low-level [gamma]-ray spectrometry.* Applied Radiation and Isotopes, 2000. **52**(3): p. 711-716.

53. Mouchel, D. and R. Wordel, *Measurement of low-level radioactivity in environmental samples by gamma-ray spectrometry.* International Journal of Radiation Applications and Instrumentation. Part A. Applied Radiation and Isotopes. **43**(1-2): p. 49-59.

54. Alessandrello, A., et al., *Measurements of internal radioactive contamination in samples of Roman lead to be used in experiments on rare events.* Nuclear Instruments and Methods in Physics Research Section B: Beam Interactions with Materials and Atoms, 1998. **142**(1-2): p. 163-172.

55. Radiochemistry. *GAMMA-RAY SPECTRUM CATALOG OF ISOTOPES*. 2003; Available from: http://www.radiochemistry.org/periodictable/gamma_spectra/.

56. Alessandrello, A., et al., *Measurements on radioactivity of ancient roman lead to be used as shield in searches for rare events.* Nuclear Instruments and Methods in Physics Research Section B: Beam Interactions with Materials and Atoms, 1991. **61**(1): p. 106-117.

57. Kozlov, V.Y., et al., *A detection system to measure muon-induced neutrons for direct dark matter searches.* Astroparticle Physics, 2010. **34**(2): p. 97-105.

58. Preusse, W. and S. Unterricker, *The contribution of cosmic ray muons to the background spectrum of gamma ray spectrometers.* Nuclear Instruments and Methods in Physics Research Section B: Beam Interactions with Materials and Atoms, 1994. **94**(4): p. 569-574.

59. Greenberg, R.R., P. Bode, and E.A. De Nadai Fernandes, *Neutron activation analysis: A primary method of measurement.* Spectrochimica Acta Part B: Atomic Spectroscopy. **In Press, Corrected Proof**.

60. Hou, X., *Activation analysis for the determination of long-lived radionuclides*, in *Radioactivity in the Environment*, P.P. Pavel, Editor 2008, Elsevier. p. 371-405.

61. Molnár, G.L., *Handbook of prompt gamma activation analysis with neutron beams*2004: Kluwer Academic Publishers.

62. Perkins, D.H., *Introduction to high energy physics*2000: Cambridge University Press.

63. Mo, L., H.Y. Wu, and C. Baldock, *Absolute Activity Determination of ¹⁹⁸ Au Solid Source Using 4πβ —γ*

Coincidence Counting Corrected by Monte-Carlo Calculation. Nuclear Science, IEEE Transactions on, 2007. **54**(3): p. 677-683.

64. Atanassov, E. and I.T. Dimov, *What Monte Carlo models can do and cannot do efficiently?* Applied Mathematical Modelling, 2008. **32**(8): p. 1477-1500.

65. Vojtyla, P., *A computer simulation of the cosmic-muon background induction in a Ge [gamma]-spectrometer using GEANT.* Nuclear Instruments and Methods in Physics Research Section B: Beam Interactions with Materials and Atoms, 1995. **100**(1): p. 87-96.

66. Hagmann, C., D. Lange, and D. Wright, *Cosmic-ray Shower Library (CRY).* 2008.

67. Project, W.U. *Neutron Activation Calculator*. 2011 19 Dec 2011; Available from: http://wise-uranium.org/rnac.html.

68. Chadwick, M.B., et al., *ENDF/B-VII.0: Next Generation Evaluated Nuclear Data Library for Nuclear Science and Technology.* Nuclear Data Sheets, 2006. **107**(12): p. 2931-3060.

69. Schumacher, M., *Photonuclear reactions.* Journal of Physics G: Nuclear Physics, 1988. **14**(S): p. S235.

APPENDICES

Appendix 1: Material Tables

```
***** Table : Nb of materials = 3 *****

Material: G4_Pb   density: 11.350 g/cm3   RadL: 5.613 mm    Nucl.Int.Length: 18.261 cm    Imean: 823.000 eV
Element: Pb (Pb)  Z = 82.0    N = 207.2   A = 207.22 g/mole
Isotope: Pb204    Z = 82      N = 204     A = 203.97 g/mole       abundance: 1.40 %
Isotope: Pb206    Z = 82      N = 206     A = 205.97 g/mole       abundance: 24.10 %
Isotope: Pb207    Z = 82      N = 207     A = 206.98 g/mole       abundance: 22.10 %
Isotope: Pb208    Z = 82      N = 208     A = 207.98 g/mole       abundance: 52.40 %      ElmMassFraction: 100.00 %
      ElmAbundance 100.00 %

Material: G4_Au   density: 19.320 g/cm3   RadL: 3.344 mm    Nucl.Int.Length: 10.539 cm    Imean: 790.000 eV
Element: Au (Au)  Z = 79.0    N = 197.0   A = 196.97 g/mole
Isotope: Au197    Z = 79      N = 197     A = 196.97 g/mole       abundance: 100.00 %     ElmMassFraction: 100.00
%ElmAbundance 100.00 %

Material: G4_AIR      density: 1.205 mg/cm3 RadL: 303.921 m Nucl.Int.Length: 710.261 m Imean:  85.700 eV
      temperature: 273.15 K pressure: 1.00 atm
Element: C (C)   Z = 6.0    N = 12.0   A = 12.01 g/mole
Isotope: C12     Z = 6      N = 12     A = 12.00 g/mole      abundance:  98.93 %
Isotope: C13     Z = 6      N = 13     A = 13.00 g/mole      abundance: 1.07 %     ElmMassFraction: 0.01 %
ElmAbundance     0.02 %
Element: N (N)   Z = 7.0    N = 14.0   A = 14.01 g/mole
Isotope: N14     Z = 7      N = 14     A = 14.00 g/mole      abundance: 99.63 %
Isotope: N15     Z = 7      N = 15     A = 15.00 g/mole      abundance: 0.37 %     ElmMassFraction: 75.53 %
      ElmAbundance 78.44 %
Element: O (O)   Z = 8.0    N = 16.0   A = 16.00 g/mole
Isotope: O16     Z = 8      N = 16     A = 15.99 g/mole      abundance: 99.76 %
Isotope: O17     Z = 8      N = 17     A = 17.00 g/mole      abundance: 0.04 %
Isotope: O18     Z = 8      N = 18     A = 18.00 g/mole      abundance: 0.20 %     ElmMassFraction: 23.18 %
      ElmAbundance 21.07 %
Element: Ar (Ar) Z = 18.0   N = 40.0   A = 39.95 g/mole
Isotope: Ar36    Z = 18     N = 36     A = 35.97 g/mole      abundance: 0.34 %
Isotope: Ar38    Z = 18     N = 38     A = 37.96 g/mole      abundance: 0.06 %
```

```
Isotope: Ar40    Z = 18     N = 40     A = 39.96 g/mole      abundance: 99.60 %    ElmMassFraction: 1.28 %
     ElmAbundance 0.47 %

***** Table: Nb of elements = 6 *****
Element: Pb (Pb) Z = 82.0   N = 207.2  A = 207.22 g/mole
Isotope: Pb204   Z = 82     N = 204    A = 203.97 g/mole     abundance: 1.40 %
Isotope: Pb206   Z = 82     N = 206    A = 205.97 g/mole      abundance: 24.10 %
Isotope: Pb207   Z = 82     N = 207    A = 206.98 g/mole     abundance: 22.10 %
Isotope: Pb208   Z = 82     N = 208    A = 207.98 g/mole     abundance: 52.40 %

Element: Au (Au) Z = 79.0   N = 197.0  A = 196.97 g/mole
Isotope: Au197   Z = 79     N = 197    A = 196.97 g/mole     abundance: 100.00 %

Element: C (C)   Z = 6.0    N = 12.0   A = 12.01 g/mole
Isotope: C12     Z = 6      N = 12     A = 12.00 g/mole abundance: 98.93 %
Isotope: C13     Z = 6      N = 13     A = 13.00 g/mole abundance: 1.07 %

Element: N (N)   Z = 7.0    N = 14.0   A = 14.01 g/mole
Isotope: N14     Z = 7      N = 14     A = 14.00 g/mole abundance: 99.63 %
Isotope: N15     Z = 7      N = 15     A = 15.00 g/mole abundance:  0.37 %

Element: O (O)   Z = 8.0    N = 16.0   A = 16.00 g/mole
Isotope: O16     Z = 8      N = 16     A = 15.99 g/mole abundance: 99.76 %
Isotope: O17     Z = 8      N = 17     A = 17.00 g/mole abundance: 0.04 %
Isotope: O18     Z = 8      N = 18     A = 18.00 g/mole abundance: 0.20 %

Element: Ar (Ar) Z = 18.0   N = 40.0   A = 39.95 g/mole
Isotope: Ar36    Z = 18     N = 36     A = 35.97 g/mole abundance: 0.34 %
Isotope: Ar38    Z = 18     N = 38     A = 37.96 g/mole abundance: 0.06 %
Isotope: Ar40    Z = 18     N = 40     A = 39.96 g/mole abundance:  99.60
```

Appendix II: GEANT4 run output with beamOn executed.

```
Idle> /run/beamOn

phot:   for  gamma    SubType= 12
      ===== EM models for the G4Region  DefaultRegionForTheWorld ======
       PhotoElectric :   Emin=        0 eV       Emax=         10 TeV

compt:   for  gamma    SubType= 13
      Lambda tables from 100 eV  to 10 TeV in 77 bins, spline: 1
      ===== EM models for the G4Region  DefaultRegionForTheWorld ======
       Klein-Nishina :   Emin=        0 eV       Emax=         10 TeV

conv:   for  gamma    SubType= 14
      Lambda tables from 1.022 MeV to 10 TeV in 77 bins, spline: 1
      ===== EM models for the G4Region  DefaultRegionForTheWorld ======
        BetheHeitler :   Emin=        0 eV       Emax=         10 TeV

msc:   for e-    SubType= 10
      Lambda tables from 100 eV  to 10 TeV in 77 bins, spline: 1
      RangeFactor= 0.04, stepLimitType: 1, latDisplacement: 1
      ===== EM models for the G4Region  DefaultRegionForTheWorld ======
          UrbanMsc93 :   Emin=        0 eV       Emax=         10 TeV

eIoni:   for  e-    SubType= 2
      dE/dx and range tables from 100 eV  to 10 TeV in 77 bins
      Lambda tables from threshold to 10 TeV in 77 bins, spline: 1
      finalRange(mm)= 1, dRoverRange= 0.2, integral: 1, fluct: 1, linLossLimit= 0.01
      ===== EM models for the G4Region  DefaultRegionForTheWorld ======
        MollerBhabha :   Emin=        0 eV       Emax=         10 TeV

eBrem:   for  e-    SubType= 3
      dE/dx and range tables from 100 eV  to 10 TeV in 77 bins
      Lambda tables from threshold to 10 TeV in 77 bins, spline: 1
      LPM flag: 1 for E > 1 GeV
      ===== EM models for the G4Region  DefaultRegionForTheWorld ======
               eBrem :   Emin=        0 eV       Emax=          1 GeV  AngularGenUrban
            eBremLPM :   Emin=        1 GeV      Emax=         10 TeV  AngularGenUrban
```

```
eIoni:   for  e+    SubType= 2
      dE/dx and range tables from 100 eV  to 10 TeV in 77 bins
      Lambda tables from threshold to 10 TeV in 77 bins, spline: 1
      finalRange(mm)= 1, dRoverRange= 0.2, integral: 1, fluct: 1, linLossLimit= 0.01
      ===== EM models for the G4Region  DefaultRegionForTheWorld ======
        MollerBhabha :   Emin=        0 eV       Emax=         10 TeV

eBrem:   for  e+    SubType= 3
      dE/dx and range tables from 100 eV  to 10 TeV in 77 bins
      Lambda tables from threshold to 10 TeV in 77 bins, spline: 1
      LPM flag: 1 for E > 1 GeV
      ===== EM models for the G4Region  DefaultRegionForTheWorld ======
              eBrem :   Emin=        0 eV       Emax=          1 GeV  AngularGenUrban
            eBremLPM :   Emin=        1 GeV      Emax=         10 TeV  AngularGenUrban

annihil:   for  e+    SubType= 5
      Lambda tables from 100 eV  to 10 TeV in 77 bins, spline: 1
      ===== EM models for the G4Region  DefaultRegionForTheWorld ======
            eplus2gg :   Emin=        0 eV       Emax=         10 TeV

msc:   for proton    SubType= 10
      Lambda tables from 100 eV  to 10 TeV in 77 bins, spline: 1
      RangeFactor= 0.2, stepLimitType: 0, latDisplacement: 1
      ===== EM models for the G4Region  DefaultRegionForTheWorld ======
          UrbanMsc90 :   Emin=        0 eV       Emax=         10 TeV

hIoni:   for  proton    SubType= 2
      dE/dx and range tables from 100 eV  to 10 TeV in 77 bins
      Lambda tables from threshold to 10 TeV in 77 bins, spline: 1
      finalRange(mm)= 1, dRoverRange= 0.2, integral: 1, fluct: 1, linLossLimit= 0.01
      ===== EM models for the G4Region  DefaultRegionForTheWorld ======
              Bragg :   Emin=        0 eV       Emax=          2 MeV
          BetheBloch :   Emin=        2 MeV      Emax=         10 TeV

hBrems:   for  proton    SubType= 3
      dE/dx and range tables from 100 eV  to 10 TeV in 77 bins
      Lambda tables from threshold to 10 TeV in 77 bins, spline: 1
      ===== EM models for the G4Region  DefaultRegionForTheWorld ======
              hBrem :   Emin=        0 eV       Emax=         10 TeV
```

```
hPairProd:   for  proton    SubType= 4
      dE/dx and range tables from 100 eV  to 10 TeV in 77 bins
      Lambda tables from threshold to 10 TeV in 77 bins, spline: 1
      ===== EM models for the G4Region  DefaultRegionForTheWorld ======
           hPairProd :   Emin=        0 eV       Emax=         10 TeV

msc:   for GenericIon    SubType= 10
      RangeFactor= 0.2, stepLimitType: 0, latDisplacement: 0
      ===== EM models for the G4Region  DefaultRegionForTheWorld ======
          UrbanMsc90 :   Emin=        0 eV       Emax=         10 TeV

ionIoni:   for  GenericIon    SubType= 2
      dE/dx and range tables from 100 eV  to 10 TeV in 77 bins
      Lambda tables from threshold to 10 TeV in 77 bins, spline: 1
      finalRange(mm)= 0.1, dRoverRange= 0.1, integral: 1, fluct: 1, linLossLimit= 0.02
      Stopping Power data for 17 ion/material pairs
      ===== EM models for the G4Region  DefaultRegionForTheWorld ======
            BraggIon :   Emin=        0 eV       Emax=          2 MeV
          BetheBloch :   Emin=        2 MeV      Emax=         10 TeV

hIoni:   for  anti_proton    SubType= 2
      dE/dx and range tables from 100 eV  to 10 TeV in 77 bins
      Lambda tables from threshold to 10 TeV in 77 bins, spline: 1
      finalRange(mm)= 1, dRoverRange= 0.2, integral: 1, fluct: 1, linLossLimit= 0.01
      ===== EM models for the G4Region  DefaultRegionForTheWorld ======
            ICRU73QO :   Emin=        0 eV       Emax=          2 MeV
          BetheBloch :   Emin=        2 MeV      Emax=         10 TeV

msc:   for kaon+    SubType= 10
      Lambda tables from 100 eV  to 10 TeV in 77 bins, spline: 1
      RangeFactor= 0.2, stepLimitType: 0, latDisplacement: 1
      ===== EM models for the G4Region  DefaultRegionForTheWorld ======
          UrbanMsc90 :   Emin=        0 eV       Emax=         10 TeV

hIoni:   for  kaon+    SubType= 2
      dE/dx and range tables from 100 eV  to 10 TeV in 77 bins
      Lambda tables from threshold to 10 TeV in 77 bins, spline: 1
      finalRange(mm)= 1, dRoverRange= 0.2, integral: 1, fluct: 1, linLossLimit= 0.01
      ===== EM models for the G4Region  DefaultRegionForTheWorld ======
               Bragg :   Emin=        0 eV       Emax=    1.05231 MeV
```

```
          BetheBloch :   Emin=  1.05231 MeV      Emax=         10 TeV

hBrems:   for  kaon+    SubType= 3
      dE/dx and range tables from 100 eV  to 10 TeV in 77 bins
      Lambda tables from threshold to 10 TeV in 77 bins, spline: 1
      ===== EM models for the G4Region  DefaultRegionForTheWorld ======
              hBrem :   Emin=        0 eV       Emax=         10 TeV

hPairProd:   for  kaon+    SubType= 4
      dE/dx and range tables from 100 eV  to 10 TeV in 77 bins
      Lambda tables from threshold to 10 TeV in 77 bins, spline: 1
      ===== EM models for the G4Region  DefaultRegionForTheWorld ======
           hPairProd :   Emin=        0 eV       Emax=         10 TeV

hIoni:   for  kaon-    SubType= 2
      dE/dx and range tables from 100 eV  to 10 TeV in 77 bins
      Lambda tables from threshold to 10 TeV in 77 bins, spline: 1
      finalRange(mm)= 1, dRoverRange= 0.2, integral: 1, fluct: 1, linLossLimit= 0.01
      ===== EM models for the G4Region  DefaultRegionForTheWorld ======
            ICRU73QO :   Emin=        0 eV       Emax=    1.05231 MeV
          BetheBloch :   Emin=  1.05231 MeV      Emax=         10 TeV

hBrems:   for  kaon-    SubType= 3
      dE/dx and range tables from 100 eV  to 10 TeV in 77 bins
      Lambda tables from threshold to 10 TeV in 77 bins, spline: 1
      ===== EM models for the G4Region  DefaultRegionForTheWorld ======
              hBrem :   Emin=        0 eV       Emax=         10 TeV

hPairProd:   for  kaon-    SubType= 4
      dE/dx and range tables from 100 eV  to 10 TeV in 77 bins
      Lambda tables from threshold to 10 TeV in 77 bins, spline: 1
      ===== EM models for the G4Region  DefaultRegionForTheWorld ======
           hPairProd :   Emin=        0 eV       Emax=         10 TeV

muMsc:   for mu+    SubType= 10
      Lambda tables from 100 eV  to 10 TeV in 77 bins, spline: 1
      RangeFactor= 0.2, step limit type: 0, lateralDisplacement: 1, polarAngleLimit(deg)= 11.45
92
      ===== EM models for the G4Region  DefaultRegionForTheWorld ======
        WentzelVIUni :   Emin=        0 eV       Emax=         10 TeV
```

```
muIoni:   for  mu+    SubType= 2
      dE/dx and range tables from 100 eV  to 10 TeV in 77 bins
      Lambda tables from threshold to 10 TeV in 77 bins, spline: 1
      finalRange(mm)= 1, dRoverRange= 0.2, integral: 1, fluct: 1, linLossLimit= 0.01
      ===== EM models for the G4Region  DefaultRegionForTheWorld ======
              Bragg :   Emin=        0 eV       Emax=        200 keV
         BetheBloch :   Emin=      200 keV      Emax=          1 GeV
        MuBetheBloch :   Emin=        1 GeV      Emax=         10 TeV

muBrems:   for  mu+    SubType= 3
      dE/dx and range tables from 100 eV  to 10 TeV in 77 bins
      Lambda tables from threshold to 10 TeV in 77 bins, spline: 1
      ===== EM models for the G4Region  DefaultRegionForTheWorld ======
             MuBrem :   Emin=        0 eV       Emax=         10 TeV

muPairProd:   for  mu+    SubType= 4
      dE/dx and range tables from 100 eV  to 10 TeV in 77 bins
      Lambda tables from threshold to 10 TeV in 77 bins, spline: 1
      ===== EM models for the G4Region  DefaultRegionForTheWorld ======
          muPairProd :   Emin=        0 eV       Emax=         10 TeV

CoulombScat:   for  mu+    SubType= 1
      Lambda tables from 100 eV  to 10 TeV in 77 bins, spline: 1
      11.4592 < Theta(degree) < 180, Eth(MeV)= 10; pLimit(GeV^1)= 0.139531
      ===== EM models for the G4Region  DefaultRegionForTheWorld ======
  eCoulombScattering :   Emin=        0 eV       Emax=         10 TeV

muIoni:   for  mu-    SubType= 2
      dE/dx and range tables from 100 eV  to 10 TeV in 77 bins
      Lambda tables from threshold to 10 TeV in 77 bins, spline: 1
      finalRange(mm)= 1, dRoverRange= 0.2, integral: 1, fluct: 1, linLossLimit= 0.01
      ===== EM models for the G4Region  DefaultRegionForTheWorld ======
            ICRU73QO :   Emin=        0 eV       Emax=        200 keV
         BetheBloch :   Emin=      200 keV      Emax=          1 GeV
        MuBetheBloch :   Emin=        1 GeV      Emax=         10 TeV

muBrems:   for  mu-    SubType= 3
      dE/dx and range tables from 100 eV  to 10 TeV in 77 bins
      Lambda tables from threshold to 10 TeV in 77 bins, spline: 1
```

```
      ===== EM models for the G4Region  DefaultRegionForTheWorld ======
              MuBrem :   Emin=        0 eV       Emax=         10 TeV

muPairProd:   for  mu-    SubType= 4
      dE/dx and range tables from 100 eV  to 10 TeV in 77 bins
      Lambda tables from threshold to 10 TeV in 77 bins, spline: 1
      ===== EM models for the G4Region  DefaultRegionForTheWorld ======
          muPairProd :   Emin=        0 eV       Emax=         10 TeV

CoulombScat:   for  mu-    SubType= 1
      Lambda tables from 100 eV  to 10 TeV in 77 bins, spline: 1
      11.4592 < Theta(degree) < 180, Eth(MeV)= 10; pLimit(GeV^1)= 0.139531
      ===== EM models for the G4Region  DefaultRegionForTheWorld ======
  eCoulombScattering :   Emin=        0 eV       Emax=         10 TeV

hIoni:   for  pi+    SubType= 2
      dE/dx and range tables from 100 eV  to 10 TeV in 77 bins
      Lambda tables from threshold to 10 TeV in 77 bins, spline: 1
      finalRange(mm)= 1, dRoverRange= 0.2, integral: 1, fluct: 1, linLossLimit= 0.01
      ===== EM models for the G4Region  DefaultRegionForTheWorld ======
              Bragg :   Emin=        0 eV       Emax=    297.505 keV
         BetheBloch :   Emin=  297.505 keV      Emax=         10 TeV

hBrems:   for  pi+    SubType= 3
      dE/dx and range tables from 100 eV  to 10 TeV in 77 bins
      Lambda tables from threshold to 10 TeV in 77 bins, spline: 1
      ===== EM models for the G4Region  DefaultRegionForTheWorld ======
              hBrem :   Emin=        0 eV       Emax=         10 TeV

hPairProd:   for  pi+    SubType= 4
      dE/dx and range tables from 100 eV  to 10 TeV in 77 bins
      Lambda tables from threshold to 10 TeV in 77 bins, spline: 1
      ===== EM models for the G4Region  DefaultRegionForTheWorld ======
           hPairProd :   Emin=        0 eV       Emax=         10 TeV

msc:   for pi-    SubType= 10
      Lambda tables from 100 eV  to 10 TeV in 77 bins, spline: 1
      RangeFactor= 0.2, stepLimitType: 0, latDisplacement: 1
      ===== EM models for the G4Region  DefaultRegionForTheWorld ======
          UrbanMsc90 :   Emin=        0 eV       Emax=         10 TeV
```

```
hIoni:   for  pi-    SubType= 2
      dE/dx and range tables from 100 eV  to 10 TeV in 77 bins
      Lambda tables from threshold to 10 TeV in 77 bins, spline: 1
      finalRange(mm)= 1, dRoverRange= 0.2, integral: 1, fluct: 1, linLossLimit= 0.01
      ===== EM models for the G4Region  DefaultRegionForTheWorld ======
            ICRU73QO :   Emin=        0 eV       Emax=    297.505 keV
         BetheBloch :   Emin=  297.505 keV      Emax=         10 TeV

hBrems:   for  pi-    SubType= 3
      dE/dx and range tables from 100 eV  to 10 TeV in 77 bins
      Lambda tables from threshold to 10 TeV in 77 bins, spline: 1
      ===== EM models for the G4Region  DefaultRegionForTheWorld ======
              hBrem :   Emin=        0 eV       Emax=         10 TeV

hPairProd:   for  pi-    SubType= 4
      dE/dx and range tables from 100 eV  to 10 TeV in 77 bins
      Lambda tables from threshold to 10 TeV in 77 bins, spline: 1
      ===== EM models for the G4Region  DefaultRegionForTheWorld ======
           hPairProd :   Emin=        0 eV       Emax=         10 TeV
================================================================================
             HADRONIC PROCESSES SUMMARY (verbose level 1)

                    Hadronic Processes for <GenericIon>
       ionInelastic  Models:            Binary Cascade: Emin(GeV)=     0  Emax(GeV)= 20

                    Hadronic Processes for <anti_neutron>
          hadElastic  Models:              hElasticLHEP: Emin(GeV)=     0  Emax(GeV)= 100000
AntiNeutronInelastic  Models:  G4LEAntiNeutronInelastic: Emin(GeV)=     0  Emax(GeV)= 25
                              G4HEAntiNeutronInelastic: Emin(GeV)=    20  Emax(GeV)= 100000

                    Hadronic Processes for <anti_proton>
          hadElastic  Models:              hElasticLHEP: Emin(GeV)=     0  Emax(GeV)= 100000
 AntiProtonInelastic  Models:   G4LEAntiProtonInelastic: Emin(GeV)=     0  Emax(GeV)= 25
                               G4HEAntiProtonInelastic: Emin(GeV)=    20  Emax(GeV)= 100000

                    Hadronic Processes for <e->
      ElectroNuclear  Models:                     CHIPS: Emin(GeV)=     0  Emax(GeV)= 30000

                    Hadronic Processes for <gamma>
```

```
   PhotonInelastic  Models:                    CHIPS: Emin(GeV)=     0  Emax(GeV)= 3.5
                                  TheoFSGenerator: Emin(GeV)=     3  Emax(GeV)= 100000

                  Hadronic Processes for <kaon+>
       hadElastic  Models:              hElasticLHEP: Emin(GeV)=     0  Emax(GeV)= 100000
 KaonPlusInelastic  Models:                     QGSP: Emin(GeV)=    12  Emax(GeV)= 100000
                                 G4LEKaonPlusInelastic: Emin(GeV)=     0  Emax(GeV)= 25

                  Hadronic Processes for <kaon->
       hadElastic  Models:              hElasticLHEP: Emin(GeV)=     0  Emax(GeV)= 100000
KaonMinusInelastic  Models:                     QGSP: Emin(GeV)=    12  Emax(GeV)= 100000
                                G4LEKaonMinusInelastic: Emin(GeV)=     0  Emax(GeV)= 25

                  Hadronic Processes for <lambda>
       hadElastic  Models:              hElasticLHEP: Emin(GeV)=     0  Emax(GeV)= 100000
  LambdaInelastic  Models:       G4LELambdaInelastic: Emin(GeV)=     0  Emax(GeV)= 25
                                  G4HELambdaInelastic: Emin(GeV)=    20  Emax(GeV)= 100000

                  Hadronic Processes for <mu->
      muMinusCaptureAtRest

                  Hadronic Processes for <neutron>
       hadElastic  Models:             hElasticCHIPS: Emin(GeV)= 0.0195  Emax(GeV)= 100000
                                    NeutronHPElastic: Emin(GeV)=     0  Emax(GeV)= 0.02
 NeutronInelastic  Models:                     QGSP: Emin(GeV)=    12  Emax(GeV)= 100000
                                 G4LENeutronInelastic: Emin(GeV)=   9.5  Emax(GeV)= 25
                                       Binary Cascade: Emin(GeV)= 0.0199  Emax(GeV)= 9.9
                                  NeutronHPInelastic: Emin(GeV)=     0  Emax(GeV)= 0.02
         nCapture  Models:                G4LCapture: Emin(GeV)= 0.0199  Emax(GeV)= 20000
                                    NeutronHPCapture: Emin(GeV)=     0  Emax(GeV)= 0.02
         nFission  Models:                G4LFission: Emin(GeV)= 0.0199  Emax(GeV)= 20000
                                    NeutronHPFission: Emin(GeV)=     0  Emax(GeV)= 0.02

                  Hadronic Processes for <pi+>
       hadElastic  Models:              hElasticLHEP: Emin(GeV)=     0  Emax(GeV)= 1
                                     hElasticGlauber: Emin(GeV)=     1  Emax(GeV)= 100000
 PionPlusInelastic  Models:                     QGSP: Emin(GeV)=    12  Emax(GeV)= 100000
                                 G4LEPionPlusInelastic: Emin(GeV)=     0  Emax(GeV)= 25

                  Hadronic Processes for <pi->
```

```
          hadElastic  Models:              hElasticLHEP: Emin(GeV)=     0  Emax(GeV)= 1
                                         hElasticGlauber: Emin(GeV)=     1  Emax(GeV)= 100000
  PionMinusInelastic  Models:                     QGSP: Emin(GeV)=    12  Emax(GeV)= 100000
                                  G4LEPionMinusInelastic: Emin(GeV)=     0  Emax(GeV)= 25

                      Hadronic Processes for <proton>
          hadElastic  Models:              hElasticCHIPS: Emin(GeV)=     0  Emax(GeV)= 100000
     ProtonInelastic  Models:                     QGSP: Emin(GeV)=    12  Emax(GeV)= 100000
                                       G4LEProtonInelastic: Emin(GeV)=   9.5  Emax(GeV)= 25
                                           Binary Cascade: Emin(GeV)=     0  Emax(GeV)= 9.9
================================================================================================
### Run 0 start.
```